2018

Components Required for the Death and Degradation of the Linker Cell in C. Elegans

Lena Marlise Kutscher

COMPONENTS REQUIRED FOR THE DEATH AND DEGRADATION OF THE LINKER CELL IN *C. ELEGANS*

A Thesis Presented to the Faculty of

The Rockefeller University

in Partial Fulfillment of the Requirements for

the degree of Doctor of Philosophy

by

Lena Marlise Kutscher

June 2018

COMPONENTS REQUIRED FOR THE DEATH AND DEGRADATION OF THE LINKER CELL IN *C. ELEGANS*

Lena Marlise Kutscher, Ph.D.

The Rockefeller University 2018

Programmed cell death (PCD) is an important process in the development of multicellular organisms. Apoptosis, a form of PCD characterized morphologically by chromatin condensation, membrane blebbing, and cytoplasm compaction, and molecularly by the activation of caspase proteases, has been extensively investigated. Studies in *C. elegans*, *Drosophila*, mice, and the developing chick have revealed, however, that developmental PCD also occurs through other mechanisms, morphologically and molecularly distinct from apoptosis. One prominent cell death program, linker cell-type death (LCD), is morphologically conserved, and independent of the key genes that drive apoptosis. Instead, LCD functions, in part, through the stress-related protein HSF-1, and subsequent upregulation of members of the ubiquitin proteasome system. How exactly HSF-1 is post-translationally regulated to either commit to cell survival or cell death is not currently known. Using a protein interaction screen and classical genetic studies, I propose that the homeodomain protein kinase HPK-1 is required to activate the heat shock function of HSF-1, thereby indirectly inhibiting its cell death role. I hypothesize that PQN-41C, a polyglutamine protein

necessary for linker cell death, binds HPK-1 to limit its HSF-1 interactions, and pushes the cell towards death.

Downstream of cell death, the linker cell must be phagocytosed and degraded by engulfing cells. This process does not rely on canonical apoptotic factors, so I carried out a forward genetic screen to identify genes involved in corpse degradation. I discovered a key protein network involved in linker cell corpse engulfment and degradation and revealed that two small GTPases, RAB-35 and ARF-6, and their regulators ensure timely phagocytosis and phagosome maturation. I also determined that the caspase CED-3 and its upstream regulator CED-4 are required not for cell death, but for proper cell corpse removal. This new role of caspase in cell corpse disposal offers an alternative function for the role of caspases in cell death, and suggests how apoptotic and non-apoptotic forms of cell death may work together to remove cells during animal development.

To Luka and Elias:

"*Think and wonder,*

wonder and think."

ACKNOWLEDGMENTS

First, I would like to thank **Shai** for his mentorship and guidance over the last six years. You have taught me how to be a better scientist, and I am so lucky to have been a student of yours. I will be sad to leave but I know I am well prepared for the next step in my career. Thank you!

Next, I would like to thank the past and present members of my thesis committee, **Hermann Steller**, **Sandy Simon**, and **Marc Tessier-Lavigne** for their scientific advice and career guidance. You have helped make this work better.

I would like to thank **Zheng Zhou** for agreeing to be my external thesis committee member and for traveling from Texas. Thank you also for your generosity with reagents and scientific advice.

I would like to thank the Dean's office (**Sid**, **Emily**, **Cris**, **Kristen**, **Marta**, and **Stephanie**) for making it so easy to be a graduate student at Rockefeller. You enabled me to focus on the science throughout my time here, and I really appreciate all your hard work.

I would like to thank past and present members of the Shaham Lab. It has been a pleasure to work in the lab, and I hope to recreate this environment if I am lucky enough to have my own lab in the future. I would like to thank the linker cell crew, **Maxime**, **Jenn**, **Andrew**, and **Mohammad**, for being so collaborative and open, and making work fun every day. I would also like to especially thank **Anu** and **Wendy** for making the late nights and hard times more enjoyable.

I would like to especially thank my collaborator and close friend, **Wolfgang Keil**. Working with you has been so fun, and your input has increased the quality of this work. I will miss our coffee breaks and daily discussions, but I hope we can continue our scientific collaboration and friendship across the pond!

I would like to thank my undergraduate mentors, **Jeff Sekelsky**, **Brian Hogan**, and **Domenic Tiani**, for instilling in me a love of science and continuing to encourage me even today.

I would like to thank the caretakers at the CFC, especially **Tashie**, **Yadira**, **Debbie**, and **Michelle**, for taking such good care of Luka and Elias, so that I could focus on my science. Your work is crucial to the success of the mothers and fathers at this university.

I would like to thank my friends **Delaney Kloesel** and **Leah Charbonneau**, whose help was crucial for the completion of this thesis. I could not have survived the last few weeks without you.

I would like to thank the **Hyatt** and **Kutscher families** for their support during my PhD, asking me about my work and accepting the fact that I always seemed to be writing something when I was visiting.

Most importantly, I would like to thank **Daniel**, for coming with me to NYC in 2011, and encouraging me every step of the way. Thanks for never complaining about the nights I would work late or every time I said 5 more minutes that turned into 30. My success is directly correlated with your support. I can't wait to start the next chapter, and I promise to work on my time estimation skills!

Table of Contents

List of Figures

List of Tables

List of Abbreviations

AMH: anti-Müllerian hormone
BAF: Boc-D-FMK
CAD: caspase activated DNase
DRG: dorsal root ganglion
ESC: embryonic stem cell
ev: empty vector
EM: electron microscopy
GCD: germ cell death
IAP: inhibitor of apoptosis protein
IBM: IAP-binding motif
ICM: inner cell mass
ISM: intersegmental muscle
kb: kilobase
LC: linker cell
LCD: linker cell-type death
LMP: lysosome membrane permeabilization
MD: Müllerian duct
MEF: mouse embryonic fibroblast
NMJ: neuromuscular junctions
PCD: Programmed cell death
PI3P: phosphatidylinositol 3-phosphate
$PI(4,5)P_2$: Phosphatidylinositol 4,5-bisphosphate
PQN: polyglutamine
PS: phosphatidyl serine
RNAi: RNA interference
ROS: reactive oxygen species
SLC: surviving linker cell
TNF: tumor necrosis factor
TUNEL: terminal deoxynucleotidyl nuclear transferase dUTP nick end-labeling UPS: ubiquitin proteasome system
WD: Wolffian duct
WT: wild type

1. Introduction

1.1. Programmed cell death

The term Programmed Cell Death (PCD) was first coined to describe cell elimination that occurs at precise locations and times during development [1], although cell death as a phenomenon had been described as early as the 1885 [2]. This process is key for sculpting tissues and organs, for removing excess or unnecessary cells, and for tissue homeostasis. The reproducible and consistent patterns of cell death in developing animals led to the idea that specific genes are driving the phenomenon. Indeed, genes promoting apoptosis, a form of PCD characterized by chromatin condensation, membrane blebbing, and cytoplasm compaction [3,4] (Figure 1-1), were initially isolated in *Caenorhabditis elegans* [5]. The discovery that the *C. elegans* caspase gene *ced-3* is required for developmental apoptosis, and the subsequent realization that caspase homologs in *Drosophila* and in vertebrates also promote apoptosis, demonstrated that underlying the stereotypical morphological signature is a conserved molecular program [6,7]. In species as diverged as *C. elegans* and the mouse, apoptosis is mediated by caspase proteases, activated by a conserved scaffolding protein called CED-4 in *C. elegans* and APAF1 in mice. Bcl-2 family proteins act upstream of CED-4/APAF1 to control its activation. This occurs by direct binding in *C. elegans* [8], or through release of mitochondrial cytochrome C, which oligomerizes APAF1 in mammals [9].

1.2. A brief introduction to developmental apoptosis in *C. elegans* and *Drosophila*

In *C. elegans*, a BH3-only-like protein, EGL-1, inhibits CED-9, a Bcl-2-like protein [10] (Figure 1-2a). This removes the inhibition that CED-9 places on CED-4, an APAF1 homolog [11]. Activated CED-4 cleaves CED-3, a caspase, into

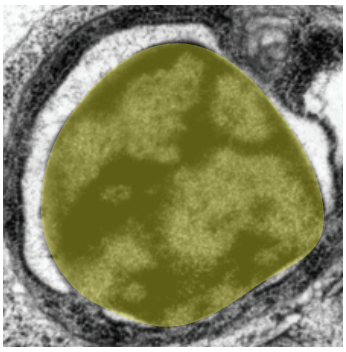

Figure 1-1. **Morphology of an apoptotic corpse.** In apoptosis, chromatin is highly condensed and darkly staining, but the nuclear envelope remains round (*C. elegans* cell, courtesy of Yun Lu).

its functional form [5]. Later, molecular apoptosis was confirmed and expanded in *Drosop*hila *melanogaster* and in mouse [12,13].

In *Drosophila*, apoptotic stimuli gather Inhibitor of Apoptosis Proteins (IAP) antagonists, including Reaper, Hid, Grim, to the mitochondria, to inhibit the IAP, Diap1 [13-16]. IAPs were found to negatively inhibit caspases in Drosophila and other organisms [17,18] (Figure 1-2b). Inhibition of IAPs allows for the APAF1-like protein Ark to activate the Caspase-9-like protein Dronc [19-21]. Downstream of Dronc, caspases DrICE and Dcp1 promote apoptosis [22,23].

1.3. A brief introduction to developmental apoptosis in mammals and evidence of alternative cell death pathways

In mammals, the core components of the apoptosis pathway combine aspects of the pathways from worms and flies, with molecular paradigms upstream of mitochondria similar to *C. elegans*, and those downstream of the mitochondria similar to Drosophila (Figure 1-2c). For example, BH3-only proteins inhibit Bcl-2 family members upon activation by an apoptotic stimulus [24], similar to *C. elegans*. This lifts the negative inhibition that Bcl-2 family members place on Bax and Bak at the mitochondria [25], allowing these proteins to form pores on the outer mitochondrial membrane and release cytochrome C [26,27]. Blocking Bax and Bak is thought to inhibit all forms of intrinsic apoptosis [28]. Additionally, this also releases IAP-binding partners to promote apoptosis [29,30], similar to *Drosophila*. Cytochrome C release leads to the activation

of the apoptosome containing multimeric APAF1, which activates the initiator caspase, caspase-9; this in turn activates the executioner caspases, caspases -3 and -7 [30,31].

Although initial reports of mice harboring knockout mutations in caspase genes, in *Apaf1*, or in both *Bax* and *Bak* suggested that these genes play important roles in vertebrate developmental cell death [13,32-36], breeding mutants onto different genetic backgrounds revealed that homozygous knockout mice were not only born, but could survive to adulthood, often exhibiting only minor defects [36-39]. For example, while initial reports suggested that mice defective in *Apaf1* exhibit inappropriate webbing between the digits of the pentadactyl limb, later analysis revealed only a delay in the process, with complete culling of the webbing within two days [34,35]. Mutations in *Caspase-3* or *Caspase-9* do not affect this process [33,40]. Furthermore, while persistence of small webs are observed in *Bax; Bak* double mutants, this surviving tissue is a small fraction of what survives in *Bmp* mutants, in which cell death is indirectly blocked [41,42].

Similarly, early studies of *Caspase-3* mutants revealed mice with apparent skull

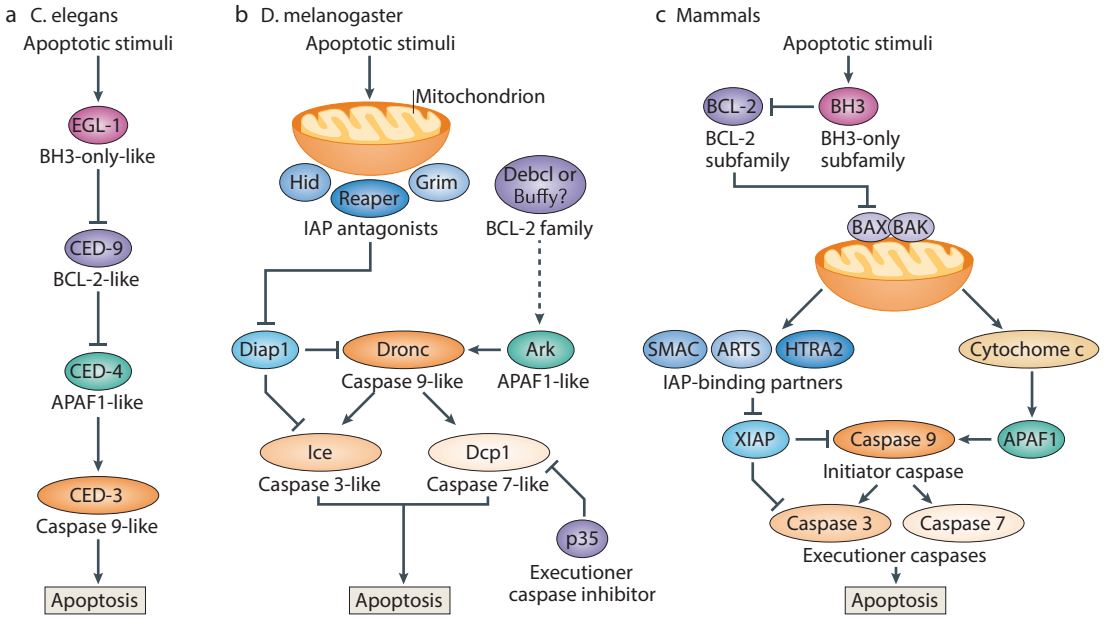

Figure 1-2. **Core components of the apoptosis pathway are conserved in worms, flies, and mammals**.
Figure adapted from [46].

fractures and protruding brain tissue, suggesting a vast excess of neurons in the brain, consistent with the observation that in some brain regions up to 80% of cells that are originally produced are thought to undergo PCD [13,43]. Subsequent examination, however, revealed no increase in neuronal cell number [44]. Rather, defects in the sutures that bind skull bones together appear to be the cause of skull disruption [45], and oozing of brain tissue is likely a consequence of the release of intracranial pressure to which the brain is normally subjected.

Although the absence of massive cell survival in *Caspase-3* or *Caspase-9* mutants could be explained by redundant activities of these enzymes, as the mouse harbors 13 caspase genes [46], only a single *Apaf1* gene is found in the murine genome [34]. Furthermore, studies of *Bax; Bak* double mutants suggest that developmental apoptosis is nearly entirely abrogated, yet some animals still develop normally to adulthood [36]. Thus, an alternative explanation may be the existence of caspase-independent non-apoptotic processes. Cells dying with non-apoptotic features during animal development have been extensively described [47], yet little is known about the underlying molecular effectors of these alternative death programs, or their *in vivo* relevance.

1.4. Non-apoptotic developmental cell death

While most developmental cell death in *Drosophila* and *C. elegans* proceeds via apoptosis, these organisms also provide highly amenable settings for non-apoptotic pathway discoveries.

1.4.1. Germ cell death in Drosophila males

Pre-meiotic male germ cells undergo stochastic PCD in the adult fly testes, and dying cells display some apoptotic features, including cytoplasmic compaction and chromatin condensation [48] (Figure 1-3a). Dying germ cells are also TUNEL-positive,

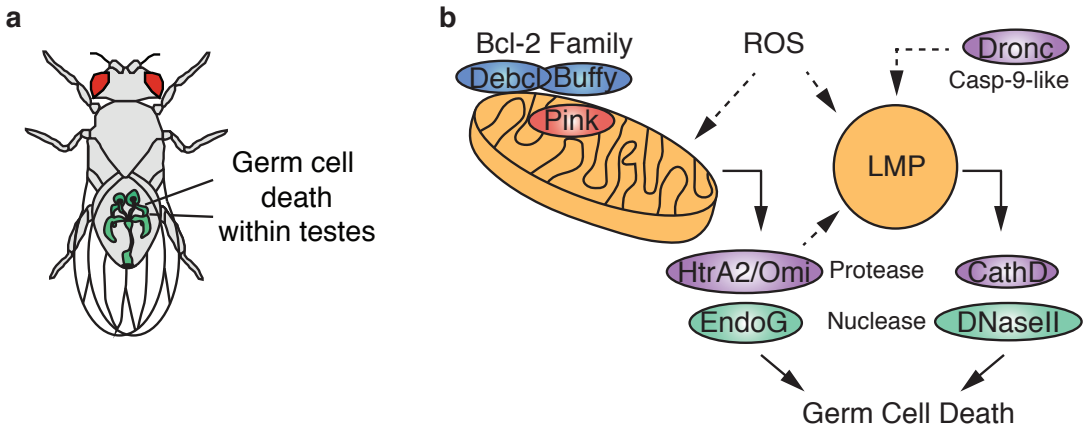

Figure 1-3. **Germ cell death in *Drosophila* males**.
(a) In adult males, germ cell death occurs within the testes (green). (b) Dronc, a Caspase-9-like protease, functions in an apoptosome-independent fashion to perhaps trigger lysosome membrane permeabilization (LMP), allowing the release of the protease CathepsinD and the nuclease DNaseII. At the mitochondria, Bcl-2 family members Debcl and Buffy function on the outer membrane, and the Parkinson-related protein Pink1 functions within. ROS may trigger release of the serine protease HtrA2/Omi and the nuclease EndoG [48].

suggesting chromosomal DNA fragmentation. Surprisingly, these wild-type cells are not stained with an antibody against cleaved Caspase-3, which binds the executioner caspases Drice and Dcp-1 [48]. Furthermore, cells still die when these caspases are knocked down, suggesting that germ cell death is non-apoptotic. Correspondingly, unlike apoptotic cells, mitochondria of dying wild-type germ cells appear deformed and swollen [48].

Although germ cell death does not employ executioner caspases, it does require an APAF1-independent function of the initiator caspase Dronc [48]. Mutations in the *Apaf1* homolog, *ark*, in fact, increase cell death, perhaps because more Dronc is now available to induce non-apoptotic death [48,49]. Mutations in *dronc* result in a 40%-60% decrease in death. This defect is specific, as lesions in the initiator caspases *strica* and *dredd* have no effect. The mechanism of Dronc action here is not fully understood. However, lysosomal biogenesis proteins and the lysosomal protease cathepsinD are

required for efficient demise, and an increase in reactive oxygen species (ROS), and acidification of the cytoplasm occur [48]. ROS and Dronc may promote lysosome membrane permeabilization, allowing release of cathepsinD and DNaseII into the cytosol [48] (Figure 1-3b). The release of DNaseII may explain TUNEL staining in the absence of cleaved Caspase-3.

Yacobi-Sharon and colleagues discovered that the mitochondrial protease HtrA2/Omi plays an important role in germ cell death [48]. *Drosophila* carrying deletions of either one or both *htrA2/omi* copies are viable, but exhibit male sterility associated with a decrease in germ cell death. *htrA2/omi* encodes a multi-domain protein containing a mitochondrial targeting sequence, an IAP-binding motif (IBM), a serine protease domain, and a protein-interaction domain. Structure-function analysis revealed that the catalytic domain, but not the IBM, is crucial for death [48]. Remarkably, *htrA2/omi* lesions in humans are associated with Parkinson's disease [48], and mutations in the Parkinson's disease- and mitochondrial-associated gene *pink1* also cause a decrease in *Drosophila* germ cell death. Overexpression of a cytosolic version of HtrA2/Omi promotes caspase-independent cell death in mammalian cells [51], accompanied by morphological similarities to *Drosophila* germ-cell death, although nuclear changes are not evident [48,51]. Roles for mitochondria in *Drosophila* germ cell death are also supported by the findings that the Bcl-2 family proteins Debcl and Buffy, and the mitochondrial nuclease EndoG, promote death [48] (Figure 1-3b).

Additionally, GCD does not function completely independent of caspases, but it provides a good model for how both caspase-dependent and independent mechanisms can work together to kill cells. Aspects of GCD may be conserved in some mammalian necrotic pathways. For example, in immortalized mouse embryonic fibroblasts (MEFs), introduction of tumor necrosis factor (TNF) can induce a non-apoptotic cell death program that does not utilize executioner caspases [52]. Instead, like GCD, lysosomes and caspase-9, but not APAF1, are required [52]. The upstream signaling and some

molecular components of TNF-induced cell death differ from GCD, but the similarities are striking nonetheless. In addition, LMP, like that observed in GCD, is important for mammary gland epithelial cell death after weaning [53].

In rodents, male germ cells also undergo stochastic cell death that may be caspase independent [54,55]. Mutations in the pro-apoptotic gene *Bax* do not block these deaths, suggesting possible involvement of non-apoptotic programs [56,57]. Furthermore, mutations in the testes-specific serine protease inhibitor *spink2* result in increased germ cell death in male mice [55]. These observations provide circumstantial evidence that conserved pathways may control stochastic germ cell death in males across species.

1.4.2. Nurse cell death in Drosophila females

In the *Drosophila* ovary, 15 nurse cells provide a developing oocyte with proteins, mRNA, and organelles [58] (Figure 1-4a). After extruding their cytoplasmic contents into the oocyte, nurse-cell remnants die. Dying wild-type cells exhibit chromatin condensation, but also autophagosomes, ruptured lysosomes, and larger vacuolar structures [59,60]. Dying cells stain with acidification markers, autophagic markers, and TUNEL [59-62], raising the possibility that more than one cell death program is involved.

Whether caspases promote nurse cell death is debated. Some studies report no activated caspases in dying cells [63,64], whereas others report immunoreactivity using an activated Caspase-3 antibody [61,62]. Mutants in *Drosophila* inducers of apoptosis (*hid, reaper, grim*) do not exhibit nurse cell survival, suggesting a caspase-independent process [65,66], and some studies suggest that overexpression of the caspase inhibitors *diap1* or *p35* also does not perturb nurse cell death [62,63]. However, other studies suggest that such overexpression weakly blocks death [67].

Genetic studies demonstrate that nurse cell death still proceeds in *dronc, dredd*, *strica, dcp-1*, or *drice* caspase single mutants [23,67,68]. However, *dredd; strica* or

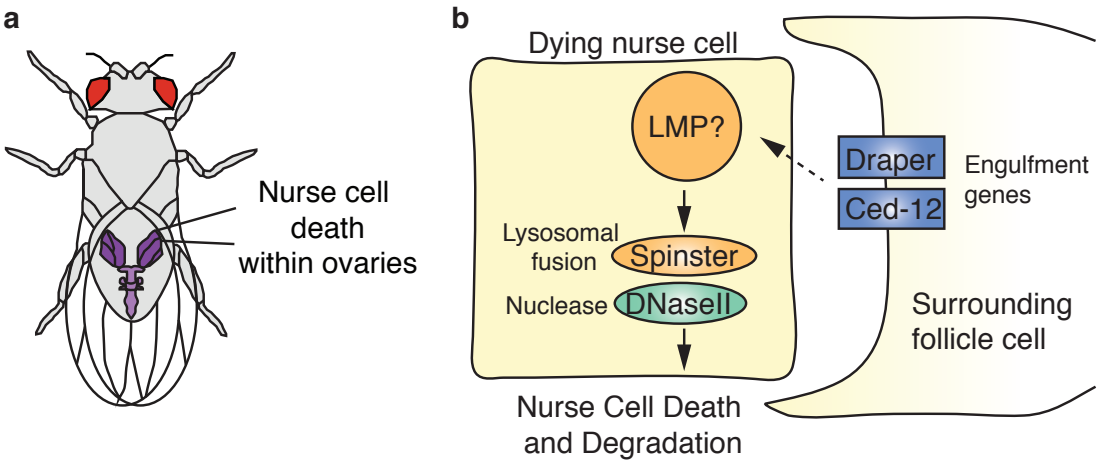

Figure 1-4. **Nurse cell death in *Drosophila* females**.
(a) In the female adult fly, nurse cell death occurs within the ovaries (purple). (b) The surrounding follicle cells may induce nurse cell death, using the engulfment receptors Draper and Ced-12 via phagoptosis. Downstream events may lead to lysosome membrane permeabilization (LMP) and the release of the lysosomal fusion protein Spinster and the nuclease DNaseII. Caspases and autophagy may be minimally involved.

dcp-1; drice double mutants exhibit weak survival, suggesting that caspases may be relevant, but functionally redundant [67]. Congruently, mutants in *Apaf1/ark*, which functions upstream of initiator caspases, also exhibit weak nurse cell death defects [66].

In developing nurse cells *in vitro*, the Caspase-3-inhibitor Z-DEVD-FMK blocks DNA fragmentation but not chromatin condensation [69]. While mutations in inhibitor of caspase-activated DNase (ICAD) cause a decrease in cleaved DNA, as assessed by a PCR assay, nurse cells still clear their DNA efficiently [70]. In another study, however, mutants in *dICAD* displayed weak nuclear persistence, similar to *Apaf1*/*ark* mutants [66]. Together, these data suggest that caspases may play some role in nurse cell death.

The role of autophagy in nurse cell death is also unclear. Despite the presence of autophagosomes, autophagy-related protein levels are not increased in dying cells [60,63]. However, one study reported that nurse cell nuclei persist in mutants of

the autophagy genes *atg1* and *atg13* [61]. This defect, however, is not fully penetrant, suggesting other processes are probably involved [61]. *atg7; dcp-1* double mutants exhibit similar defects to *atg7* single mutants [71], indicating that these other pathways may be caspase independent.

Lysosomes may play important roles in nurse cell death and removal (Figure 1-4b). Mutants in the lysosomal nuclease *DNaseII* and the lysosomal trafficking protein *deep orange/Vps18* exhibit persisting nurse cell nuclei [60,71], as do mutants in the lysosomal fusion protein *Spinster* and the lysosomal protease *CathepsinD* [60]. While Deep Orange is required in the engulfing follicle cells, DNaseII and Spinster appear to function cell autonomously [60]. Thus, lysosomes may have multiple activities in nurse cell death, although these results are complicated by the fact that some of these mutants perturb cytoplasm transfer to the oocyte, which may delay or impede death [59].

Recent research raises the possibility that the primary nurse-cell-death mechanism may be phagoptosis (primary phagocytosis), such that death of nurse cells is non-autonomously promoted by surrounding follicle cells [72]. Consistently, mutants in the engulfment genes *draper* and *ced-12* display nurse cell survival, and Draper is required for nurse cell acidification [72]. Furthermore, ablation of surrounding follicle cells strongly inhibits nurse cell death, although cytoplasm transfer is also blocked, complicating interpretation of the persistent nuclei phenotype [72]. However, it is possible that nurse cell death may be an example of assisted suicide.

1.4.3. Salivary gland cell death in Drosophila larvae

Drosophila salivary glands are larva-specific structures that are rapidly degraded after puparium formation [73,74] (Figure 1-5a). Dying wild-type cells exhibit apoptotic features, but also an abundance of autophagosomes, and nuclear separation from the cytoplasm [75,76]. Both autophagy and caspase genes are induced during

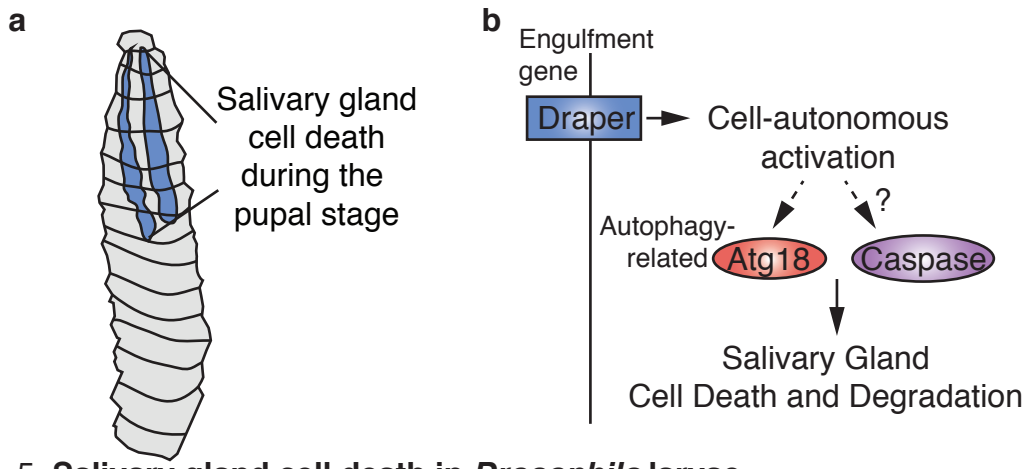

Figure 1-5. **Salivary gland cell death in *Drosophila* larvae**.
(a) After puparium formation, large larval salivary glands (blue) die and degrade before the adult fly hatches. (b) The engulfment gene Draper is required cell-autonomously within the salivary glands to drive cell death, and may lead to downstream activation of autophagy genes like Atg18. Caspases may work in parallel.

salivary gland cell death [77,78], although the precise contribution of each is not fully understood. Caspases may be dispensable for cell death. Loss-of-function mutants in *dronc* or *drice* caspase genes or in *Apaf1*/*ark* do not strongly perturb salivary gland death and degradation [74,79]. While expression of the caspase inhibitor p35 halts DNA fragmentation and nuclear lamin cleavage [75,76], it does not result in intact cells [78]. Instead, fragments appear to persist inappropriately [74], suggesting a cell degradation role for caspases.

Autophagy is induced prior to salivary gland cell death, and in the absence of the autophagy-related gene *atg18*, salivary glands are not properly degraded, exhibiting vacuolated cell fragments [74] (Figure 1-5b). These findings provide *in vivo* evidence for a role of autophagy in degrading dying cells [74]. Combining autophagy and caspase inhibition blocks gland degradation further, but not cell death, suggesting these pathways function in parallel [74]. Cell death can be inhibited by overexpression of the PI3K active subunit Dp110 and p35, suggesting involvement of a PI3K target [74].

The salivary glands are large structures, and their phagocytosis by neighboring

cells is not well understood. The engulfment gene *draper* is required to induce autophagy cell-autonomously in the salivary gland cells, and not for engulfment [76,80], suggesting an unexpected and intimate connection between engulfment and degradation genes. Such a connection had been described for nurse cell death (see above) [72]. In *C. elegans*, engulfment genes also appear important in some contexts for promoting nuclease activation for cell degradation [81].

1.4.4. Linker cell death in C. elegans

The *C. elegans* male-specific linker cell leads gonad elongation. During the L4 larva-to-adult transition, the cell dies, allowing gonad-cloaca fusion for sperm release and male fertility (Figure 1-6a). The dying linker cell is engulfed by its neighboring U.l/rp cells [82]. Morphologically, wild-type linker cell death is non-apoptotic: chromatin is not condensed, the nuclear envelope becomes crenellated, and mitochondria and endoplasmic reticulum swell [82] (Figure 1-7). Death proceeds even when all four *C. elegans* caspase genes are inactivated, and mutations in other core apoptotic genes also fail to prevent death [82,83]. Thus, linker cell death represents the first example of a non-apoptotic caspase-independent cell death process required for development. The morphology of dying linker cells is frequently seen in vertebrate development, and we have termed this appearance linker cell-type death (LCD). Importantly, although invaginated membranes are often artifacts of EM fixation, this is not the case for linker cell nuclear crenellation, as this feature is detected in the living animal under light microscopy. In vertebrate settings, LCD ultrastructural features are distinguished from EM artifacts or natural variability as they are seen only at specific developmental times, and accompany only populations of dying cells and not their neighbors (see below).

Work in the lab revealed multiple control pathways promoting linker cell death. This death must be tightly regulated, as premature demise blocks gonad elongation, resulting in sterility [84]. Two opposing Wnt pathways control death onset (Figure 1-6b).

Figure 1-6. **The linker cell dies independent of caspases.**
(a) The linker cell (green) is a male-specific cell that leads the elongation of the developing gonad. Once it reaches its destination, it dies, and is engulfed by the U.l/rp cells (purple), allowing fusion of the gonad with the cloaca. (b) Multiple regulatory pathways are required to ensure the linker cell dies at the proper place and time. These pathways include two antagonistic Wnt pathways (blue), the developmental timing protein LIN-29 (red), Sarm/TIR-1, the MAPKK SEK-1, and the polyglutamine protein PQN-41 (green), and the nuclear hormone receptor NHR-67 (purple). These pathways converge on the heat shock factor HSF-1, which acts in parallel with the SET-16 histone methyltransferase complex (orange). The pro-death function of HSF-1 competes with its pro-survival function. HSF-1 may transcriptionally upregulate the E2 ubiquitin-conjugating enzyme LET-70 (purple). The transfer of ubiquitin from the E1 UBA-1, through LET-70, to an E3 complex may confer substrate specificity leading, perhaps to degradation of key proteins by the proteasome, resulting in linker cell death.

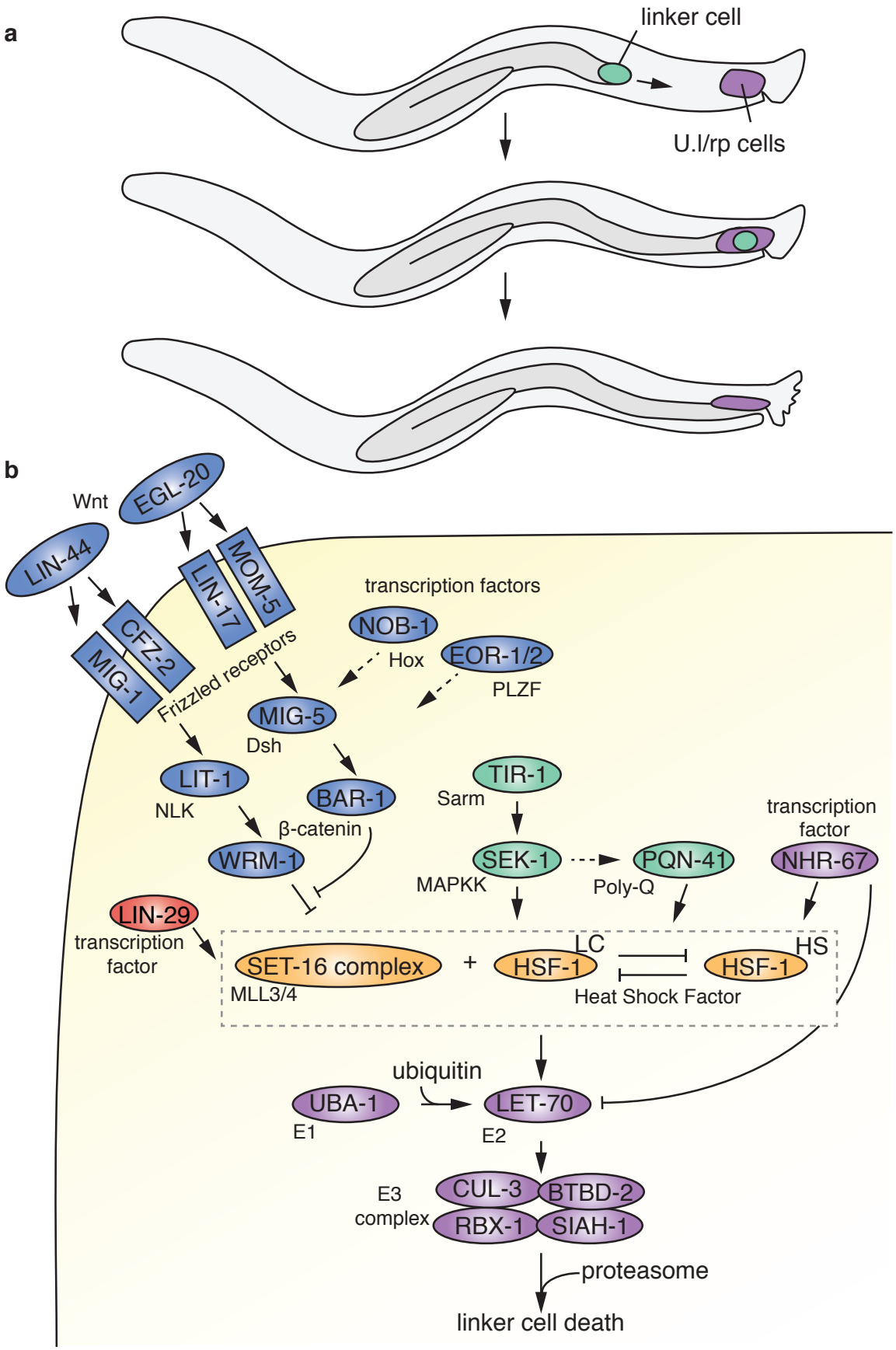
a
linker cell
U.l/rp cells
b
Wnt
EGL-20
LIN-44
LIN-17
MOM-5
CFZ-2
MIG-1
Frizzled receptors
transcription factors
NOB-1
Hox
EOR-1/2
PLZF
MIG-5
Dsh
LIT-1
NLK
BAR-1
β-catenin
WRM-1
TIR-1
Sarm
SEK-1
MAPKK
PQN-41
Poly-Q
transcription factor
NHR-67
LIN-29
transcription factor
SET-16 complex
MLL3/4
+
HSF-1
LC
HSF-1
HS
Heat Shock Factor
ubiquitin
UBA-1
E1
LET-70
E2
E3 complex
CUL-3
BTBD-2
RBX-1
SIAH-1
proteasome
linker cell death

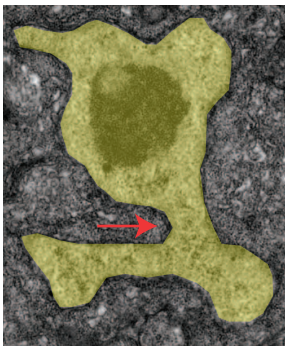

Figure 1-7. **Dying linker cells have uncondensed chromatin and crenellated nuclei.**
In linker cell death, the nuclear envelope is crenellated, with indentations apparent even using Nomarski optics. Reprinted from [87].

One pathway, consisting of the Wnt ligand LIN-44, secreted by some tail cells, the Frizzled receptors MIG-1 and CFZ-2, the Nemo-like kinase LIT-1, and the β-catenin WRM-1, all acting in the linker cell, appears to block linker cell death, and may prevent premature death [85]. The LIN-44/Wnt pathway is inhibited by a second Wnt pathway, consisting of EGL-20/Wnt, secreted by the engulfing cells, and LIN-17/Frizzled and MOM-5/Frizzled, acting within the linker cell with MIG-5/Disheveled and BAR-1/β-catenin, which promotes death [85]. Two transcription factors, NOB-1/Hox and the EOR-1/-2/PLZF complex, likely control the EGL-20/Wnt pathway [86].

In parallel, TIR-1, the *C. elegans* ortholog of the human Sarm protein, activates the MAPKK protein SEK-1 to promote linker cell death [87]. SEK-1 may promote expression of the polyglutamine-repeat protein PQN-41. PQN-41 expression is induced in the linker cell at the onset of death, and a GFP-tagged version forms puncta within the linker cell [87]. How exactly PQN-41 promotes cell death is currently unknown.

The zinc finger protein LIN-29, a component of a developmental timing program [88], also promotes death, as does the nuclear hormone receptor NHR-67 [86]. These genes appear to act independently of and in parallel to the Wnt and MAPKK pathways [86], and ensure that the linker cell is dying in the correct place at the right time.

Linker cell death can be restored to mutants carrying lesions in the upstream control pathways by a gain-of-function mutation in HSF-1, a highly conserved transcriptional regulator of the heat-shock and other stress responses. HSF-1 loss-

of-function blocks linker cell death. Thus, HSF-1 likely functions downstream of or in parallel to the regulators described above [85]. A pro-death role for HSF-1 is surprising, as HSF-1 is typically responsible for promoting survival in response to stress. In animals exposed to a heat shock 4h before death onset, the linker cell survives inappropriately, suggesting that the pro-death and pro-survival functions of HSF-1 may compete [85]. We hypothesize that HSF-1 is post-translationally modified, and these modifications promote either the cell survival or cell death role, depending on context. Which genes are responsible for these modifications in LCD is currently unknown, however.

Genetically, HSF-1 functions at the same step as the SET-16 H3K4 histone methyltransferase complex, similar to the mammalian MLL3/4 complex. *C. elegans* complex components include SET-16, SWD-2.2, UTX-1, ASH-2, RBBP-5, WDR-5, and PIS-1, and mutations or RNAi against any of these components promotes inappropriate survival [86].

Genetic, expression, and functional studies suggest that HSF-1 may work by transcriptionally activating components of the ubiquitin proteasome system [85]. The single *C. elegans* E1 enzyme, UBA-1, is required for cell death through activity of the E2 ubiquitin-conjugating enzyme LET-70, homologous to mammalian UBE2D2. LET-70/UBE2D2 appears to act through an E3 ubiquitin ligase complex comprising the cullin CUL-3, the ring box protein RBX-1, the BTB domain containing protein BTBD-2, and perhaps SIAH-1 [85]. The identities of substrates binding to this E3 complex are unknown, but may provide critical clues to how this caspase-independent cell death is executed. It is possible, for example, that degradation of a critical substrate through this E3 complex is the key to the lethal effects of the pathway. Correspondingly, proteasome 19S regulatory domain components are required for linker cell death [85].

Molecular components related to those promoting linker cell death have been implicated in degeneration and death in other settings. Wallerian degeneration is a process by which the distal process of an injured neuronal axon degenerates,

leaving the cell body intact. Wallerian degeneration slow (Wld^S) mice have persistent axotomized axons [89] caused by an abnormal protein fusion between an NAD^+ synthesis protein, NMNAT, and the ubiquitin factor E4B (Ube4b) [90]. Recent work has revealed that mutations in *dSarm*, the *Drosophila* homolog of *C. elegans tir-1* required for linker cell death, also suppress Wallerian degeneration in the fly [91]. Likewise, murine *Sarm* promotes Wallerian degeneration *in vivo* [91]. Overexpression of the SAM-TIR domains of murine Sarm in cell culture promotes death that appears non-apoptotic, as it proceeds in the presence of caspase inhibitors [92].

In wild-type mice, injury to cortical and dorsal root ganglion (DRG) neurons causes degeneration of the axotomized axon [91]. In *Sarm1*$^{-/-}$ neurons, however, the axons persist over an 18h period. *In vivo*, axotomy at the sciatic nerve in wild-type animals causes the axons to degenerate and a disintegration of the integrity of the neuromuscular junctions (NMJ). In *Sarm1*$^{-/-}$ animals, the axons persist and remain innervated to the NMJs. When the SAM-TIR domains of Sarm1 are overexpressed (Sarm1 lacking first 408 amino acids) in DRG cells in culture, the cells die in a non-apoptotic manner [92]. Pro-apoptotic factors, caspase inhibitors, calpain inhibitors, or extracellular calcium chelation do not inhibit this SAM-TIR-induced cell death [92]. In primary DRG, mitochondrial depolarization by the protonophore molecule CCCP results in axon degeneration and cell death [93]. This induced cell death is non-apoptotic, but requires Sarm1 to degenerate and kill the cells, even in the presence of mitochrondrial depolarization. The authors designate this cell death as sarmoptosis [93]. It remains unclear, however, if this cell death occurs in normal mammalian development, and how different it is from LCD.

In the linker cell, TIR-1/Sarm1 regulates expression of the polyQ repeat protein, PQN-41 [87]. While PQN-41 function is not well understood, its sequence raises the hypothesis that polyQ-expansion neurodegenerative diseases, such as Huntington's disease, may be instances of a developmental program gone awry [94]. Supporting

this, in a mouse Huntington's disease model, dying cells exhibit swollen mitochondria and golgi, and crenellated nuclei, strikingly reminiscent of linker cell death [95] (Figure 1-8a,b). TUNEL staining is not detected in dying neurons [96]. Crenellated nuclei are also found in dying cells of other polyQ disease models and in human patients [97-102] (Figure 1-8c-e).

Intersegmental muscles (ISMs) of the moth, *Manduca sexta* may also prove fertile ground for exploring similarities with linker cell death. Wild-type ISM cells that die during metamorphosis exhibit non-apoptotic features: chromatin condensation is not seen, nor are DNA fragmentation, or membrane blebbing [103]. However, ubiquitin expression is induced, similar to linker cell death [104]. Furthermore, an E1 ubiquitin-activating enzyme, several E2 ubiquitin-conjugating enzymes, and E3 ubiquitin ligases are induced [105]. Molecular characterization of these proteins and their targets may expose similarities to linker cell death.

1.5. Non-apoptotic cell death in mammalian development

Although non-apoptotic cell death pathways have been described in vertebrate cells, including necroptosis, ferroptosis, or pyroptosis, none appear to be required for normal development, as elimination of key genes regulating these processes does not affect development or developmental cell death [106,107]. Nonetheless, evidence that non-apoptotic cell death has important roles in vertebrate development abounds, including but not limited to, the formation of the mammalian palate [108] (Figure 1-8f), cornification of epidermal keratinocytes [109], and lysosome-mediated mammary gland involution after lactation [53]. In the following subsections, I highlight four additional salient examples that raise the possibility that non-apoptotic cell death programs may indeed be the norm during vertebrate development. Whether such programs back up, act in parallel, or function independently of apoptosis is not easy to distinguish, as a key test for their non-apoptotic nature is whether they proceed without apoptotic genes-

Figure 1-8. **Crenellated nuclei (pseudocolored yellow, red arrows) are prevalent in disease models and in normal development.**
(a) In a mouse model of Huntington's disease, crenellated nuclei are prominent in almost all the cells of the striatum [95]. Black arrow, neuronal nuclear inclusion. (b) They are also prevalent in dark neurons of a mouse model of Huntington's disease [96]. (c) In brain autopsy samples of a Huntington's disease patient, crenellated nuclei with uncondensed chromatin are present [102]. (d) In a cell line overexpressing a pathogenic Ataxin-3, crenellated nuclei were apparent prior to non-apoptotic cell death [99]. (e) In the CAG repeat disease dentatorubral-pallidoluysian atrophy, autopsy samples from patients have nuclear membrane indentations in some granule cells in the cerebellar cortex [100]. Star, intranuclear inclusion. (f) Dying cells from the developing palatal shelf display crenellated nuclei [108]. (g) While *Caspase-9* null ESCs rarely die after UV treatment, those that do display LCD features, including open chromatin, swollen organelles, and crenellated nuclear envelope [32]. Ch, chromatin. (h) Degenerating motoneurons in *Bak* knockout mice have crenellated nuclei, and are small and atrophied [112]. N, nucleus. m, mitochondria. rer, rough endoplasmic reticulum. Black arrow, synapse. Dotted line, soma. (i) Degenerating motoneurons in a wild-type stage 24 chick spinal cord have indented nuclei [115]. (j) Non-apoptotic dying retinal ganglion cells in the same organism have crenellated nuclei after axotomy [117]. (k) Peripherally deprived ciliary ganglion neurons in the embryonic chick display highly indented nuclei [118]. N, nucleus. (l) Avian motoneurons in culture adopt either an apoptotic morphology, or an LCD morphology as shown here, with highly crenellated nuclei, and swollen organelles at later timepoints (not shown) [119]. Scale bar = 1 μm. (m) In the presence of caspase inhibitors, motoneurons in the chick acquire non-apoptotic morphology [120]. n, nucleus. (n) Mouse uterine epithelial cells die shortly after implantation, and these cells display irregularly shaped nuclei [125]. (o) Regressing Müllerian duct cells in wild-type mice have open chromatin, crenellated nuclei, and swollen organelles [130]. MD, Müllerian duct epithelial cell. (p) Explant cultures of degenerating Müllerian duct cells from rats share the same features [133]. Adapted from [235].

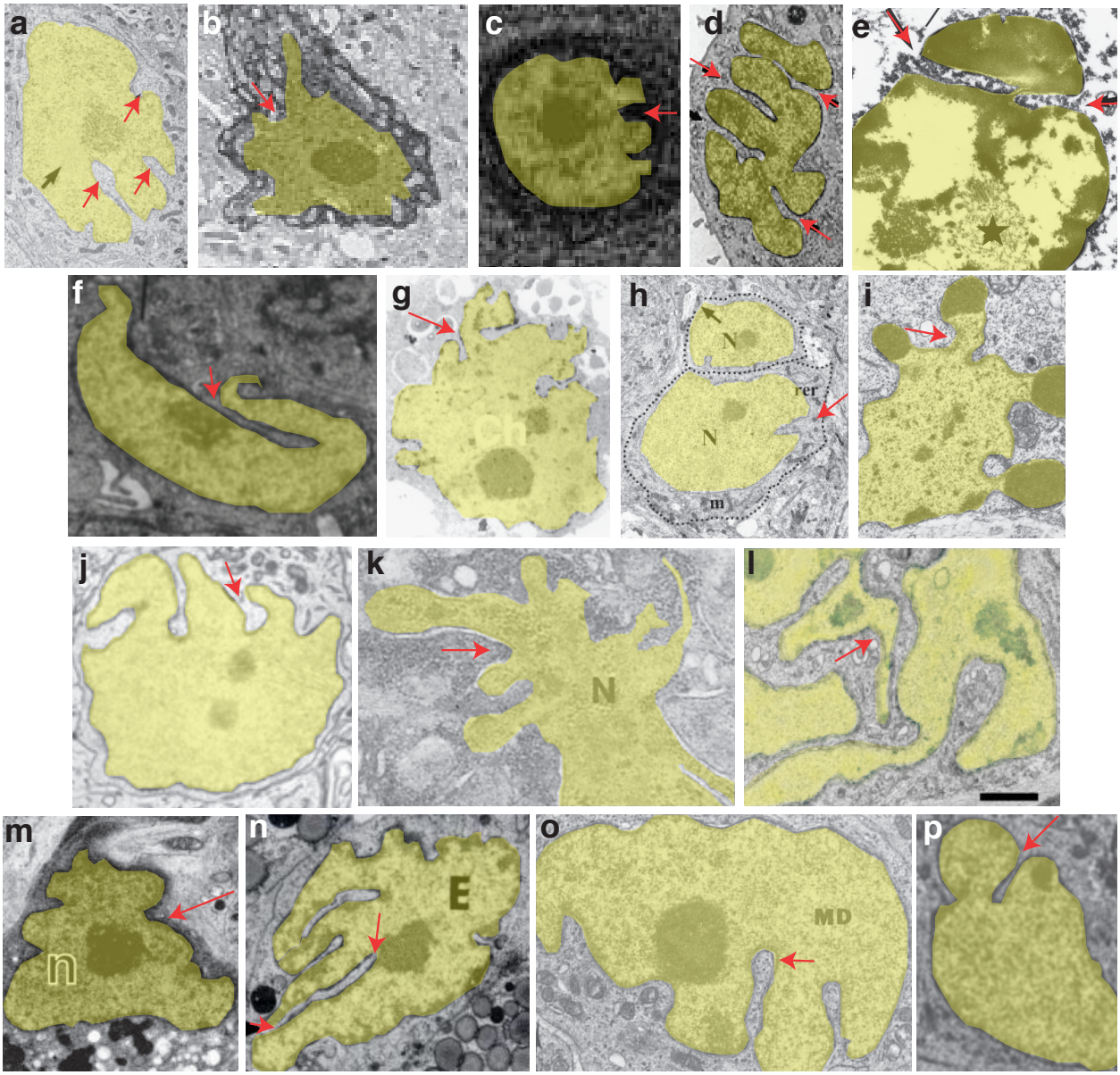
a
b
c
d
e
f
g
h
N
rer
N
m
i
j
k
N
l
m
n
E
o
MD
p

inherently unnatural settings. I have therefore focused on processes that are genetically non-apoptotic, and which also have obvious non-apoptotic features in the developing wild-type animal.

1.5.1. Cell death in the vertebrate nervous system

Initial studies of mice harboring lesions in core apoptotic components, including *Apaf1*, the initiator *Caspase-9*, and the executioner *Caspase-3*, suggested important roles for these genes in nervous system development. *Apaf1*$^{-/-}$, *Caspase-3*$^{-/-}$, and *Caspase-9*$^{-/-}$ animals exhibited exencephaly associated with neural tube defects, and most animals died perinatally or shortly after birth [13,32-35], and presented with mitotically active immature neurons [110]. Later studies revealed that genetic background was a strong contributor to these defects, and that mice carrying the same lesions in other genetic contexts could develop normally to adulthood. For example, *Caspase-3*$^{-/-}$ mice in a C57BL/6J genetic background survive to adulthood, but the same mutation in 129X1/SvJ mice induces perinatal lethality [37]. How then does cell death still occur? A number of studies suggest that alternative cell death pathways are likely to be at least as important as apoptosis in these mutants.

While embryonic stem cells (ESCs) lacking *Caspase-9* exhibit resistance to pro-apoptotic agents [32], some mutant cells die and exhibit non-apoptotic LCD-like morphology, including a crenellated nuclear envelope, uncondensed chromatin, and swollen organelles (Figure 1-8g), suggesting that a process akin to linker cell death may be at play. Supporting this, death of post-mitotic spinal cord and brain stem motoneurons (Figure 1-9a) appears to proceed normally in *Caspase-3*$^{-/-}$ and *Caspase-9*$^{-/-}$ animals even though TUNEL staining decreases [110], suggesting that caspase-activated DNase (CAD), one of the enzymes responsible for cleaving chromosomal DNA during apoptosis [111], is not induced. Thus, cells appear to be dying in the absence of caspase activation. Indeed, dying cells lacking *Caspase-3* or

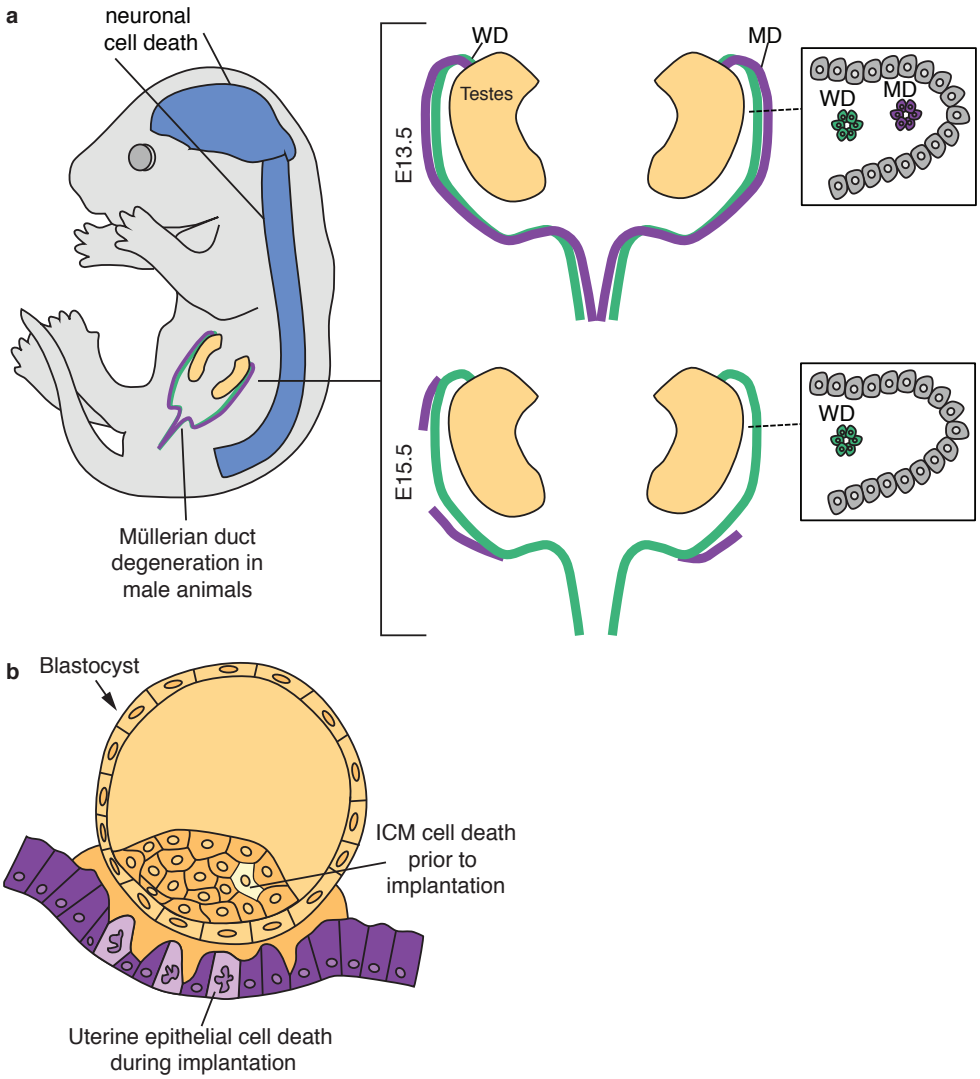

Figure 1-9. **Non-apoptotic cell death occurs in vertebrate development**.
(a) In the developing mouse embryo, neurons within the brain and spinal cord (blue) die. In male mice at E13.5, the Müllerian duct (MD, purple) and the Wolffian duct (WD, green) are both present in the immature reproductive system. Signal from the testes cause the Müllerian duct to degenerate by E15.5. (b) Cell death occurs in the inner cell mass of the blastocyst (yellow) prior to implantation. Uterine epithelial cells die upon implantation of the blastocyst and may be entosed by the trophoblast cells.

Caspase-9 have different morphologies than wild-type cells, with reduced chromatin condensation [110]. Similar studies in *Bax*$^{-/-}$ animals reveal an increase in cell number, but the extra cells are small and atrophied, are not synaptically connected, and exhibit crenellated nuclei [112] (Figure 1-8h). In *Apaf1*$^{-/-}$ mutants, spinal and cranial

motoneurons, and DRG sensory cell death numbers are normal compared to wild type, again suggesting that caspase-independent cell death mechanisms are important in the developing nervous system [113].

As in the mouse, motoneurons are normally produced in excess during chick spinal cord development, and many subsequently die [114]. Ultrastructurally, these dying wild-type cells possess either apoptotic or non-apoptotic morphologies, the latter exhibiting dilated organelles, open chromatin, and an irregular nucleus [115,116] (Figure 1-8i). Axotomized retinal ganglion cells or peripherally deprived ciliary ganglion cells have the same indented nuclear structure [117,118] (Figure 1-8j,k). Interestingly, wild-type chick motoneurons in culture can adopt similar morphologies (Figure 1-8l), and while these dying cells can be engulfed, they lack cleaved Caspase-3 staining or TUNEL staining [119]. *In vivo*, these motoneurons still die in the presence of the Caspase-3 inhibitor Ac-DEVD-CHO or the stronger pan-caspase inhibitor Boc-D-FMK (BAF) [120]. Intriguingly, all of the dying cells treated with caspase inhibitors have a crenellated nucleus, open chromatin, and swollen organelles [120], all features of LCD (Figure 1-8m).

1.5.2. Cell death in the inner cell mass (ICM)

Cell death is an early occurrence in vertebrate development, and is already evident in the inner cell mass (ICM), prior to implantation [121] (Figure 1-9b). These cell deaths in a wild-type mouse blastocyst are characterized by condensed chromatin and loss of nuclear membrane integrity, but also swelling of the endoplasmic reticulum [122]. Single mutants of apoptotic factors do not seem to block blastocyst development, suggesting that cell death likely proceeds normally [121]. Supporting this notion, when hamster or mouse embryos are cultured from the 8-cell stage to the blastocyst stage *in vitro* in the presence of the Caspase-3 inhibitor Ac-DEVD-CHO, no noticeable effects on development are observed [123]. Dying cells in the ICM of wild-type bovine

blastocysts exhibit a mix of apoptotic and non-apoptotic features [124]. Some dying cells have condensed chromatin but weak TUNEL staining, while others have moderate TUNEL staining [124]. Furthermore, only low transcript levels of key apoptotic factors, including *Caspase-3*, *Caspase-9*, *Caspase-8* and *Fas/FasLG*, are detected [124]. Thus, caspases, and perhaps other apoptotic proteins, may not be required for cell death in the ICM.

1.5.3. Death of uterine epithelial cells during implantation

At the site of implantation, uterine epithelial cells die and are internalized by embryonic trophoblast cells [125] (Figure 1-9b). These dying epithelial cells in normal development exhibit compacted chromatin, but also swollen organelles and irregular nuclear envelopes [125,126] (Figure 1-8n). One set of studies reported activated Caspase-3 in TUNEL-positive dying cells in wild-type hamster and mouse uterine epithelial cells at the site of implantation [123]. Additionally, inhibiting Caspase-3 with *N*-acetyl-DEVD-CHO in the uterus stopped implantation in both species, suggesting that Caspase-3 may be necessary for cell death [123]. However, *Caspase-3*$^{-/-}$ or *Apaf1*$^{-/-}$ adult female mice are fully fertile [37,38]. Furthermore, a subsequent detailed examination of the process revealed that neither cleaved Caspase-3 nor TUNEL are detected in dying wild-type epithelial cells immediately adjacent to trophoblast cells [127]. Entosis, engulfment of a living cell followed by degradation, has been a suggested mechanism, as the small GTPase ROCK, which controls entosis in cell culture [128], appears to be required [127]. The ultrastructure of these dying cells was not reported, but could be used to distinguish among different alternative cell death mechanisms.

1.5.4. Cell death in the Müllerian duct

In developing mammals, sex specification occurs early in embryogenesis.

Initially, both sexes form a Wolffian duct (WD), which develops into male urogenital structures, and a Müllerian duct (MD), which gives rise to the female reproductive tract. In females, the WD degenerates, whereas the MD regresses in males [129] (Figure 1-9a). MD regression occurs at day E13.5 [130], and is initiated by the secreted TGF-β protein AMH (anti-Müllerian hormone) [131]. In the absence of AMH, the MD persists, and results in female organs alongside the male urogenital system. This leads to male infertility, as the ectopic female organs physically block sperm release [132].

The morphology of dying wild-type MD epithelial cells in rats, mice, and rabbits, is entirely non-apoptotic: chromatin in degenerating cells does not condense, and the nuclear envelope is crenellated [130,133,134] (Figure 1-8o). These features are highly reminiscent of linker cell death in *C. elegans*, suggesting that MD degeneration proceeds in a similar fashion. Degeneration of female rabbit WD cells is also accompanied by crenellated nuclei [134]. MD and WD degeneration can be faithfully reproduced in an organ culture system, and dying cells here exhibit open chromatin and nuclear crenellation [135] (Figure 1-8p).

Regressing wild-type MD cells are TUNEL-positive [136], and cleaved Caspase-3 is detected in some dying cells [132]. However, neither *Caspase-3* nor other apoptosis mutants are reported to harbor defects in urogenital tract development. There are conflicting reports regarding the sterility of *Apaf1*$^{-/-}$ mutants males; however, not all males are infertile [38,39]. *Caspase-3*$^{-/-}$ male mice in the C57BL/6J genetic background are fully fertile [37]. Thus, it is possible that LCD is the main cell death mechanism during MD and WD degeneration, with *Apaf1* and *Caspase-3* either playing minor roles, or specifically promoting cell corpse degradation (e.g. [120]).

While the genes directly driving MD epithelial cell death are unknown, some of the upstream signaling events have been explored. Wnt7a signaling from MD epithelial cells allows surrounding mesenchymal cells to respond to testes-derived AMH [137], likely by regulating expression and/or activation of receptors in the mesenchymal

cells [138-140]. Receptor engagement leads to activation of SMAD1/5/8 proteins, which in turn induce expression of Wnt4, and possibly other Wnts [140]. Possible autocrine signaling then leads to the activation of β-catenin, which may dimerize with LEF1/TCF to promote regression in the adjacent epithelial cells [136]. β-catenin accumulates in the mesenchymal cytoplasm, and is present near the plasma membrane of MD epithelial cells [136]. Mesenchyme-specific knockdown of β-catenin prevents MD degeneration [132]. While both MD regression and linker cell death in *C. elegans* use β-catenin signaling to initiate cell death, β-catenin appears to function cell non-autonomously in the MD.

The matrix metalloproteinase MMP2 may be involved in signaling to initiate regression [141]. *Mmp2* is expressed at higher levels in the mesenchyme of males, and this increased expression is abolished in the absence of AMH [141]. In organ culture, blocking MMP2 activity prevents MD degeneration, while activating MMP2 causes degeneration, even in the absence of AMH [141]. However, MMP2 mutant mice are fertile, suggesting other genes may be involved [142]. Roles for MMPs in linker cell death have not been described, but the adjacent gonad is known to secrete these proteins [143].

Together, the examples described make a compelling case for the prevalence of caspase-independent non-apoptotic cell death during vertebrate development, with LCD playing, perhaps, an important role.

1.6. Phagocytosis and degradation of dying cells

After cell death, the dying corpse must be recognized and engulfed by neighboring cells or professional phagocytes. Clearance of cells undergoing programmed cell death is important during development of multicellular organisms, and failure to remove dying cells is implicated in developmental abnormalities [144] and autoimmune disease [145]. Studies of the nematode *C. elegans* uncovered

genes required for engulfment and degradation of cells dying by apoptosis [146-151]. Homologous genes regulate apoptotic cell clearance in *Drosophila* and vertebrates, as do a number of species-specific genes [152-154].

1.6.1. Recognition and engulfment of apoptotic corpses

In *C. elegans*, neighboring cells, rather than specialized phagocytes, engulf dying cells [155,156]. Two distinct, parallel pathways are responsible for apoptotic corpse recognition [146,157]. In pathway A, *ced-1*/Megf-10, *ced-6*/Gulp, and *ced-7*/Abca1 function at the cell membrane to recognize the cell corpse, likely through phosphatidyl serine (PS) exposure [158-160] (Figure 1-10a). PS is also actively exposed on cells dying by necrosis in *C. elegans*, and requires the same engulfment machinery as apoptotic cells, as well as necrotic specific genes [161].

In pathway B, *ced-2*/CrkII, *ced-5*/Dock180, and *ced-12*/Elmo function within the cytoplasm of the phagocyte to promote activation of *ced-10*/Rac [162-165]

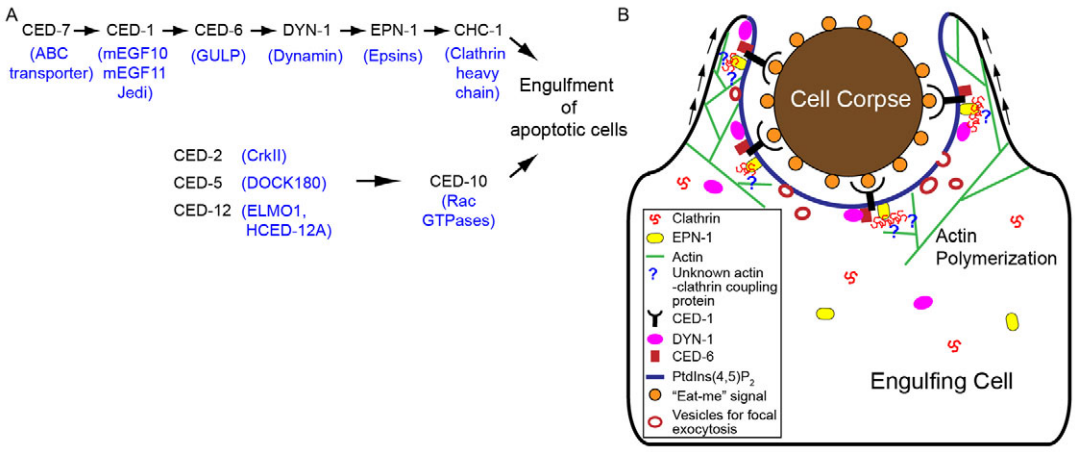

Figure 1-10. **Phagocytosis of *C. elegans* apoptotic corpses.**
(a) In *C. elegans*, two parallel pathways mediate the engulfment of apoptotic corpses. *C. elegans* proteins in black, and mammalian homologs in blue. (b) Actin (green) is polymerized in the engulfing cell to extend pseudopods around the corpse, mediated by clathrin and unknown coupling proteins. “Eat-me” signals, such as phosphatidyl serine are exposed on the dying cell. Adapted from [168].

(Figure 1-10a). Genes from these two pathways have also been implicated in axon pruning and the diurnal renewal of photoreceptor cells, among other processes [166,167].

In WT embryos, engulfment, which begins with the budding of pseudopods and ends when the phagocytic cup closes completely, takes on average 7 min [168]. Pseudopod extension around embryonic apoptotic corpses relies in part on the *C. elegans* clathrin gene (*chc-1*) and epsin (*epn-1*), which is able to induce membrane curvature [168] (Figure 1-10a,b). Both genes act downstream of the *ced-1* pathway, along with the dynamin *dyn-1* [149,168].

Many of the genes identified in *C. elegans* have functional homologs in both *Drosophila* and vertebrates [169-171]. In these other organisms, professional phagocytes exist alongside 'amateur' phagocytes. For example, in *Drosophila*, macrophage-like plasmatocytes migrate freely within the embryo to engulf foreign particles and dying cells [172]. The CD36-like receptor *Croquemort* is required in Drosophila for the engulfment of apoptotic corpses but not bacteria, suggesting that different receptors are required for different particles [152].

1.6.2. Degradation of apoptotic corpses

Once a dying corpse is internalized by a neighboring cell or professional phagocyte, its compartment is progressively acidified and recycled (Figure 1-11). Degradation of a refractile apoptotic embryonic corpse in *C. elegans* takes approximately 40-50 min in wild-type animals [149,173,174].

After internalization, a series of membrane composition changes and changes in associated proteins results in the progressive acidification of the phagosome and eventual degradation of the corpse in *C. elegans* embryos. Initially, phosphatidylinositol 3-phosphate (PI3P) is produced on nascent phagosomes by the PI3-kinases *piki-1* and *vps-34* in *C. elegans* [175]. PI3P is loaded onto the phagosome in a wavelike fashion,

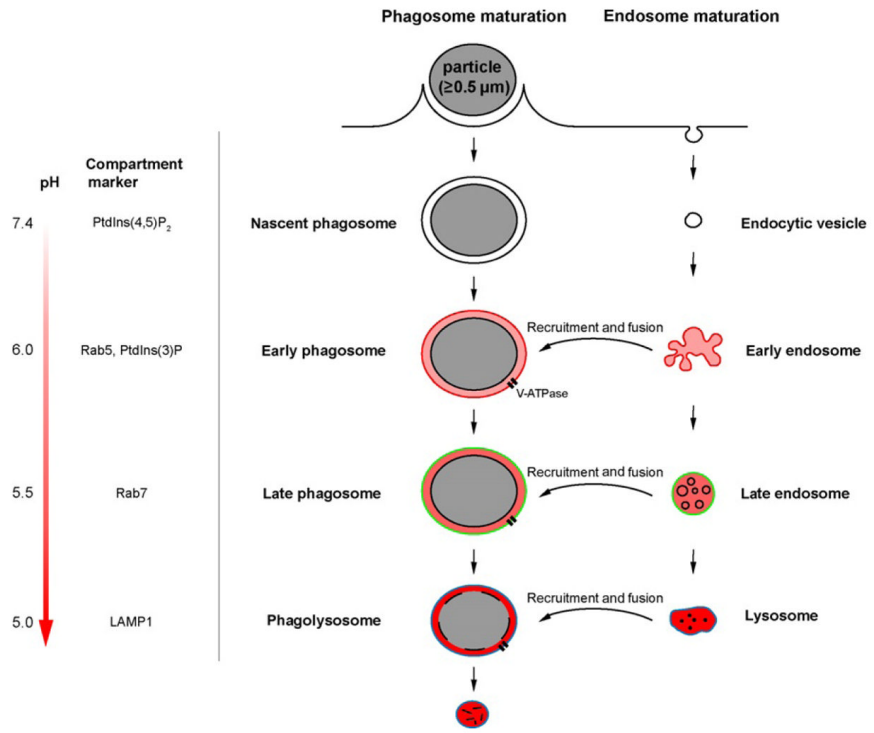

Figure 1-11. **Degradation of internalized apoptotic corpse.**
After an apoptotic corpse is phagocytosed, phosphatidylinositol 4,5-bisphophate (PtdIns(4,5)P_2) is removed from the nascent phagosome and replaced with phosphatidylinositol 3-phosphate (PtdIns(3)P). Next, RAB-5-positive early endosomes are recruited and fused to the early phagosome. RAB-7-positive late endosomes are recruited and fused to the late phagosome, and eventually lysosomes are recruited and fused to form the phagolysosome. These membrane compartment fusions acidify the phagolysosome, eventually degrading the apoptotic corpse. Adapted from [253].

which requires the PI3-phosphatase MTM-1 [175]. This allows the recruitment of FYVE-domain containing proteins such as the sorting nexins SNX-1, SNX-6 and LST-4/SNX-9 [176]. Mutations in these genes lead to an excess of engulfed but undegraded apoptotic corpses.

Next, early endosomes marked by the small GTPase RAB-5 are recruited and fuse to the nascent phagosome [147]. These RAB-5-positive endosomes are recruited immediately after phagosome sealing in *C. elegans*, likely by DYN-1 [147,174]. RAB-5 to RAB-7 conversion by SAND-1 and CCZ-1 allows the fusion of late endosomes and

eventually lysosomes to the corpse-containing phagosome [148,177]. RAB-7 may function downstream at the lysosome-phagosome fusion step, and remains on the phagosomal membrane until the corpse is completely degraded [149,150].

RAB-2 promotes the fusion of lysosomes to the phagosome, and also plays a separate role in acidification of the phagosome lumen [149,151]. RAB-14 plays similar roles to RAB-2, and the two proteins likely function in partially redundant pathways for recruiting and tethering lysosomes to phagosomes [150,151]. Proteomic approaches in cell culture have revealed more than a dozen Rabs associated with the phagosome, suggesting that other, yet-to-be identified, RAB proteins are also involved [178,179].

In mammalian systems, most of the studies of phagosome maturation in macrophages have focused on the internalization of opsonized latex beads or bacteria, and many of the genes and pathways discussed above are conserved in these processes [179]. The core molecules are the same, with roles for PI3-kinase, Rab5 and Rab7 well-established [180]. There is reason to suspect that the process and dynamics of apoptotic corpse engulfment differs from engulfment of foreign objects, however, especially since engulfment and degradation of cells dying by apoptosis does not elicit an immune response [181].

1.6.3. Engulfment and degradation of non-apoptotic corpses

While the molecular and genetic characterization of some non-apoptotic cell death processes has advanced considerably, whether common clearance mechanisms are used for apoptotic and non-apoptotic dying cells remains a major open question. It has been shown that apoptotic engulfment genes in *C. elegans* are not responsible for engulfment of the linker cell corpse [82], but whether these and other genes function in linker cell corpse degradation is unknown. The genes responsible for both the death and degradation of the linker cell are the basis of my thesis.

I was interested in how the polyglutamine protein PQN-41C induces cell death,

so I investigated the function PQN-41C by determining the role of its interacting partners, which is discussed in Chapter 2. To identify genes necessary for death and degradation, I carried out a forward genetic screen and identified the protein networks for two small GTPases, and their role in phagosome maturation; these results comprise the bulk of my thesis and are discussed in Chapter 3. Lastly, I found that the caspase CED-3 has an unknown and surprising role in linker cell corpse degradation, but not death, which is discussed in Chapter 4. In Chapter 5, I synthesize these results and place them into a broader context of non-apoptotic cell death and degradation, and I speculate on how these processes may be conserved in mammalian systems.

2. PQN-41C interacts with an inhibitor of linker cell death, HPK-1

2.1. Summary

PQN-41C is a polyglutamine protein required for efficient linker cell death. PQN-41C is comprised almost entirely of coiled coil domains [87], which can act as protein binding platforms [182]. To determine additional binding partners of PQN-41C, I carried out a protein interaction screen using a yeast two-hybrid system against a *C. elegans* cDNA library. I recovered 33 possible interacting partners, and I performed RNAi against each of these genes to identify putative roles in linker cell death. I focused on *hpk-1*, a gene encoding a homeodomain protein kinase, which appears to function as an inhibitor of linker cell death. I performed epistasis experiments with known linker cell death genes and found that loss of *hpk-1* suppressed the linker cell survival defects of known regulators. However, *hpk-1* did not suppress defects in *hsf-1*(lf), suggesting that HPK-1 acts upstream or in parallel to HSF-1. Subsequent analysis revealed that HSF-1-GFP fails to form stress granules upon heat shock in the absence of *hpk-1*. Additionally, the heat-shock-related linker cell survival defect is suppressed in the absence of *hpk-1.* Together, these results suggest that HPK-1 promotes the heat shock function of HSF-1, and inhibition of HPK-1 is required for efficient cell death, which may be regulated through PQN-41C.

2.2. PQN-41C interacts with proteins of different functions

Previous work in the lab suggested that the long isoforms of PQN-41, A and B, promote cell survival, while the shorter isoform PQN-41C promotes cell demise [87]. All of these isoforms share a polyglutamine repeat region, while the A and B isoforms have long N-terminal tails with coiled-coil domains [87]. Both coiled-coil domains and polyglutamine repeats are thought to act as protein binding platforms [183], raising the possibility that the distinct interactomes of each of these PQN-41 isoforms may confer

their opposing functions. To try and determine these interactomes, I attempted a yeast two-hybrid screen using each of these isoforms as bait, but I failed to see expression of LexA-PQN-41A or LexA-PQN-41B (Figure 2-1a). I did see expression of LexA-PQN-41C, which did not autoactivate under His-Leu-Trp-Ade- conditions (Figure 2-1b), so I decided to continue screening using PQN-41C only.

Using a *C. elegans* cDNA library from L4 hermaphrodites, I transformed $9.3x10^6$ colonies, and I recovered 71 candidate clones over a 9-day screening period (Table 2-1). These clones represent 38 genes, with gene ontology classifications of proteolysis, PQN-domain, ubiquitin-related, DNA-related, and RNA-related, among others (Table 2-1).

I identified PQN-41C as interacting with another isoform of PQN-41 in the yeast

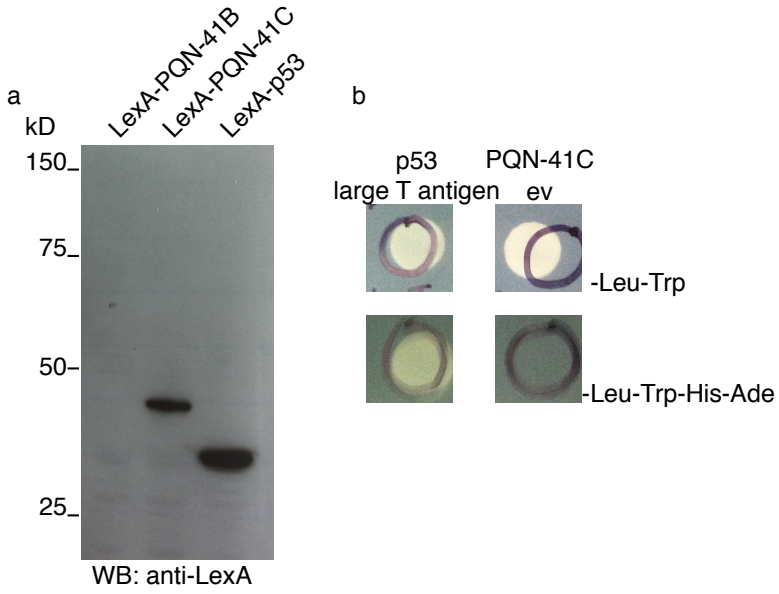

Figure 2-1. **Controls for PQN-41C yeast two hybrid screen**.
(a) Total protein from yeast cells expressing LexA-PQN-41B, LexA-PQN-41C, or LexA-p53 (positive control) was extracted and probed with an anti-LexA antibody to determine protein expression levels. (b) Yeast expressing p53 and large T antigen (positive control) or PQN-41C and empty vector (ev) were tested for interaction or self-activation, respectively, on minimal media plates.

Table 2-1. **List of PQN-41C interacting proteins and their surviving linker cell phenotype upon knockdown.**

Gene	No. of Y2H hits	Function	RNAi phenotype (N)	Notes
empty vector			3% (137)	
asp-3	1	Proteolysis	6% (95)	1
F32A5.3	1	Proteolysis	4% (91)	
K10C2.1	2	Proteolysis	6% (100)	1
F57F5.1	1	Proteolysis	n.d. (arrest)	
nep-17c	1	Proteolysis	8% (130)	1
pqn-41	2	Coil-coiled domain	18% (96)***	1
npp-4	2	Coil-coiled domain	11% (127)*	1
R11A8.7	1	Coil-coiled domain	6% (103)	Y2H clone corresponds to b/c/e isoforms; 1
pqn-59	9	Coil-coiled domain/ proteolysis	10% (81)	
H34I24.3	1	Coil-coiled domain	6% (88)	
pqn-85	1	Coil-coiled domain/ DNA-related	18% (82)**	2
tag-214	1	Ubiquitin-related	n.d. (slow growth)	
F52G3.1	1	Ubiquitin-related	6% (82)	
sao-1	1	Ubiquitin-related	11% (158)*	
etr-1	2	RNA-related	9% (87)	Y2H clone corresponds to e/f/g isoforms; 1
asd-1	1	RNA-related	3% (97)	
asd-2	2	RNA-related	2% (118)	1
pes-4	1	RNA-related	10% (94)*	
chd-7	2	DNA-related	14% (119)*	1
zfp-1	1	DNA-related	16% (101)**	
tag-153	7	DNA-related	10% (167)*	2
eef-2a	1	DNA-related	n.d. (arrest)	
T19D12.2	1	DNA-related	5% (76)	a/c isoforms; 1
aco-2	1		33% (79)***	a/c isoforms
aldo-2a	1		15% (95)*	
meg-1/2	3		7% (150)	1
M02E1.1a	2	Unknown function	3% (104)	1
hpk-1	4	kinase	0.7% (136)	
C18E3.9	1	Unknown function	4% (74)	
clec-49/50	1	lectin	3% (144)	1
F57F4.4	1		7% (160)	1
gdi-1a	1		8% (150)	1
yars-1	1	tRNA synthetase	4% (134)	
vit-4	1	Yolk protein	Didn't assay	
vit-3	1	Yolk protein	Didn't assay	
vit-6	1	Yolk protein	Didn't assay	

1. cloned targeting region into L4440 from Y2H (Ahringer clone incorrect or non-existent). 2. cloned from cDNA library (Ahringer clone incorrect or non-existent). **: P<0.0001, **: p<0.001, *: p<0.05, Fishers exact test. RNAi clones obtained from [243] unless otherwise noted. Strain contains *rrf-3* mutation for increased RNAi-senstivity, *him-5* for males, and a GFP linker cell marker.

two-hybrid screen (Table 2-1), so I tested the other two isoforms for interaction. I found that PQN-41A-LexA interacts with PQN-41B and PQN-41C, and that PQN-41C indeed interacts with itself (Figure 2-2). This preliminary result suggests that perhaps PQN-41C forms dimers or oligomers to drive its cell death function.

2.2.1. Knockdown of some potential interacting partners causes a linker cell survival defect

I knocked down each of the candidate interacting partners in an RNAi-sensitized background (Table 2-1). Seven genes gave a significant number of surviving linker cells upon knockdown, and one gene appeared to accelerate linker cell death or degradation.

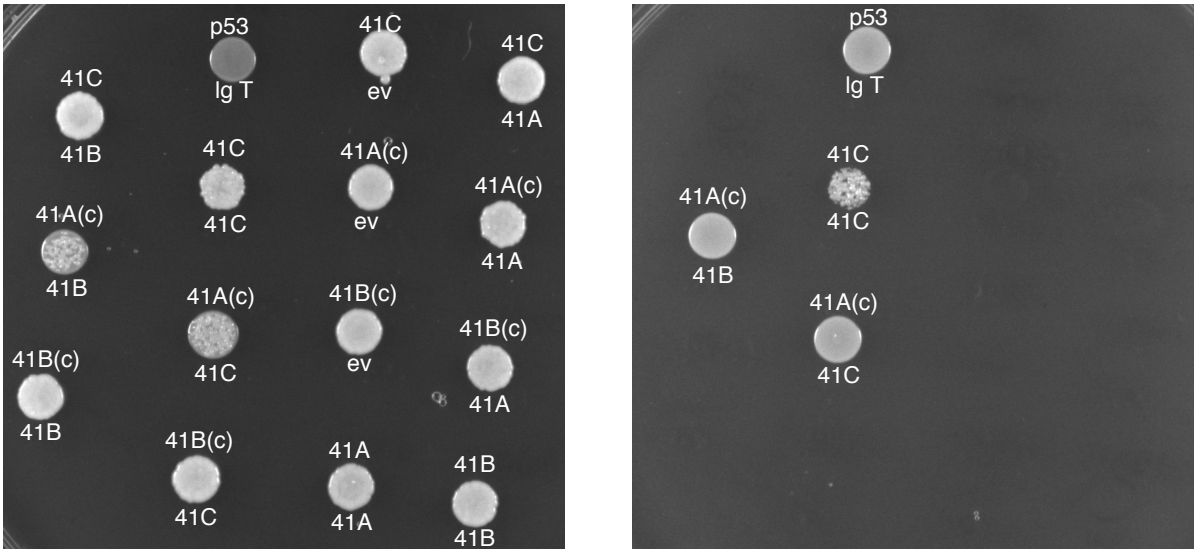

Figure 2-2. **PQN-41C interacts with itself.**
Interactions between the PQN-41 isoforms were tested using a yeast two-hybrid assay. LexA-tagged components listed above the interaction spot, and GAD-tagged components listed below the interaction spot. LexA was located N-terminally unless otherwise noted (labeled as (c)). Left panel shows effect of transformed proteins on yeast growth, and right panel shows growth on minimal media, indicating physical interaction. p53 + large T antigen included as a positive control.

These candidates were investigated further and are discussed below.

2.2.1.1. aco-2

Knockdown of the mitochondrial aconitase *aco-2* increased the number of surviving linker cells (SLCs) to 33% (Table 2-1). In these animals, the linker cell often detached from the gonad, so that the gonad itself never completely migrated to the tail of the animal (Figure 2-3). The linker cell failed to migrate completely in 18% of the animals (N=8/45). The spermatids were also defective, with 98% of spermatids appearing to have excessive vacuolization (N=44/45, Figure 2-3). Knockdown of *aco-2* in a *pqn-41*(*ns294*) background was additive, suggesting these genes function in the same pathway (Table 2-2). *aco-2* appears to function cell-autonomously, as knockdown

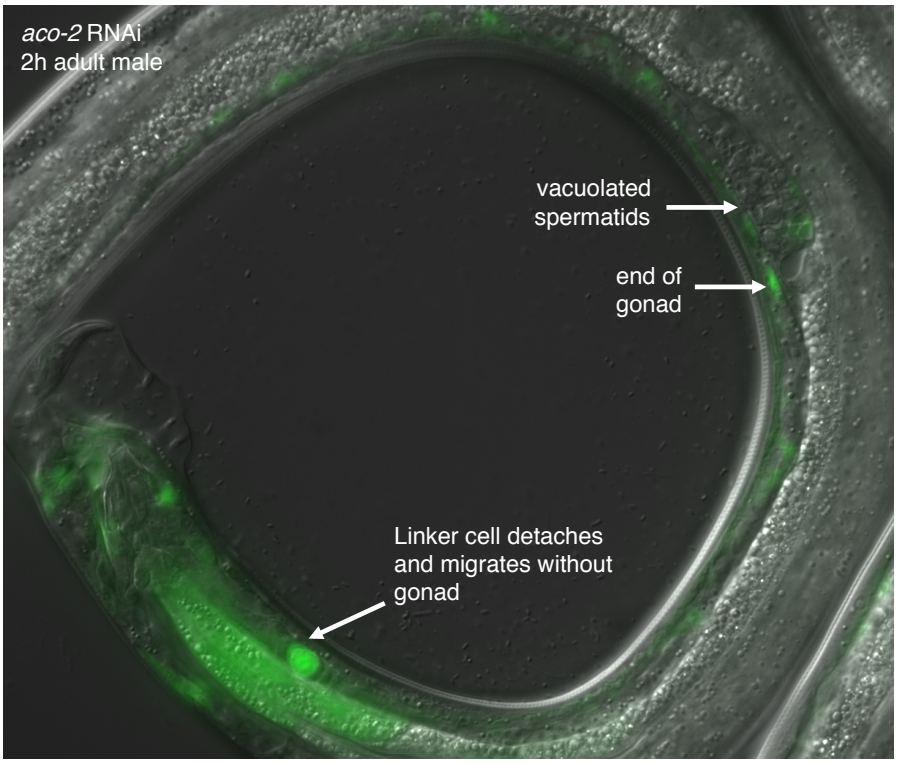

Figure 2-3. **Knockdown of *aco-2* leads to incompletely migrated gonads and vacuolated spermatids**.
L1 synchronized RNAi-sensitized animals were fed bacteria expressing double-stranded *aco-2* RNA. Males were scored 2h after the L4 to adult transition. Image is a representative example. Strain contained *rrf-3*(*pk1426*) II; *him-8*(*e1489*) IV; *qIs56* V.

Table 2-2. ***zfp-1* acts synergistically with *pqn-41*.**

Gene	%Surviving linker cells (N)	Predicted if additive
empty vector	25% (107)	
aco-2	50% (102)	50%
pqn-85	39% (83)	39%
zfp-1	44% (62)*	37%
aldo-2	22% (49)	36%
chd-7	29% (56)	36%
tag-153	12% (42)	33%

* = results indicate synergy. Strains contain *pqn-41*(*ns294*), *him-5*(*e1490*) for males and *qIs56* linker cell marker. Animals were scored 0-2h after the L4 to adult transition.

specifically in the linker cell resulted in a significant increase of SLCs (Table 2-3). The migration defect appears to be cell non-autonomous, however (Table 2-3). I obtained a temperature sensitive allele *or1565ts* from Bruce Bowerman's lab, but these animals failed to grow after hatching at 25°C. A more sensitive time course should be developed, perhaps shifting to 25°C prior to the commitment to cell death at the L3 or early L4 larval stage.

2.2.1.2. zfp-1

Knockdown of the zinc finger protein *zfp-1* resulted in 16% SLCs (Table 2-1). I obtained a deletion allele of *zfp-1*, *ok554*, which skips exons 6 and 7; these exons do not include the zinc finger domain or the PQN-41 interacting region, so *ok554* may be a hypomorphic allele, as confirmed by a weaker SLC defect in these animals (Table 2-4). *zfp-1* appears to function cell autonomously in linker cell death, as knockdown specifically in the linker cell caused a significant increase in the number of SLCs, although there was also an increased number of migration defective cells (Table 2-3).

To determine its genetic interaction with *pqn-41*, I knocked down *zfp-1* in RNAi-sensitized *pqn-41*(*ns294*) animals. Interestingly, the two genes appear to function synergistically, together having a defect of 44% surviving linker cells (Table 2-2).

Table 2-3. ***aco-2*, *zfp-1*, *eef-2*, and *tag-214* function cell autonomously.**

Gene	WT background %SLC (N)	LC-specific RNAi %SLC (N)	%LCs with migration defect
e.v.	3% (157)	11% (47)	0
aco-2	21% (43)*	20% (91)*	1%
pqn-85	13% (53)*	9% (114)	2%
zfp-1	13% (46)*	23% (47)*	9%
aldo-2	8% (51)	n.d.	n.d.
chd-7	4% (46)	11% (55)	2%
tag-153	n.d.	3% (40)	0
hpk-1	n.d.	5% (70)	0
eef-2	let	20% (54)*	n.d.
F57F5.1	let	7% (119)	n.d.
tag-214	slow growth	18% (56)*	n.d.

n.d. = not determined, let = lethal, e.v. = empty vector; * p<0.5, Fishers exact test, Strains contain *rde-1*(*ne219*) for abrogation of systemic RNAi, *nsIs387* for RNAi in the linker cell only, *him-8*(*e1489*) for males, and *qIs56* as a linker cell marker. Animals were scored 0-2h after the L4 to adult transition. Knockdown of genes in a wild-type background (not RNAi-sensitized, no *rde-1* mutation) included as reference.

Animals doubly mutated for *zfp-1*(*ok554*) and *pqn-41*(*ns294*) together developed slowly, and had incomplete male tail development. This developmental defect precluded me from scoring the SLC phenotype effectively in this background. However, this result suggests these genes function together in similar processes during development, as well as in LCD.

2.2.1.3. pqn-85

Knockdown of the NIPBL ortholog *pqn-85* in an RNAi-sensitized background resulted in 18% SLCs (Table 2-1). Decreasing *pqn-85* levels in *pqn-41*(*n294*); *rrf-3* animals caused an additive increase of SLCs (Table 2-2). Knockdown of this gene in a wild-type background, however, only had a 13% SLC defect, and knockdown only in the linker cell had no significant increase in the defect compared to empty vector control (Table 2-3). I obtained two alleles of *pqn-85*, *tm2338* and *tm2334*/+.

Table 2-4. **Genetic mutants of Y2H hits do not recapitulate their RNAi phenotype in most cases**.

Genotype	%SLC (N)	Notes
Wild type	3% (157)	
zfp-1(*ok554*)	11% (47)	Weak allele; skips exon 6 and 7 which do not include ZnF or interacting region
chd-7(*tm6138*)	4% (53)	In frame deletion of exon 3
chd-7(*tm6139*)	2% (49)	In frame deletion
chd-7(*gk290*)	12% (50)	In frame deletion at C term
chd-7(*gk306*)	5% (38)	In frame deletion at C term
tag-153(*ok699*)	4% (26)	Strong LOF (out of frame deletion)
aco-2(*or1565ts*)^	n.d.	Temp. sensitive allele
hpk-1(*pk1393*)	6% (87)	Putative null

^obtained from Bruce Bowerman; n.d. = not determined. Animals were scored 0-2h after the L4 to adult transition. Strains also contain either *him-5*(*e1490*) or *him-8*(*e1489*) for males, and *qIs56* or *nsIs65* linker cell marker.

Unfortunately, *tm2338* did not have the annotated mutation, and *tm2334* animals were inviable as homozygous animals. Therefore, I was unable to adequately follow up on this gene.

2.2.1.4. chd-7

chd-7 encodes a chromodomain helicase, homologous to mammalian *CHD8*. Mutations in *CHD8* are a risk factor for autism [184]. Knockdown of *chd-7* in an RNAi-sensitized background resulted in a 14% surviving linker cell (SLC) defect. I obtained four alleles of *chd-7*, all of which resulted in in-frame deletions of various parts of the protein (Table 2-4). The defects ranged from 2% SLC to 12% SLC, but all alleles were unlikely to be true null alleles, based on predicted protein translation. Unfortunately, knockdown of *chd-7* in a wild-type RNAi background or in the linker cell specifically did not increase the number of SLCs compared to WT (Table 2-3), suggesting that the original RNAi phenotype may have been a false positive.

To determine if an odd genetic interaction was occurring between *chd-7* and

rrf-3, the gene that confers RNAi sensitivity when mutated, I crossed *chd-7*(*gk290*) and *chd-7*(*gk306*) to *rrf-3*(*pk1426*), and found that the double mutants had a significant number of SLC compared to the *chd-7* mutants alone (*chd-7*(*gk290*); *rrf-3*(*pk1426*): 17% (N=46); *chd-7*(*gk306*); *rrf-3*(*pk1426*): 14% (N=58)). This result suggests that there may be an unknown genetic interaction between *chd-7* and *rrf-3* that is somehow influencing linker cell survival. Knocking down *chd-7* in a *pqn-41*(*ns294*); *rrf-3* background did not significantly increase the number of SLCs compared to each gene alone (Table 2-2).

2.2.1.5. tag-153

tag-153 encodes a NOT-domain-containing protein, which is typically found in negative regulators of transcription [185]. It is homologous to *CNOT2* in humans. Knockdown of *tag-153* in an RNAi-sensitized background resulted in a weak phenotype of 10% SLC (Table 2-1). I obtained a strong loss-of-function allele, *ok699*, which encodes a large deletion that results in an out-of-frame coding sequence. This allele did not recapitulate the RNAi phenotype, however, and had a SLC defect similar to wild type (Table 2-4). Intriguingly, linker-cell-specific knockdown of *tag-153* resulted in a decreased number of SLC compared to the empty vector control (Table 2-3); knockdown of *tag-153* in *pqn-41*(*ns294*); *rrf-3* animals also decreased the number of surviving cells by half (Table 2-2).

2.2.1.6. aldo-2

aldo-2 encodes an aldolase, a glycolytic enzyme. Knockdown in an RNAi sensitized background resulted in a 15% SLC defect, but only 8% when knocked down in an otherwise wild type background (Tables 2-1, 2-3). Knockdown of *aldo-2* in *pqn-41*(*ns294*); *rrf-3* animals did not enhance the *pqn-41* phenotype (Table 2-2). *aldo-2* is expressed in many cells in the animal, although I did not see expression within the linker cell specifically.

2.2.1.7. Knockdown of tag-214, F57F5.1, and eef-2 resulted in slow growth or larval lethality

Knockdown of *tag-214*, a gene encoding an E3 ubiquitin ligase similar to *RBBP6*, *F57F5.1*, a gene encoding an ortholog of cathepsin B, or *eef-2*, a gene encoding the translation elongation factor EF-2, resulted in either larval lethality or slow larval development (Table 2-1). Because of this, I was unable to determine the effect on linker cell death using whole animal knockdown experiments. Therefore, I knocked down each of these genes in a linker-cell-specific manner, and I found that both *eef-2* and *tag-214* had a significant number of surviving cells when knocked down in the inker cell (Table 2-3).

2.2.2. Knockdown of some potential interacting partners reduces the number of aberrantly surviving cells

Knockdown of two genes, *asd-2*, which encodes an RNA binding protein similar to mammalian QKI, and *hpk-1*, which encodes a homeodomain protein kinase similar to HIPK1/2 in vertebrates, did not have a SLC defect (Table 2-1). Instead, knockdown of these genes resulted in a decreased number of dead or dying linker cells, suggesting that these genes may be inhibitors of cell death (*asd-2*: 42% remaining corpses, $p=0.0011$ compared to WT; *hpk-1*: 17% remaining corpses, $p<0.0001$ compared to WT, Fishers exact test). Because of the weaker phenotype of *asd-2,* I decided to focus on the role of *hpk-1* in linker cell death first.

2.3. PQN-41C interacts with the homeodomain protein kinase, HPK-1, an inhibitor of linker cell death

I recovered four independent yeast two-hybrid colonies of *hpk-1*, with the interacting region near the Ser/Thr kinase domain (Figure 2-4). A literature search of *hpk-1* homologs revealed a putative interaction with the heat shock factor HSF-1, a

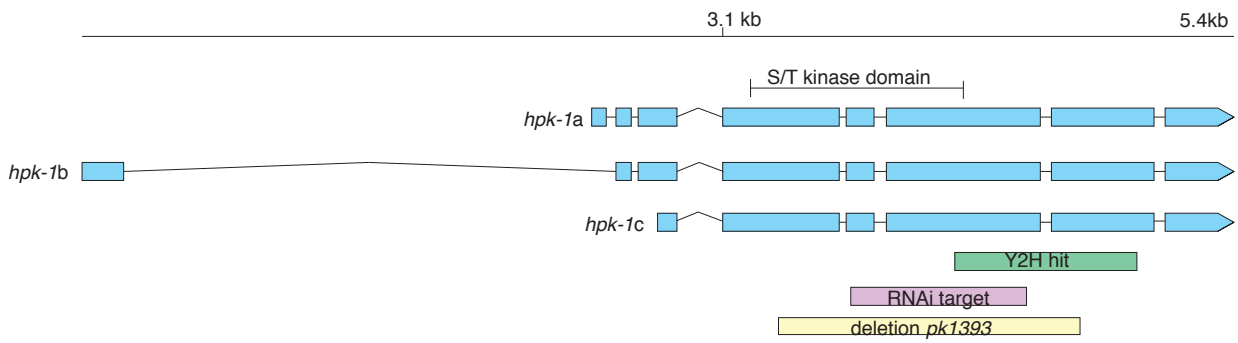

Figure 2-4. **Genetic information for *hpk-1*.**
hpk-1 has three isoforms, all of which contain a Ser/Thr kinase region. Shown is the location of the Y2H interacting fragment (green), the location of the RNAi targeting construct (purple), and the out-of-frame deletion caused by *pk1393* (yellow).

known linker cell death gene (see Discussion). Therefore, I wanted to determine how *hpk-1* is involved in linker cell death, as well as its interactions with known linker cell death genes, including HSF-1.

2.3.1. Knockdown of hpk-1 decreases the number of surviving cells

As mentioned above, knockdown of *hpk-1* in an RNAi-sensitized background decreased the number of SLCs and remaining corpses 2h after the L4 to adult transition compared to WT (Table 2-1). Knockdown specifically in the linker cell also caused a decrease in the number of surviving cells, compared to the empty vector control (Table 2-3). I obtained a putative null of *hpk-1*, *pk1393*, which deletes the majority of the kinase domain (Figure 2-4). This allele had a similar number of SLCs compared to WT (Table 2-4), and was used for further genetic interaction studies.

2.3.2. Knockdown of hpk-1 suppresses the linker cell death defects of regulatory genes required for LCD

I wanted to determine how *hpk-1* interacts with known linker cell death genes, so

I knocked down *hpk-1* in strains where those genes were mutated. Knockdown of *hpk-1* in *pqn-41*(*ns294*); *rrf-3* animals resulted in half the number of SLCs compared to *pqn-41* alone (Figure 2-5). Similar results were seen with the upstream activator of *pqn-41, sek-1*(*ag1*) animals, and in the Wnt *egl-20*(*n585*) (Figure 2-5).

Next, I wanted to verify these results using genetic double mutants. Because *hpk-1* and other cell death genes result in male infertility [82,185], I used artificial insemination to generate these strains (see Methods). *pqn-41*(*ns294*); *hpk-1*(*pk1393*) double mutants only had a slight decrease in SLCs compared to *pqn-41*(*ns294*) alone (Table 2-5). This difference in phenotypes between the genetic mutants and the RNAi phenotype could perhaps be explained by the fact that *ns294* is not a complete null of

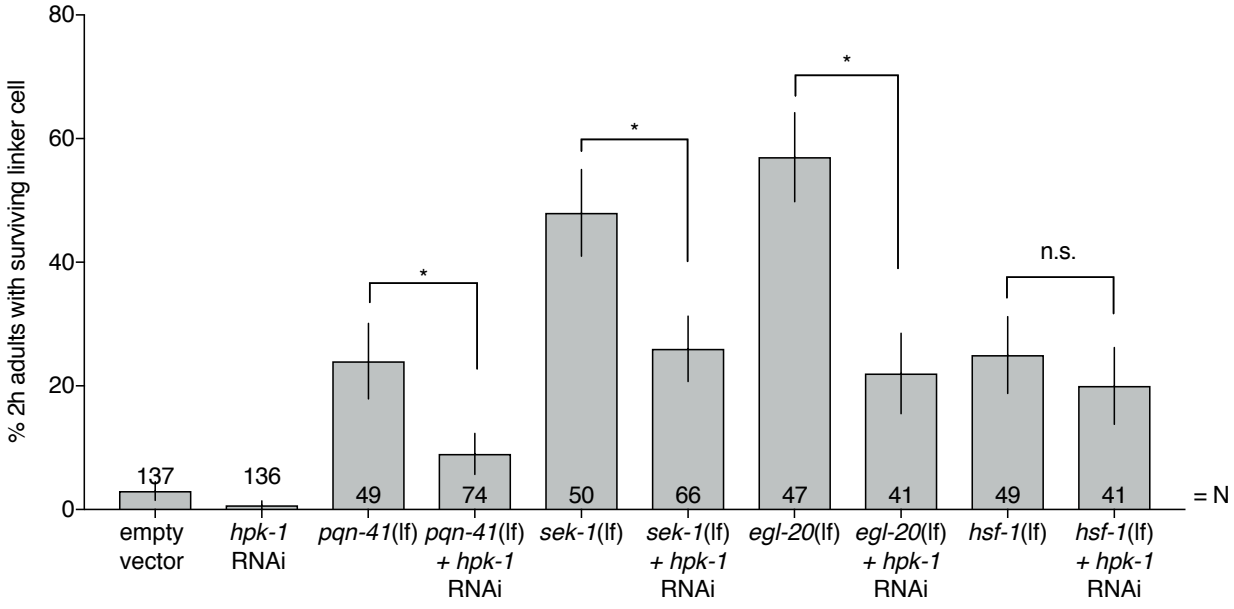

Figure 2-5. **Knockdown of *hpk-1* suppresses the surviving linker cell defects of known linker cell death regulators**.
Linker cell survival in indicated genotypes. Animals scored 0-2 h after the L4 to adult transition. Strains contain *lag-2*p::GFP linker cell reporter and *him-5*(*e1490*). Number of animals scored inside bars. Error bars, standard error of the proportion. n.s., $p>0.05$, *, $p<0.05$, Fisher's exact test.

pqn-41.

Despite multiple attempts, I was unable to generate double *sek-1*(*ag1*) *hpk-1*(*pk1393*) animals, suggesting that these genes are synthetically lethal. Double *egl-20*(*n585*); *hpk-1*(*pk1393*) animals recapitulated the RNAi phenotype, with loss of *hpk-1* suppressing the *egl-20* phenotype by half (Table 2-5). I also examined *bar-1*(*ga80*) *hpk-1*(*pk1393*) animals and found that *hpk-1* enhanced the *bar-1* defect to almost 100% (Table 2-5). Oddly, application of RNAi in *bar-1*(*ga80*) animals also enhanced the SLC defect (91% SLCs in empty vector RNAi (N=55) compared to 56% SLCs with no RNAi application (N=41)), suggesting that lacking *bar-1* and undergoing a stress-related event at the same time may affect linker cell death.

Knocking down *hpk-1* by RNAi did not suppress defects in *hsf-1*(*sy441*) or *let-70*(*ns770*), however, suggesting HPK-1 functions upstream or in parallel to HSF-1 (Figure 2-5, [187]). Double *hsf-1*(*sy441*); *hpk-1*(*pk1393*) genetic mutants were indistinguishable from *hsf-1*(*sy441*) animals as well (Table 2-5).

2.4. HPK-1 acts upstream or in parallel to HSF-1

The epistasis data between *hpk-1* and known linker cell death genes suggested that *hpk-1* acts upstream or in parallel to *hsf-1*. Therefore, I investigated the relationship

Table 2-5. ***hpk-1*(*pk1393*) suppresses defects of some linker cell regulatory genes**.

Genotype	%SLC (N)
pqn-41(*ns294*)	20% (44)
pqn-41(*ns294*); *hpk-1*(*pk1393*)	16% (77)
egl-20(*n585*)	50% (46)
egl-20(*n585*); *hpk-1*(*pk1393*)	24% (90)
bar-1(*ga80*)	56% (41)
bar-1(*ga80*) *hpk-1*(*pk1393*)	92% (76)
hsf-1(*sy441*)	25% (49)
hsf-1(*sy441*); *hpk-1*(*pk1393*)	20% (41)

Animals were scored 0-2h after the L4 to adult transition. Strains also contain *him-5*(*e1490*) for males, and *qIs56* linker cell marker.

between HPK-1 and HSF-1 further with Mohammad Alam, a rotation student at the time.

2.4.1. HSF-1 fails to form heat shock granules in the absence of hpk-1

In yeast, the HPK-1 homolog Yak1 phosphorylates Hsf1 to enhance its DNA binding activities [188]. We wanted to determine if something similar was occurring in *C. elegans,* so we examined the formation of HSF-1-GFP granules upon heat shock, which can be used as a proxy for DNA binding [189]. We found that these granules failed to form in *hpk-1*(*pk1393*) animals after an 8 min heat shock at 35°C, suggesting that HPK-1 is required for HSF-1 granule formation (Figure 2-6).

2.4.2. The linker cell dies appropriately after heat shock in the absence of hpk-1

Because of the dual role that HSF-1 plays in both cell survival and cell death, linker cell death is sensitive to changes in temperature and stress events immediately

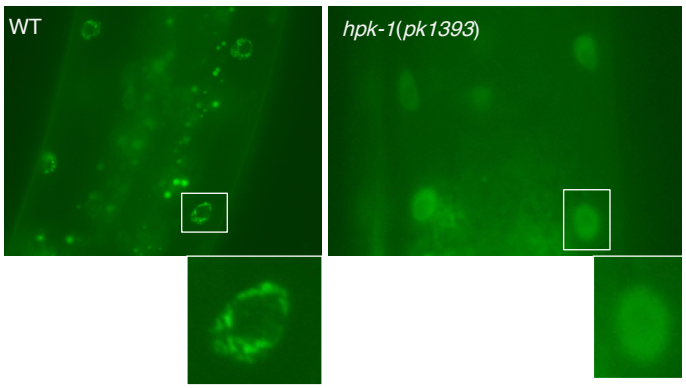

Figure 2-6. **HPK-1 is required for HSF-1 granule formation after heat shock.** HSF-1-GFP granule formation was examined in wild-type (left) and *hpk-1*(*pk1393*) (right) animals. Animals were heat shocked for 8 min at 35°C and examined immediately after for formation of nuclear puncta. Inset shows increased magnification of boxed nucleus.

prior to cell death onset [85]. In wild-type animals, a brief heat shock 4h prior to LCD resulted in a 13% surviving linker cell defect (N=61), in support of previously published results [85]. In *hpk-1*(*pk1393*) animals, however, the linker cell dies appropriately after heat shock (6% SLC, N=120). This result suggests that HPK-1 is required to drive the heat shock response of HSF-1, and its absence allows HSF-1 to carry out its pro-death function, even when the heat shock response has been activated.

2.5. Discussion

From a protein interaction screen, I recovered 33 putative interactors of PQN-41C. *pqn-41* is expressed in many cells within the animal [87]. Therefore, these proteins could be interacting with PQN-41C in the linker cell, or in non-death-related functions of PQN-41C, such as egg laying (Andrew Schwendeman, *unpubl. data*). To determine which genes function to linker cell death, I knocked down each of the putative interacting proteins in an RNAi-sensitized background. I found that knockdown of ten of these genes had a significant number of surviving linker cells. Additionally, two of the candidate genes caused a decrease in the number of surviving cells and cell corpses upon knockdown.

One immediate question that comes to mind is why were these ten genes not recovered from the genome-wide RNAi screen carried out by Elyse Blum and Mary Abraham? For five of these genes, the answer is simple: they were either misrepresented or missing from the original RNAi screening library. I generated these RNAi clones myself. Another possibility is that because the original RNAi screen was carried out under the dissecting scope without a close watch on time, some of the weaker candidate genes were missed. My subsequent screen was performed under high magnification, exactly 2h after the L4 to adult transition. This step is crucial for detecting genes with weak phenotypes (<20% surviving linker cells). Lastly, some of the genes I recovered could also be false positives, as some of the genetic mutants I tested

do not phenocopy the RNAi data.

As a next level of stringency, I wanted to test which of the ten genes I isolated functioned cell-autonomously. I integrated an extrachromosomal array carrying *mig-24*p::*rde-1* in an *rde-1*(*ne219*) background to examine linker cell specificity. This strain also allowed me to examine the linker-cell-specific defects of the three genes that caused lethality upon RNAi. This next round of screening revealed that *aco-2*, *zfp-1*, *eef-2*, and *tag-214* function cell autonomously. *tag-214* is a particularly intriguing result, as it encodes an E3 ubiquitin ligase, and may be an interesting gene to follow up on in the future.

From these different tests, I isolated a few candidate genes that may be worthy of future study. The aconitase, *aco-2*, is responsible for the 2-step dehydration/ hydration reaction that converts citrate to isocitrate in the Krebs cycle [190]. The human homolog, *ACON2,* is implicated in human prostate cancer and neurodegenerative disorders, and downregulation is observed in Huntington's mouse models and patients [191,192]. Knockdown of *aco-2* caused the largest surviving linker cell defect of all the genes tested; these animals also had an interesting phenotype where the linker cell would detach from the gonad and continue migrating on its own. A major question that remains is whether the defect in *aco-2* is caused by a general defect in metabolism or is more specific to linker cell death. While initially I considered that not having enough ATP would be a reason for a cell to die, it is likely that linker cell death is an energy-dependent process. Perhaps linker cell death cannot be carried out without energy, and perhaps a cell dying from energetic failure would adopt a different morphology. Further study into the function of metabolism on linker cell death is likely warranted.

Another interesting gene I identified is *zfp-1*. *zfp-1* encodes a protein homologous to human AF10, implicated in leukemia as a result of translocation with MLL [193]. ZFP-1 contains leucine zippers, zinc fingers, and PHD/LAP domain. In *C. elegans*, *zfp-1* has been implicated as a common mediator of lifespan regulation through the insulin-

signaling pathway and after dietary restriction [194]. In linker cell death, *zfp-1* had a weak defect upon knockdown, but *zfp-1* synergistically enhanced the *pqn-41*(*ns294*) defect. Since *pqn-41*(*ns294*) is not a complete null, it would be prudent to test whether we also see enhancement in the newly generated *pqn-41*(*ns807*) allele, which removes the entire 34 kb locus.

zfp-1(*ok554*) appeared to be a hypomorphic allele with respect to its linker cell defect. When I generated the genetic double mutant between *zfp-1*(*ok554*) and *pqn-41*(*ns294*), however, these animals had extreme developmental defects, including defects in egg laying and tail development. The defect in tail development was so severe that it precluded me from easily scoring the linker cell death phenotype. These phenotypes suggest that *zfp-1* and *pqn-41* may be working in other parallel in other cellular contexts as well.

I recovered two other proteins with polyglutamine (PQN) domains, *pqn-85*, a gene implicated in DNA repair, and *pqn-59*, which is similar to the ubiquitin-associated protein UBAP2. Both of these genes had weak RNAi phenotypes, but it may be interesting to create a triple mutant between the three PQN genes to determine how they influence each other. I find it intriguing that we have three putative genes implicated in linker cell death that all contain polyglutamine repeats, especially given the prevalence of these genes in neurodegenerative disorders.

The negative regulator of transcription, TAG-153, had a weak surviving linker cell defect upon knockdown by RNAi. The loss-of-function allele, *ok699*, had no appreciable defect, however. Interestingly, knocking down *tag-153* in a *pqn-41*(*ns294*) background suppressed the *pqn-41* defects by half. To determine how these genes work together, it would be prudent to create a double mutant allele between *tag-153*(*ok699*) and *pqn-41*(*ns294*) or *pqn-41*(*ns807*) to see whether this suppression also occurs in the genetic double mutants.

The best candidate I recovered and likely the gene that warrants the

most attention is the homeodomain protein kinase *hpk-1.* Knockdown of *hpk-1* in *pqn-41*(*ns294*), *egl-20*(*e585*), and *sek-1*(*ag1*) animals suppressed their defects by half. This result suggests that *hpk-1* may function as an inhibitor of linker cell death, downstream of these genes. *hpk-1* RNAi in *hsf-1*(*sy441*) mutants did not affect the number of SLCs, suggesting that *hpk-1* may function upstream or in parallel to *hsf-1.* Consistent with this, Jennifer Malin found that knockdown of *hpk-1* in *let-70*(*ns770*) animals also does not affect the *let-70*(*ns770*) defect [187].

Yeast lacking the *hpk-1* homolog, Yak1, have a reduced resistance to heat stress [195]. Yak1 phosphorylates Hsf1 in *vitro*, which enhances its DNA binding ability [188]. These results support our finding that HSF-1-GFP fails to form stress granules after heat shock when HPK-1 is missing. It should be noted that the result we obtained is the opposite reported by [196], although they used knockdown of *hpk-1* by RNAi rather than a genetic mutant to examine this function.

HSF-1 in the linker cell can function in either a pro-survival, stress-related role or a pro-death role [85]. The pro-death role of HSF-1 competes with its pro-survival role at the start of linker cell death, likely through post-translational modifications. In mammalian systems, sumoylation of HSF-1 inhibits its transcriptional activity [197], and in *C. elegans*, HPK-1 antagonizes sumoylation of HSF-1 in order to positively modulate its heat shock response [197]. One hypothesis we had from these results is that because sumoylation of HSF-1 negatively affects its transcription of heat-shock-related genes, then perhaps sumo-HSF-1 could have a distinct function in its cell death role. Additional experiments are needed to test this hypothesis.

In *C. elegans,* HPK-1 promotes the pro-survival, stress-related role of HSF-1 during early larval stages [196,198], and perhaps likely also in the linker cell. In the absence of HPK-1, the pro-survival function of HSF-1 is weakened, pushing the system towards cell death. In fact, *hpk-1*(*pk1393*) animals are unable to mate, although their spermatids are fully functional. Perhaps in these animals the linker cell is dying

prematurely and affecting gonad fusion to the cloaca. This hypothesis could be easily tested in the long-term imaging device recently developed by Wolfgang Keil in our lab (see Chapter 3).

I first stumbled upon HPK-1 through a protein interaction screen of PQN-41C. Knockdown of *hpk-1* by RNAi in a *pqn-41* loss-of-function background suppressed the surviving linker cell defects in *pqn-41* animals by half. When I made a double mutant between *hpk-1*(*pk1393*) and *pqn-41*(*ns294*), however, the suppression was weaker. To analyze these interactions further, it would be useful to determine if *hpk-1*(*pk1393*) is able to suppress the defects seen in the complete null of *pqn-41*. If our model is correct (Figure 2-7), knocking out *hpk-1* in a complete null background of *pqn-41* should reduce the defects of *pqn-41.* Additionally, because *pqn-41* is a cold-sensitive protein, and *hpk-1* plays a role in the heat shock response, it will be useful to determine how the double mutant behaves at 15°C and at 25°C.

One model of how these proteins are working in the linker cell is that PQN-41C

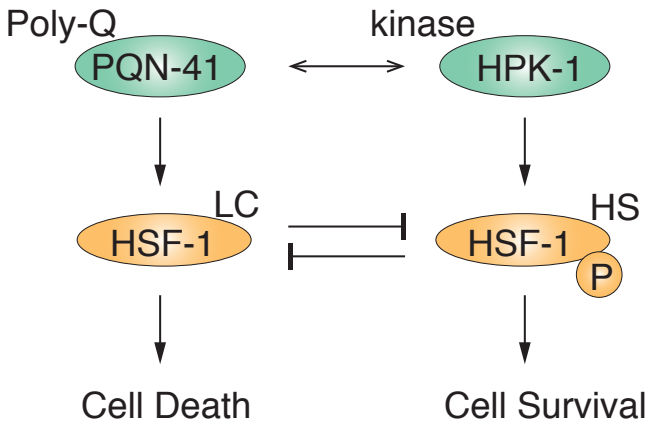

Figure 2-7. **Model for how PQN-41C, HPK-1, and HSF-1 function in linker cell death**.
PQN-41C acts upstream of HSF-1, likely promoting its cell death function. PQN-41C interacts physically with HPK-1, perhaps inhibiting its pro-survival role of HSF-1 modulation after stress conditions.

binds HPK-1 at the onset of linker cell death, inhibiting its pro-survival function towards HSF-1 (Figure 2-7). One way to test this hypothesis is with an in vitro phosphorylation assay. Incubating HPK-1 and HSF-1 together with radioactive phosphate may result in some of the phospho-groups transferring to HSF-1. If we now add recombinant PQN-41C to this reaction, perhaps phosphate is no longer incorporated. Given that these proteins are relatively unstable, this hypothesis may be more difficult to test in actuality, but it would be a worthwhile experiment.

In addition to the interplay between PQN-41C, HSF-1, and HPK-1, I also observed some other interesting defects while trying to determine the function of *hpk-1* in linker cell death. *hpk-1*(*pk1393*); *sek-1*(*ag1*) double mutants were synthetically lethal, suggesting that these genes may function in parallel in vital cellular processes. I also found that *bar-1*(*ga80*) *hpk-1*(*pk1393*) double mutants have a SLC defect of nearly 100%. *bar-1*(*ga80*) is not a complete null, making interpretation of this data difficult. In Xenopus and Drosophila, however, HIPK1 can repress or activate β-catenin targets, depending on the developmental context [199,200], suggesting that these genes function together in other cellular systems. One hypothesis I had about their function in the linker cell is that lacking both genes may alter the linker cell's stress levels and promote the stress-related function of HSF-1, independent of HPK-1. For example, *bar-1*(*ga80*) animals fed empty vector control RNAi bacteria have linker cell defects of 91%, compared to 56% in *bar-1*(*ga80*) animals under normal, non-RNAi conditions. This result suggests that *bar-1* animals are ultrasensitive to perturbations in stress activation (simply activating the RNAi pathway in this background is enough to nearly inhibit linker cell death completely).

Another hypothesis is that HPK-1 phosphorylates BAR-1 and stabilizes it. In *ga80* mutants, this stabilization is crucial for mutated BAR-1 to maintain some of its protein levels and carry out partial wild-type function. In the absence of HPK-1, this stabilization is lost, and *bar-1*(*ga80*) *hpk-1*(*pk1393*) double mutants could represent total BAR-1 loss

with respect to its linker cell function. This hypothesis is derived from the fact that HIPK2 stabilizes β-catenin homologs in Xenopus [200], Drosophila [199] and *in vitro* [199].

The interplay between PQN-41, HPK-1, HSF-1, and BAR-1 represents an exciting avenue of future research and may tell us more about the fine-tuning of linker cell death onset.

3. RAB-35 and ARF-6 GTPases mediate engulfment and clearance following linker cell-type death

3.1. Summary

Following death, the linker cell must be engulfed and degraded. Therefore it is a particularly attractive in vivo model for investigating the clearance of a cell that normally dies non-apoptotically: the time of linker cell death onset is predictable, the process can be followed in live animals, and engulfment events can be dissected genetically.

In this chapter, I show that engulfment and degradation of the linker cell differs in mechanics and genetics from apoptotic cell clearance. I demonstrate that, unlike apoptotic cell corpses, the linker cell is simultaneously engulfed by two U cell-descendent phagocytes, resulting in cell splitting. Apoptotic engulfment genes are not required for this novel form of engulfment. Rather, I find that the GTPase RAB-35 is a key coordinator of at least two steps in linker cell degradation. Early on, RAB-35 localizes to extending phagocyte pseudopods, and prevents premature onset of phagocytosis. Once engulfment has occurred, RAB-35 drives degradation of the linker cell by promoting recruitment of RAB-5 and then RAB-7 GTPases onto phagosome membranes, and subsequent lysosomal fusion and degradation. I demonstrate that both activities of RAB-35 require inactivation of another conserved small GTPase, ARF-6, which I show functions as a clearance inhibitor. RAB-35 physically interacts with the ARF-6 GTPase activating protein CNT-1, providing a plausible mechanism for ARF-6 inhibition. Furthermore, while RAB-35 localizes to engulfing-cell and phagosome membranes during most of linker cell clearance, ARF-6 only transiently persists at the membrane, and its timely removal depends on RAB-35.

3.2. Linker cell corpse clearance occurs by a novel mechanism

3.2.1. The dying linker cell is simultaneously engulfed by two neighboring cells

Linker cell death and clearance occurs during the transition from the fourth larval stage to the adult, and can take up to 8 hours to complete [82,201]. To examine this process at high spatiotemporal resolution, I used a long-term imaging microfluidic device that Wolfgang Keil, a postdoc in the lab, previously developed [198] to simultaneously image the linker cell (*mig-24*p::Venus) and the engulfing cells (*lin-48*p::mKate2) in live animals (Figure 3-1). Animals were loaded into the device, and z-stacks were acquired every 8 min for > 20h (Figure 3-1). Animal development and linker cell death kinetics were not affected by either imaging or fluorescent reporter identity (Figure 3-1b, Table 3-1, top). The timings of characteristic events accompanying linker cell degradation

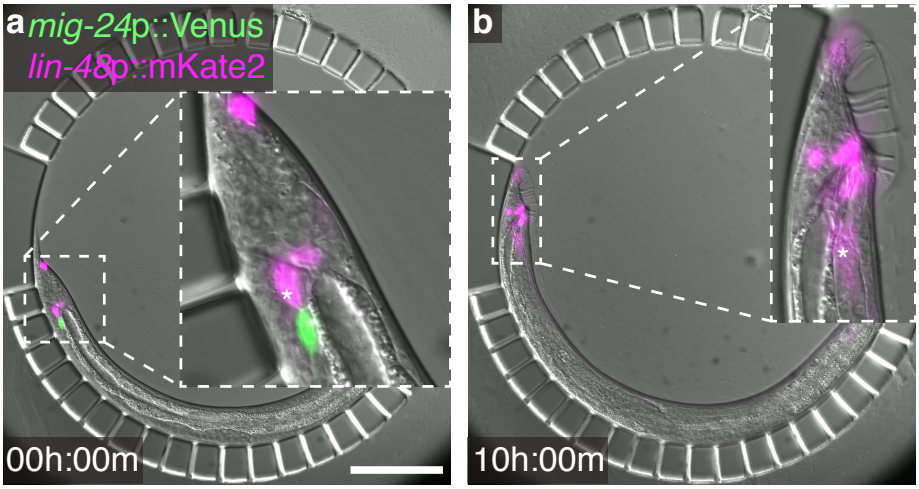

Figure 3-1. **Microfluidic device for long-term imaging of linker cell death.** (a,b) *C. elegans* male immobilized in a microfluidic chamber (see [198]) at (a) first contact between linker cell (green) and engulfing U.l/rp cell (magenta, asterisk), and (b) after 10 hours. All males examined in all figures in Chapter 3 carry the male-producing *him-5*(*e1490*) or *him-8*(*e1489*) mutation. Scale bar, 100 µm.

Table 3-1. **Reporter identity does not affect linker cell degradation** (mean ± SE of proportion).

Genotype	% linker cell corpses in 24h adults	N
qIs56[LCp::GFP]	12 ± 3.2	100
nsIs65[LCp::Venus]	11 ± 3.1	100
nsIs60[LCp::Venus]	5 ± 2.1	103
arf-6(*ns388*); *nsIs65*	64 ± 4.8	101
rab-35(*b1013*); *nsIs65*	79 ± 4.0	102
nsIs589[UCp::mKate2]; *nsIs65*	5 ± 5.0	101
arf-6(*ns388*); *nsIs589; nsIs65*	57 ± 6.6	56
rab-35(*b1013*); *nsIs589; nsIs65*	54 ± 8.4	35
nsIs653[UCp::mKate2-PH]; *nsIs65*	1 ± 1.0	104
nsIs60; nsIs622[UCp::mCh-RAB-5]	0	100
nsIs592[UCp::mCh-RAB-7]; *nsIs65*	8 ± 2.8	91
nsIs586[UCp::CTNS-1-mKate2]; *nsIs65*	3 ± 1.7	101
nsIs650[LCp::mKate2]	4 ± 2.0	101
nsIs595[UCp::YFP-RAB-35]; *nsIs650*	2 ± 1.4	101
rab-35(*b1013*); *nsIs595; nsIs650*	1 ± 1.0	100
arf-6(*tm1447*); *nsIs595; nsIs650*	3 ± 1.7	101
nsIs625[UCp::ARF-6-YFP]*; nsIs650*	10 ± 3.9	59
arf-6(*tm1447*); *nsIs625; nsIs650*	4 ± 2.6	55
rab-35(*b1013*)*; nsIs625; nsIs650*	51 ± 6.9	53
arf-6(*tm1447*); *rab-35*(*b1013*)*; nsIs625; nsIs650*	43 ± 5.2	90
nsIs636[UCp::ARF-6 (D92N)-YFP]; *nsIs650*	56 ± 4.9	101
rab-35(*b1013*)*; nsIs713*[UCp::YFP-RAB-35]; *nsIs65*	0	53

UCp = *lin-48*p; LCp = *mig-24*p, except for *qIs56*, which is *lag-2*p. All animals carried a *him-5*(*e1490*) mutation in addition to the transgenes listed above.

were noted, with time zero corresponding to the time of first contact between the linker cell and the U.lp or U.rp engulfing cells (Figure 3-2a), and are consistent with previous reports [82,201].

I found that after first contact, the linker cell migrates so that it becomes sandwiched between the U.lp and U.rp cells (Figure 3-2b), whose cell nuclei are displaced anterior to the linker cell. Linker cell nuclear crenellation also becomes apparent at this time (Figure 3-2c). Remarkably, following linker cell nuclear changes, both U.l/rp cells simultaneously attempt to engulf the linker cell (Figure 3-2d, Figure 3-3). During this process, which I term *competitive phagocytosis*, linker cell

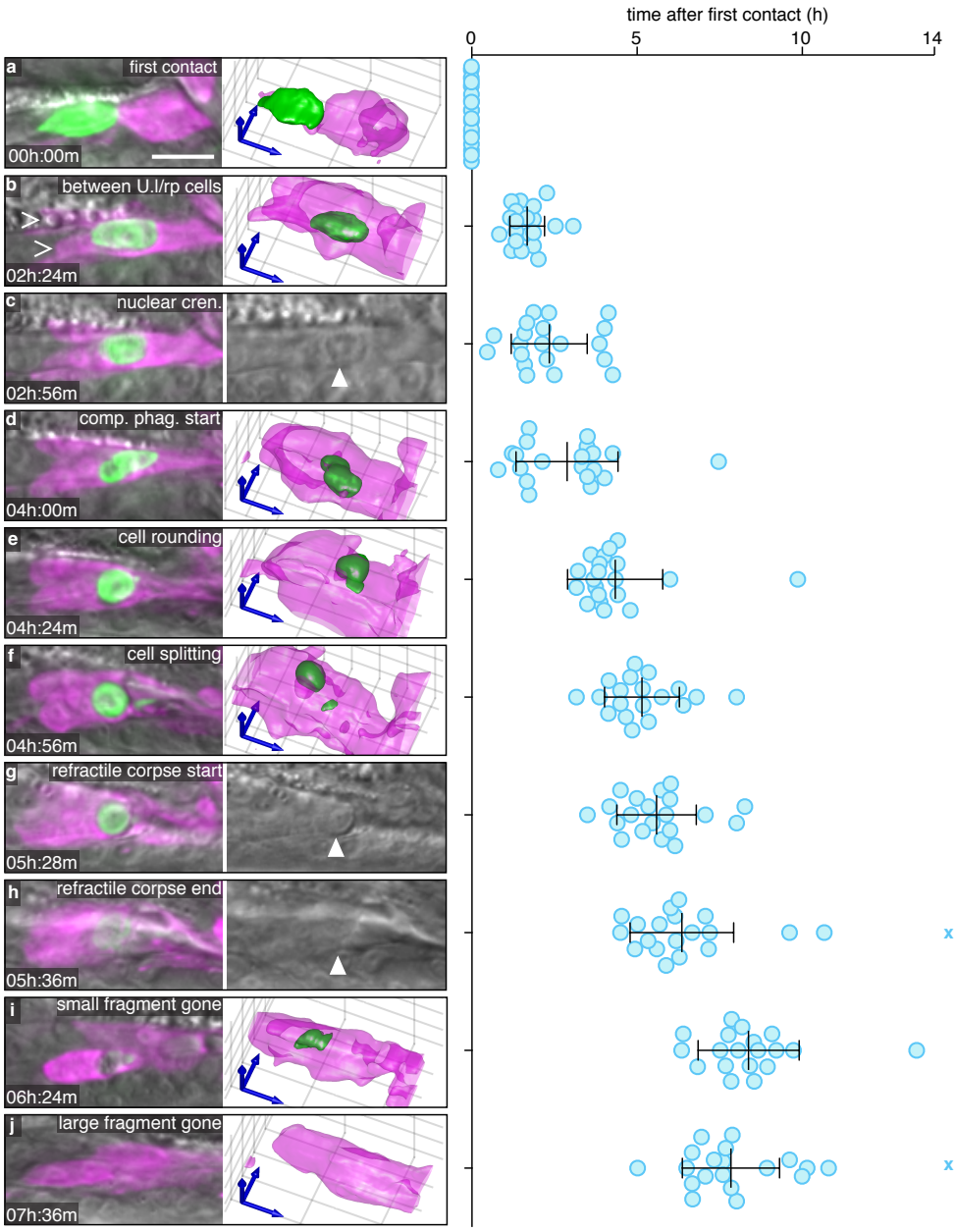

Figure 3-2. **Linker cell death and degradation.**

(a) Left: Maximum intensity projection showing linker cell at first contact with U.l/rp cells. Right: 3D rendering. Scale bar, 10 µm. (b-j) Stereotypical events during linker cell dismantling. Images as in (a), except that in (c,g,h) a single DIC slice is shown instead of 3D rendering. Right, time of events in individual animals (blue circles) after first contact. X, event did not occur during imaging. Bars, mean ± sd. Arrowhead, linker cell. (b) Linker cell between U.l/rp cells (caret) (c) Nuclear crenellation onset. (d) Competitive phagocytosis begins. (e) Linker cell rounding (f) Linker cell corpse splits. (g) Onset of refractility. (h) End of refractility. (i) Small fragment disappears. (j) Large fragment disappears.

rounding (Figure 3-2e) is followed by splitting of the linker cell into two fragments (Figure 3-2f). The larger linker cell remnant contains the nucleus, and is equally likely to be found within U.lp or U.rp (8/19 and 11/19, respectively; p=0.5, χ^2-test). The cell engulfing the nucleus-containing fragment is more likely to be binucleate (17/19; p=0.0006, χ^2-test), a result of an earlier unrelated U cell descendent fusion event [202], suggesting that the larger U.l/rp cell engulfs a larger portion of the linker cell. The larger linker cell remnant, but not the smaller, then becomes refractile by DIC microscopy (Figure 3-2g-h). The two linker cell fragments are degraded with similar kinetics (Figure 3-2i-j). Competitive phagocytosis does not result in extensive leakage of linker cell cytoplasm, as I never observed reporter protein outside the cell (N=35).

To identify the precise time point at which the linker cell fragments become

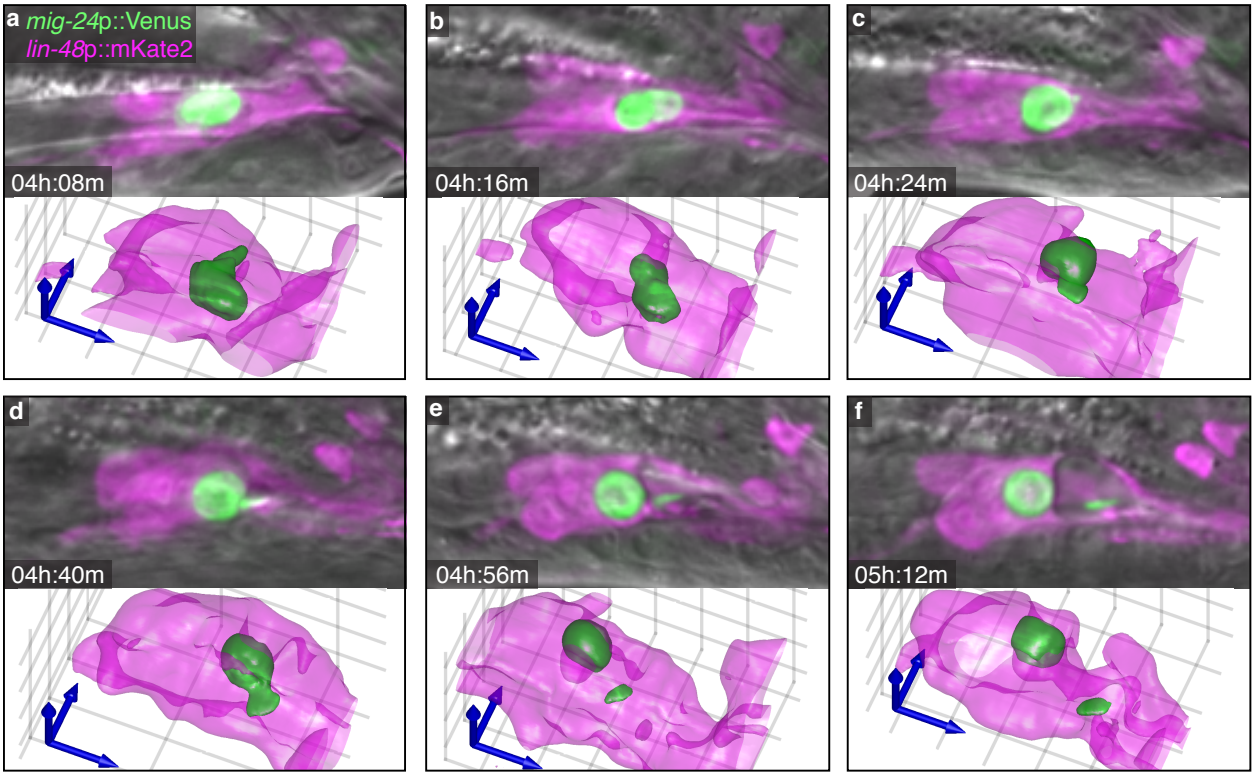

Figure 3-3. **Competitive phagocytosis is dynamic.**
Additional frames of animal shown in Figure 3-2, demonstrating back-and-forth tugging events leading to linker cell splitting. Scale bar, 10 µm.

internalized, I followed linker cell death in animals expressing the mKate2-PH reporter, derived from PLC-δ1, which marks the plasma membrane and membranes of open phagosomes by binding $PI(4,5)P_2$ [203]. Localization of this reporter around the linker cell ceases soon after cell splitting (Figure 3-4), suggesting that linker cell fragmentation and U.l/rp internalization are coupled.

The unique mechanics governing linker cell dismantling raise the question of whether U cell descendants are specifically equipped for linker cell clearance. To test this, I examined animals carrying a mutation in the gene *him-4*, in which linker cell migration is defective, and the cell ends up near the head [82]. In these animals, linker cell death occurs fairly reliably, as determined by onset of nuclear crenellation [82]. However, while engulfment and degradation by neighboring cells can occur, it is inefficient (62 ± 6.9% remaining corpses in 24h adult males, N=50, $p<0.0001$ compared to wild type, Fisher's exact test). Thus, U.l/rp cells exhibit specialization for linker cell clearance.

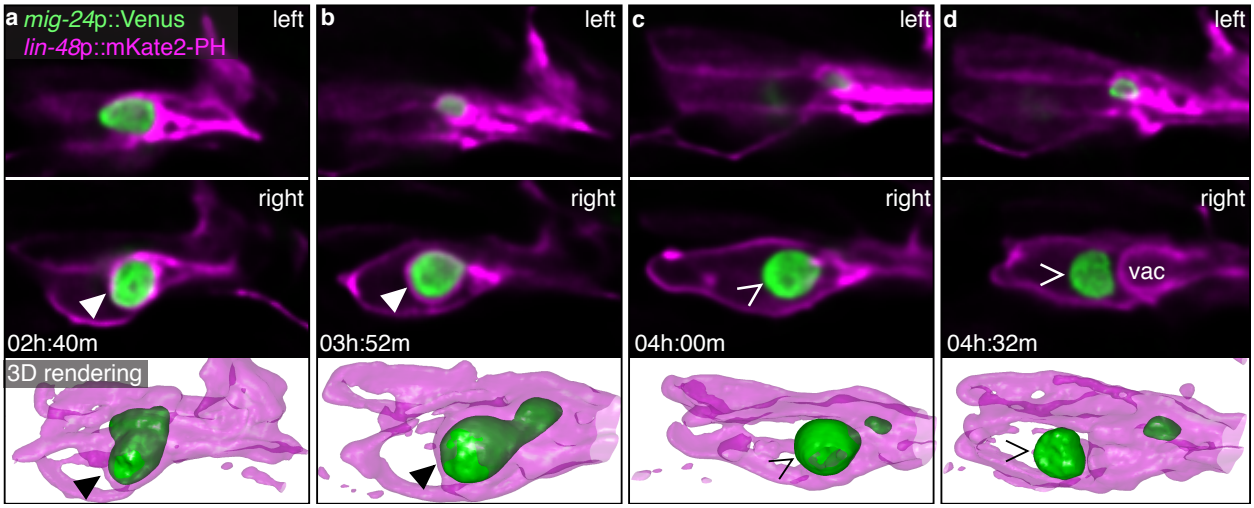

Figure 3-4. **mKate2-PH is removed from the plasma membrane immediately after splitting, indicating internalization.**
Linker cell splitting correlates with loss of mKate2-PH, an open phagosome marker. Scale bar, 10 μm. (a-b) Arrowhead, mKate2-PH plasma membrane marker around linker cell prior to cell splitting (c-d) Caret, mKate2-PH plasma membrane marker absent from phagosome after cell splitting.

3.2.2. Apoptotic engulfment genes are not required for linker cell clearance

It was previously reported that linker cell engulfment can occur in animals lacking apoptosis engulfment genes [82]; however, whether the cell is eventually degraded in these settings was not examined. To look at this in detail, I followed linker cell engulfment in animals lacking components of each or both parallel pathways that together drive apoptotic cell engulfment. Animals were scored 24h after the L4-to-adult transition, when the majority of animals have cleared the linker cell corpse [201]. I found that linker cell engulfment is only weakly perturbed by mutations in some known engulfment genes (Table 3-2). Furthermore, double mutants between engulfment genes in different pathways do not strongly affect linker cell clearance. Consistent with this observation, when I expressed MFG-E8-GFP, a phosphatidylserine binding protein [204,205], in U cell descendants, I did not observe fluorescence accumulation around the linker cell (5 lines, >100 animals scored in total). Nonetheless, I did find that mutations in the phagosome maturation gene *sand-1* significantly inhibit clearance of linker cell debris (Table 3-2).

Thus, while genes promoting cell corpse degradation following engulfment are shared between linker cell death and apoptosis, upstream genes required for phagocytosis and the initiation of degradation are different. Linker-cell-specific engulfment genes remain, therefore, to be discovered.

3.3. A forward genetic screen to identify new factors in engulfment and clearance

To identify components of the linker cell engulfment machinery, I sought mutants in which linker cell engulfment and/or degradation are defective. To do so, I mutagenized hermaphrodites carrying a *lag-2*p::GFP linker cell reporter and a *him-5* mutation, which increases the proportion of male progeny (Figure 3-5a). After two generations, males were screened for linker cell persistence. It was previously

Table 3-2. **Canonical apoptotic engulfment genes play a minor role in linker cell corpse removal**

(mean ± SE of proportion).

Genotype	Mammalian homolog	% linker cell corpses in 24h adults	N
WT		12 ± 3.2	100
ced-1(*e1735*)	CD91	14 ± 3.4	103
ced-6(*n2095*)[a]	Gulp	9 ± 2.9	100
ced-7(*n1892*)	ABCA	7 ± 2.3	120
ced-2(*e1752*) [a]	CrkII	20 ± 4.0*	102
ced-5(*n1812*) [a]	Dock180	12 ± 2.9	125
ced-12(*k149*)	Elmo	27 ± 4.5*	96
ced-10(*n1993*)	Rac1	26 ± 4.5*	97
ced-1; ced-5		21 ± 3.2	162
ced-7; ced-10		27 ± 4.5*	98
nuc-1(*e1392*)	DNaseII	31 ± 4.5**	104
cep-1(*gk138*)	p53	12 ± 3.2	103
ced-8(*n1891*)	XK	7 ± 2.5	104
dyn-1(*ky51*)	dynamin	22 ± 4.1	103
ttr-52(*tm2003*)	transthyretin-like	7 ± 2.5	101
ttr-52(*tm2078*)	transthyretin-like	4 ± 1.9	102
psr-1(*ok714*)	phosphatidylserine receptor	7 ± 2.5	103
psr-1(*tm469*)	phosphatidylserine receptor	4 ± 2.6	56
piki-1(*ok2346*)	PI3K	13 ± 3.4	94
unc-108(*n3263*)	Rab2	5 ± 2.3	88
sand-1(*or552*)	Mon1	38 ± 4.9***	97
sand-1(*ok1963*)	Mon1	58 ± 4.8***	104
rme-1(*b1045*)[b]	EHD4	19 ± 6.1	42
scav-1(*ok2598*)	Scarb1	12 ± 5.1	41
scav-2(*ok877*)	CD36	4 ± 2.7	54
scav-3(*ok1286*)	CD36	3 ± 2.1	64
scav-5(*ok1606*)	Scarb1	5 ± 2.9	56
cdh-3(*gk178860*)	cadherin	13 ± 4.5	56
cdh-3(*pk87*)	cadherin	3 ± 2.8	36

[a]*nsIs1*[*lag-2*p::GFP, *rol-6*(+)];[b]*nsIs65*[*mig-24*p::Venus]; *him-8*; *: $p < 0.05$, Fisher's exact test; **: $p < 0.005$, Fisher's exact test; ***: $p < 0.0001$, Fisher's exact test. All animals carried a *him-5*(*e1490*) mutation and *qIs56*[*lag-2*p::GFP] linker cell marker, unless otherwise noted.

shown that animals defective in linker cell death exhibit gonadal blockage, and can be sterile [82]. I therefore directly collected spermatids from mutant males by impaling a needle into the gonad, and used these spermatids to artificially inseminate wild-type hermaphrodites [206] (Figure 3-5b-d, see Methods for details). Cross progeny were then

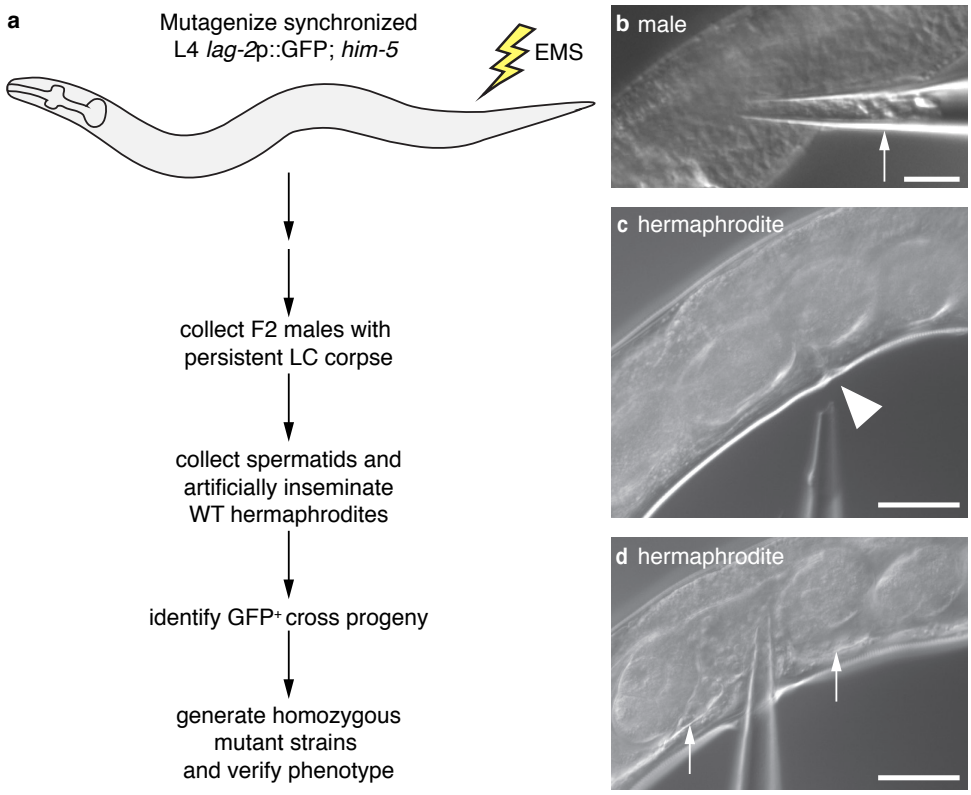

Figure 3-5. **Genetic screen for linker cell degradation mutants**.
(a) Genetic screen scheme. (b-d) Artificial insemination procedure. (b) Needle filled with buffer plunged into a 24h mutant adult male gonadal cavity. Spermatids automatically flow into the needle (arrow). (c) Needle aligned with a wild type hermaphrodite vulva (arrowhead). (d) Needle inserted into the vulva and spermatids released. Released spermatids fill the hermaphrodite gonadal cavity (arrows).

used to establish mutant lines.

I screened 15000 genomes, and isolated 181 males for artificial insemination. From these, I had 66 successful inseminations (36% success rate), and obtained 59 mutants lines (some of the successful inseminations only produced male cross-progeny). 44 of these strains were confirmed under the compound microscope, as having some defect in linker cell death or degradation, while the rest were considered to be false positives (Appendix).

I divided each of the remaining strains into five categories: I. weakly surviving, II. relatively healthy, III. odd death, IV. delayed death, and V. persistent corpse (see Appendix for descriptions of classifications and phenotype analysis of the remaining mutants). For my thesis work, I focused on the three strongest mutants in the class V, and the subsequent analyses are described in this chapter.

3.4. RAB-35 pathway

3.4.1. RME-4/DENND1 promotes linker cell engulfment and degradation

One mutant, *ns410*, exhibits persistent refractile linker cell corpses, and was further studied (Figure 3-6a). Using standard genetic mapping, coupled with whole genome sequencing, I identified a mutation predicted to generate a G100E alteration

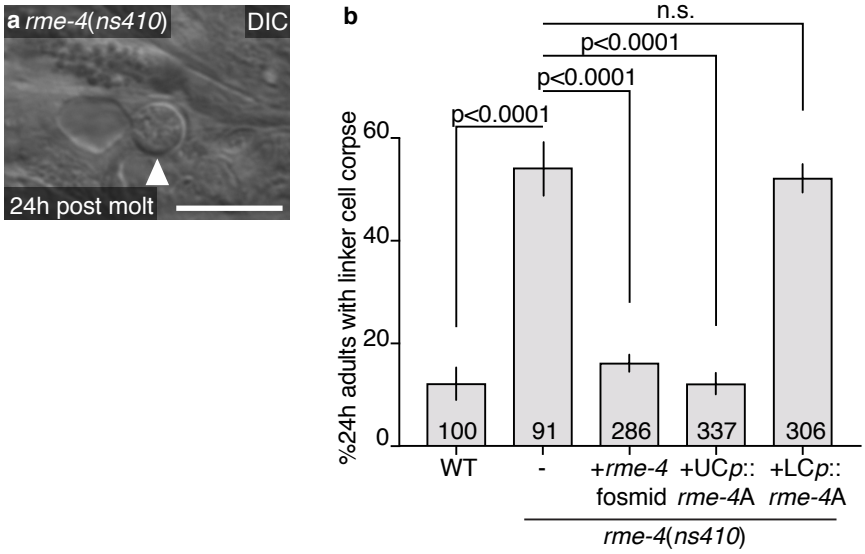

Figure 3-6. ***ns410* is a mutation in *rme-4*.**
(a) DIC image of persistent linker cell corpse (arrowhead) in *rme-4*(*ns410*). Scale bar, 10 µm. (b) Linker cell degradation in indicated genotypes. Strains contain *lag-2*p::GFP linker cell reporter and *him-5*(*e1490*). UCp, *lin-48*p. LCp*, mig-24*p. Number of animals scored inside bars. Average of at least three independent lines. Error bars, standard error of the proportion or standard error of the mean. n.s., p>0.05, Fisher's exact test.

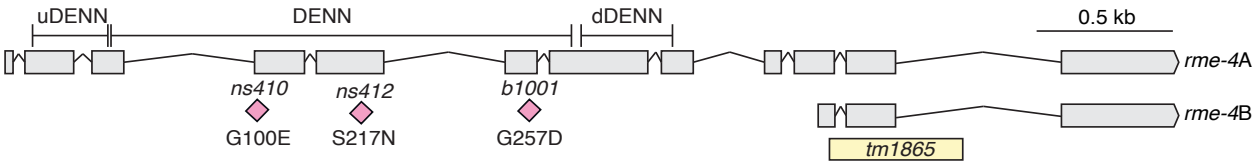

Figure 3-7. ***rme-4* gene locus**.
Pink diamonds, locations of point mutations. Yellow box, deletion allele *tm1865*.

in the DENN domain protein RME-4, homologous to vertebrate DENND1 [204] (Figure 3-7). Linker cell degradation is restored to *ns410* mutants by expressing a fosmid spanning the genomic region of *rme-4* (Figure 3-6b). Furthermore, two other *rme-4* alleles, *ns412* (S217N; isolated in my screen) and *b1001* (G257D; a previously characterized loss-of-function lesion [207]) also promote linker cell degradation defects, as does the *rme-4(tm1865)* deletion allele (Figure 3-8). *rme-4*(*tm1865*) mutants exhibit a weaker linker cell survival defect, perhaps because the truncated RME-4 protein produced in this mutant is present at half wild-type levels [204]. RNAi against *rme-4*

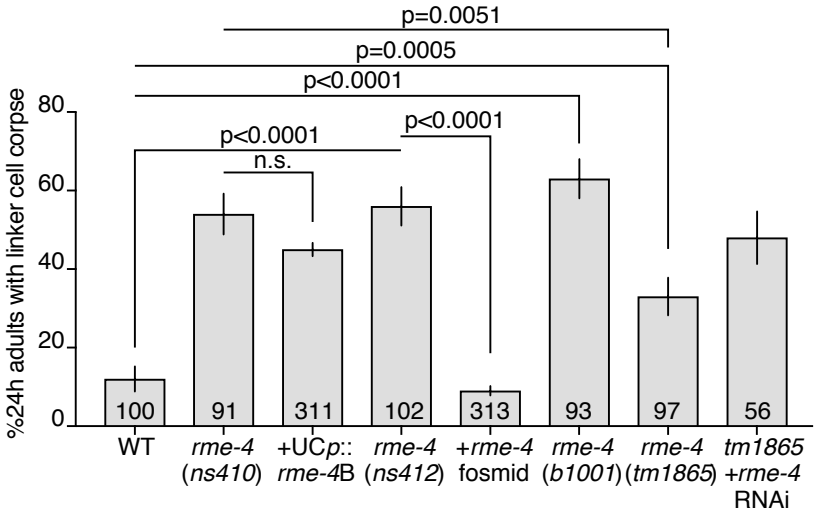

Figure 3-8. **Phenotypic analysis of other mutations in *rme-4*.**
Linker cell degradation in indicated genotypes. Strains contain *lag-2*p::GFP linker cell reporter and *him-5*(*e1490*). UCp, *lin-48*p. LCp*, mig-24*p. Number of animals scored inside bars. Average of at least three independent lines. Error bars, standard error of the proportion or standard error of the mean. n.s., p>0.05, Fisher's exact test.

exacerbates the defect of animals carrying this allele (Figure 3-8). Taken together, these results demonstrate that the *rme-4* gene is required for linker cell corpse degradation.

RME-4 is widely expressed and found in the linker cell and in its engulfing cells (Figure 3-9). To determine where RME-4 functions, I expressed cDNAs for either the *rme-4*A or *rme-4*B transcript (Figure 3-7) in either the linker cell or the engulfing cells. I found that the longer A isoform restores linker cell degradation when expressed in U cell descendants, but not when expressed in the linker cell (Figure 3-6). B isoform expression in the engulfing cells has no effect (Figure 3-8). Thus, RME-4A is the active isoform driving linker cell engulfment, and it does so by acting in the engulfing cells.

3.4.2. RAB-35 GTPase Is a key linker cell degradation regulator controlled by RME-4/DENND1 and TBC-10/TBC1D10A

The RME-4 DENN domain was previously proposed to drive the guanine nucleotide exchange reaction (GEF function) of the small GTPase RAB-35 [207,208]. The *ns410*, *ns412*, and *b1001 rme-4* alleles are predicted to cause single amino-acid changes within this domain, suggesting that RME-4 could function as GEF during linker cell degradation. To test this directly, I examined two *rab-35* mutants, *tm2058* and

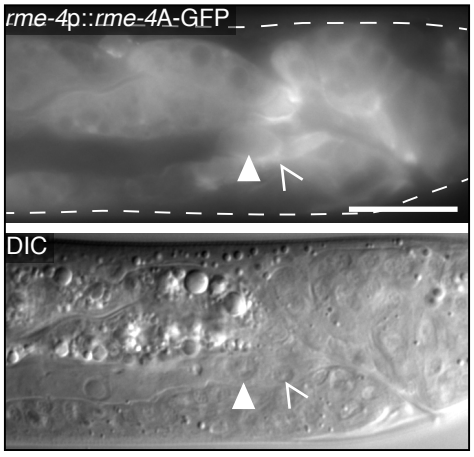

Figure 3-9. ***rme-4* translational reporter expression**.
Arrowhead, linker cell. Caret, U.lp or U.rp cell. Top: GFP. Bottom: DIC. Scale bar, 10 µm.

b1013, that carry a small deletion surrounding the start codon, and an early Q69Ochre stop mutation, respectively (Figure 3-10a). I found that both lesions inhibit linker cell corpse degradation, and persistent corpses resemble those seen in *rme-4* mutants (Figure 3-10b,c). While *rab-35* is broadly expressed (Figure 3-11), I found that linker cell degradation is restored to *rab-35* mutants by expression of *rab-35* cDNA in engulfing cells, but not in the linker cell (Figure 3-10b). Thus, RAB-35 is required in engulfing cells

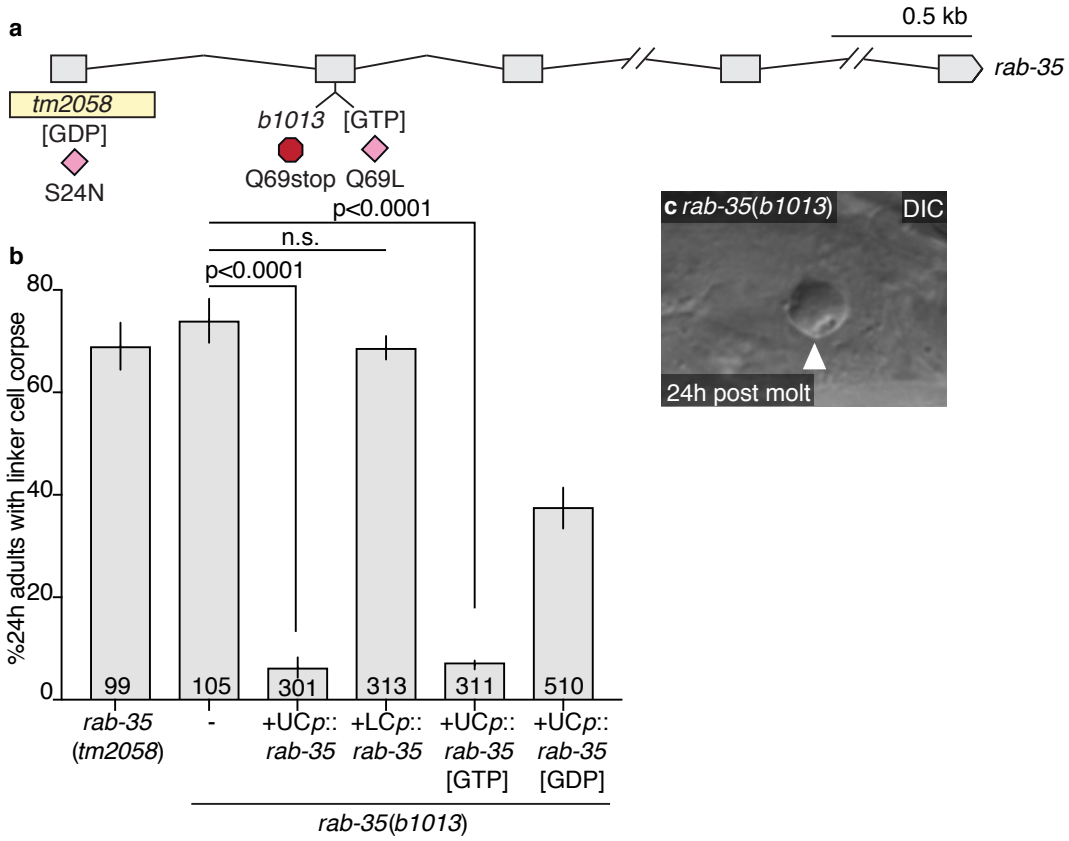

Figure 3-10. **Mutations in *rab-35* cause a persistent corpse defect**.
(a) *rab-35* gene locus. Yellow box, deletion allele *tm2058*. Pink diamonds, point mutations. Red octagon, early stop allele *b1013.* (b) Linker cell degradation in indicated genotypes. Strains contain *lag-2*p::GFP linker cell reporter and *him-5*(*e1490*). UCp, *lin-48*p. LCp*, mig-24*p. Number of animals scored inside bars. Average of at least three independent lines. Error bars, standard error of the proportion or standard error of the mean. n.s., p>0.05, Fisher's exact test. (c) DIC image of persistent linker cell corpse (arrowhead) in *rab-35*(*b1013*).

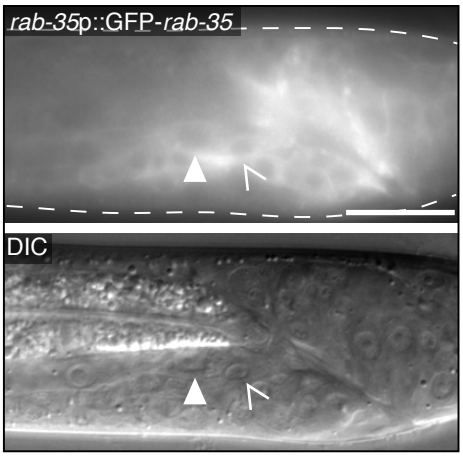

Figure 3-11. ***rab-35* translational reporter expression**.
Arrowhead, linker cell. Caret, U.lp or U.rp cell. Top: GFP. Bottom: DIC. Scale bar, 10 µm.

for linker cell degradation.

RAB-35 and other small GTPases cycle between GTP and GDP bound forms. If RME-4 functions as a RAB-35 GEF, I expect RAB-35[GTP] to be the active form of the protein in linker cell degradation. Indeed, I found that expression of RAB-35(Q69L), predicted to lock the protein in the GTP-bound configuration, fully restores linker cell degradation to *rab-35*(*b1013*) mutants (Figure 3-10b). A GDP-bound mimetic, RAB-35(S24N), however, only partially rescues *rab-35*(*b1013*) linker cell defects. Furthermore, I found that RAB-35(S24N) protein selectively binds RME-4A (but not RME-4B) in a yeast two-hybrid assay [204] (Figure 3-12). Thus, RAB-35 functions with RME-4 in engulfing cells, and RAB-35[GTP] is likely the relevant active form driving linker cell clearance.

I next sought to identify the GTPase activating protein (GAP) completing the RAB-35 GTPase cycle. I reasoned as follows: weak RME-4 (GEF) mutations should result in some RAB-35[GTP] production, but perhaps not enough for efficient linker cell degradation. Combining an *rme-4*(weak) mutation with a RAB-35 GAP mutation, which would block RAB-35[GTP] hydrolysis, could, however, allow sufficient accumulation of

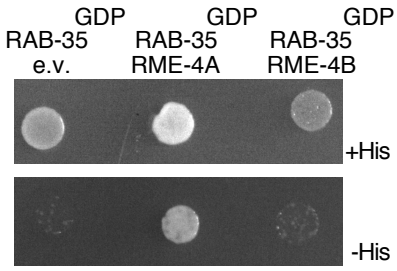

Figure 3-12. **RAB-35[GDP] interacts with RME-4A**.
Yeast two-hybrid assay with LexA-RAB-35[S24N] (GDP) as bait, and Gal4-AD (GAD) empty vector, GAD-RME-4A, or GAD-RME-4B as prey. Top: histidine present. Bottom: histidine absent. Growth on -His plates, physical interaction.

RAB-35[GTP] for efficient linker cell degradation. I therefore screened for the effects of mutations in *C. elegans* homologs of the known mammalian Rab35 GAP genes *tbc-7/Tbc1D24, tbc-10/Tbc1D10A,* and *tbc-13/Tbc1D13* [209]. Mutations or knockdown of these genes alone have no effect on linker cell corpse degradation, nor do they rescue linker cell degradation defects of animals carrying the strong *rme-4*(*ns410*) mutation, in which no RAB-35[GTP] is predicted to accumulate (Figure 3-13a). However, combining the *tbc-10*(*gk388086*) allele with the weak *rme-4*(*tm1865*) allele restores normal linker cell degradation (Figure 3-13b). Thus, TBC-10 is likely the RAB-35 GAP.

Supporting this notion, while TBC-10 protein is widely expressed (Figure 3-13c), specific expression of TBC-10 in U cell descendants of *rme-4*(*tm1865*); *tbc-10*(*gk388086*) double mutants reintroduces the linker cell degradation defect. Similar expression of a TBC-10(R225A) protein, containing a lesion in the putative catalytic arginine finger, has no effect (Figure 3-13b).

Taken together, these results suggest that RAB-35[GTP] is a key regulator of linker cell degradation, and that its activity is controlled by RME-4/GEF and TBC-10/GAP.

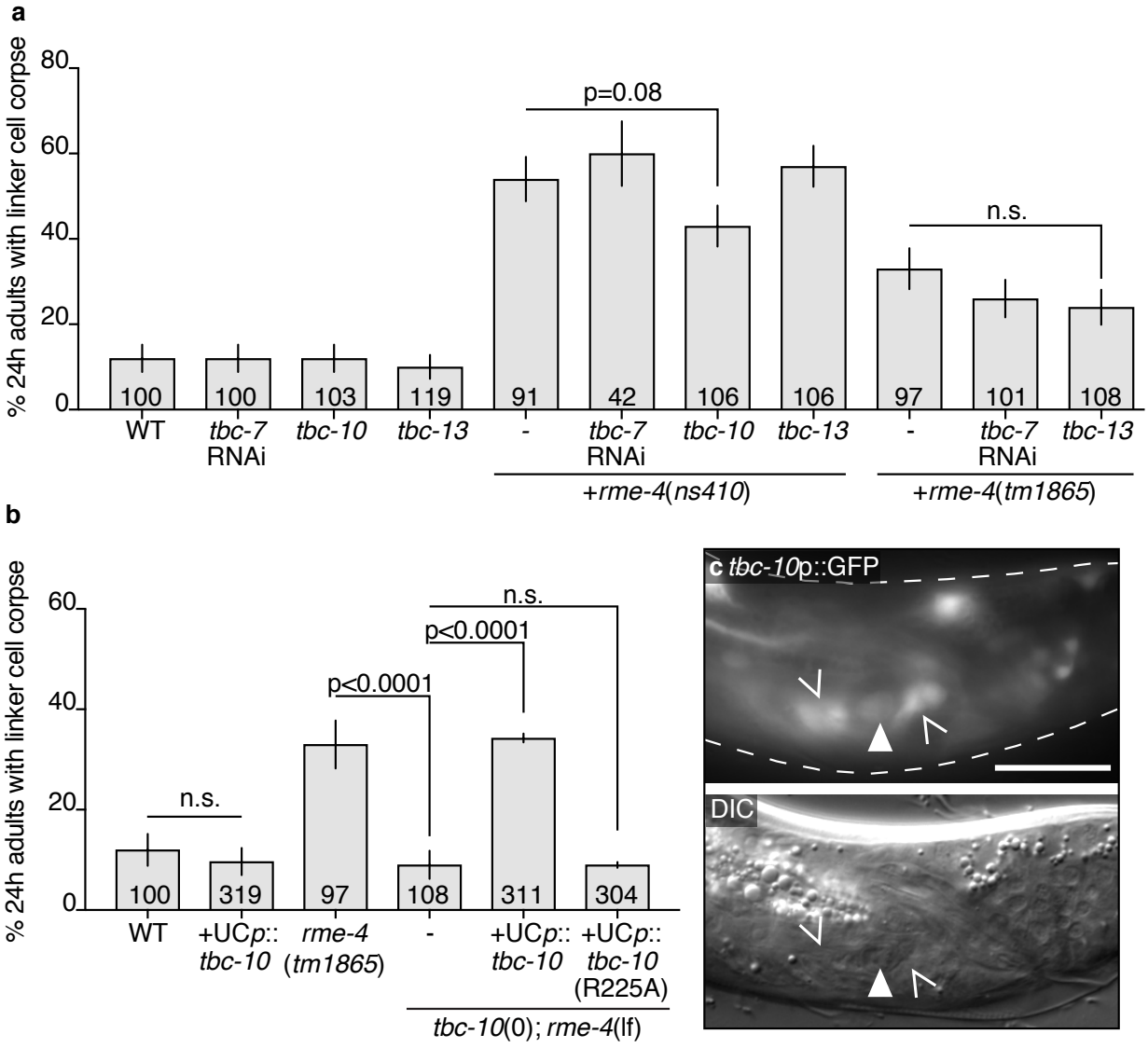

Figure 3-13. **TBC-10 is the putative RAB-35 GAP in linker cell corpse removal**. (a,b) Linker cell degradation in indicated genotypes. Strains contain *lag-2*p::GFP linker cell reporter and *him-5*(*e1490*). UCp, *lin-48*p. LCp*, mig-24*p. Number of animals scored inside bars. Average of at least three independent lines. Error bars, standard error of the proportion or standard error of the mean. n.s., p>0.05, Fisher's exact test. (**c**) *tbc-10* transcriptional reporter. Arrowhead, linker cell. Caret, U.l/rp cells. Top: GFP. Bottom: DIC. Scale bar, 10 µm.

3.4.3. RAB-35 promotes timely onset of linker cell engulfment and is required for subsequent phagosome maturation

To define more specifically the defects associated with loss of RAB-35, I imaged *rab-35*(*b1013*) mutants using the microfluidic setup, and quantified hallmark linker cell death and degradation events over > 24h (Table 3-1). I found no significant differences compared to wild-type animals in the onset or duration of developmental milestones (e.g. tail-tip retraction or appearance of rays; Figure 3-14a-c), or in appearance of linker cell death hallmarks (e.g. nuclear crenellation; Figure 3-14d-i). However, competitive phagocytosis of the linker cell begins prematurely in *rab-35* mutants (Figure 3-15a), initiating before the linker cell has the opportunity to intercalate between the U.l/rp cells (Figure 3-15b). While subsequent linker cell splitting occurs at the same time as in wild-type animals (Figure 3-14g), formation of the larger refractile corpse is delayed (Figure 3-15c), and refractility can last much longer (Figure 3-15d). Mutations in *rab-35* delay degradation of the large fragment, if it occurs at all (Figure 3-15e,f). The smaller linker cell fragment is degraded as in the wild type (Figure 3-14h). Thus, RAB-35 plays roles in both engulfment initiation and phagosome maturation.

Consistent with a role in engulfment initiation, I found that RAB-35, tagged with the fluorescent reporter YFP, localizes to extending pseudopods early on, and remains enriched around the larger linker cell-containing phagosome for an extended period of time, until late stages of linker cell degradation (Figure 3-16).

Some aspects of phagosome maturation have been previously characterized. I therefore sought to address where in this process RAB-35 functions. To do so, I first generated animals expressing both YFP-RAB-35 and either mCherry-RAB-5, marking early phagosomes, mCherry-RAB-7, marking late phagosomes, or CTNS-1-mKate2, marking the phagolysosome (Table 3-1). In wild-type animals, RAB-35 and RAB-5 transiently co-localized on the phagosome membrane in 5/6 animals examined (Figure 3-17a-d). In three of six animals, RAB-5 enrichment was seen in only a single

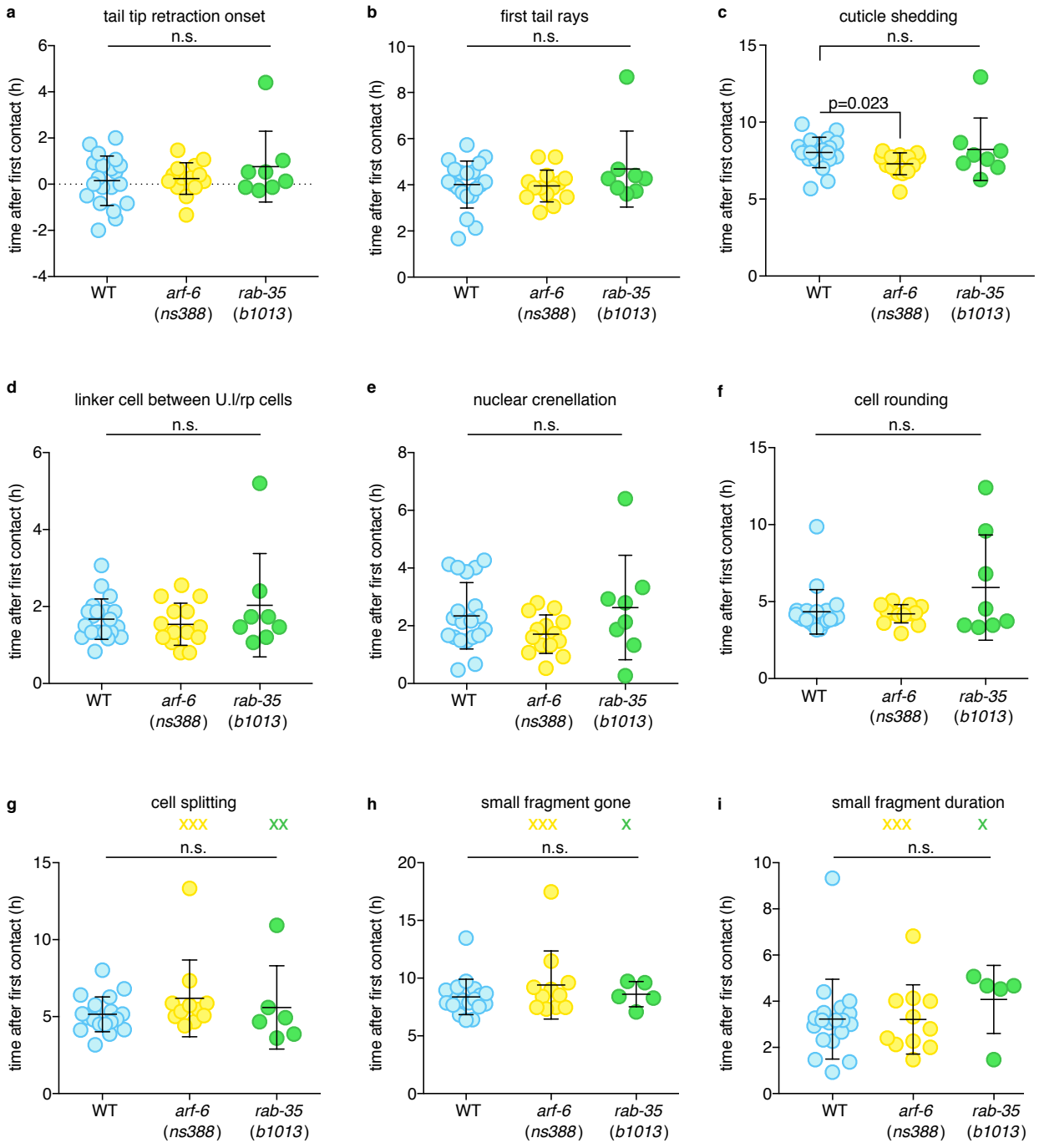

Figure 3-14. **Characterization of stereotypical events during linker cell clearance in *rab-35* and *arf-6* mutants**.

(a-i) Strains contain linker cell reporter [*mig-24*p::Venus], U.l/rp cell reporter [*lin-48*p::mKate2], *him-5*(*e1490*). Dots, individual events in single animals in hours with respect to first contact. X, event did not occur; not factored into statistical analysis. Bars, mean ± std. n.s., p>0.05, Student's t-test.

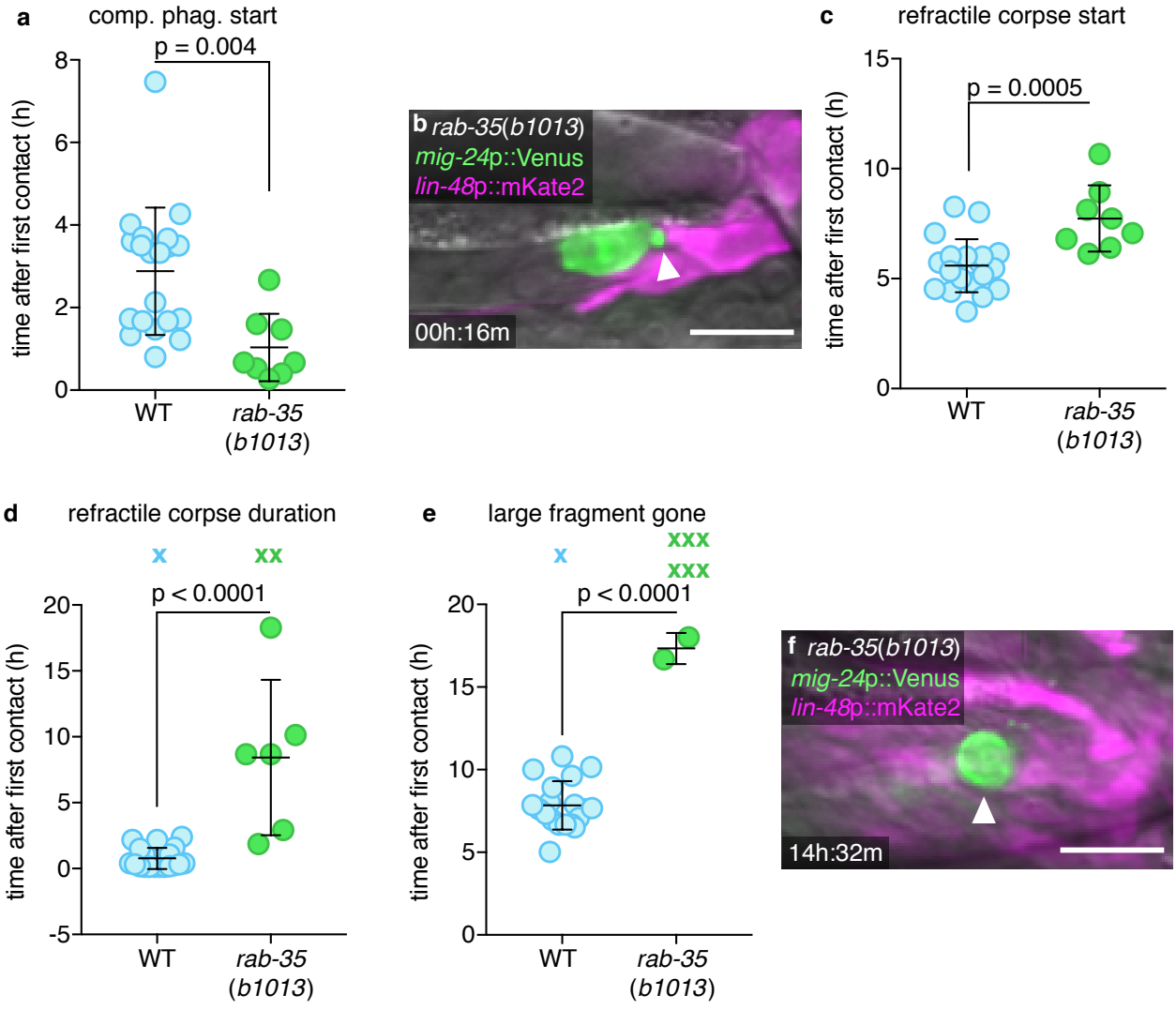

Figure 3-15. **RAB-35 plays roles in both engulfment initiation and phagosome maturation.**

Strains contain linker cell reporter [*mig-24*p::Venus], U.l/rp cell reporter [*lin-48*p::mKate2], *him-5*(*e1490*). (a) Competitive phagocytosis onset in individual animals (circles). Bars, mean ± sd. Student's t-test. WT, wild-type. (b) Arrowhead, early competitive phagocytosis in *rab-35*(*b1013*). (c-e) Quantification of linker cell events as in (a). X, Event persisting or not observed by end of imaging; not included in statistical analysis. (f) Arrowhead, persistent large cell fragment in *rab-35*(*b1013*).

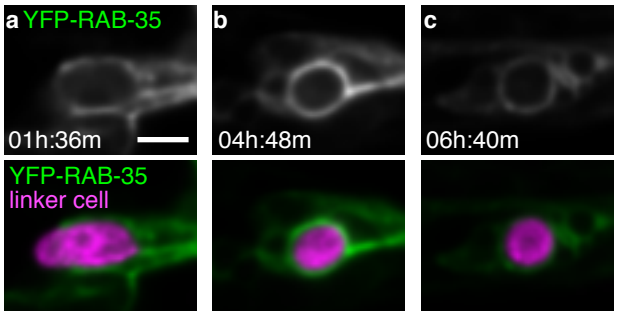

Figure 3-16. **RAB-35 localizes to extending pseudopods and remains around the phagosome.**
Top: Localization of YFP-RAB-35 within U.l/rp cells. Bottom: YFP-RAB-35 (green), and linker cell (*mig-24*p::mKate2; magenta). Scale bar, 5 µm.

frame over a 20h experiment (images acquired every 8 min), suggesting that RAB-5 can move quickly on and off the phagosome membrane. RAB-7 and RAB-35 co-localization is more sustained (Figure 3-18a-d, 7/7 animals). Furthermore, as RAB-35 disappears from the phagosome membrane, mCherry-RAB-7 fluorescence accumulates within the phagosome (Figure 3-18c,d). Such internalization of RAB-7 had not been previously reported in other settings. CTNS-1 and RAB-35 exhibit minimal co-localization (Figure 3-19), suggesting that RAB-35 is removed from the phagosome membrane once lysosomal fusion occurs.

I next examined reporter localization in *rab-35*(*b1013*) mutants. I found that RAB-5 fails to localize to the phagosome membrane in these animals (Figure 3-17e-g, 5/7 animals). Similarly, RAB-7 does not accumulate on the phagosome surface, and is not taken up into the phagosome (Figure 3-18e-g, 5/5 animals).

These studies, therefore, support the idea that RAB-35 acts early in phagosome maturation, and is required for recruiting RAB-5 and RAB-7 for proper degradation to ensue.

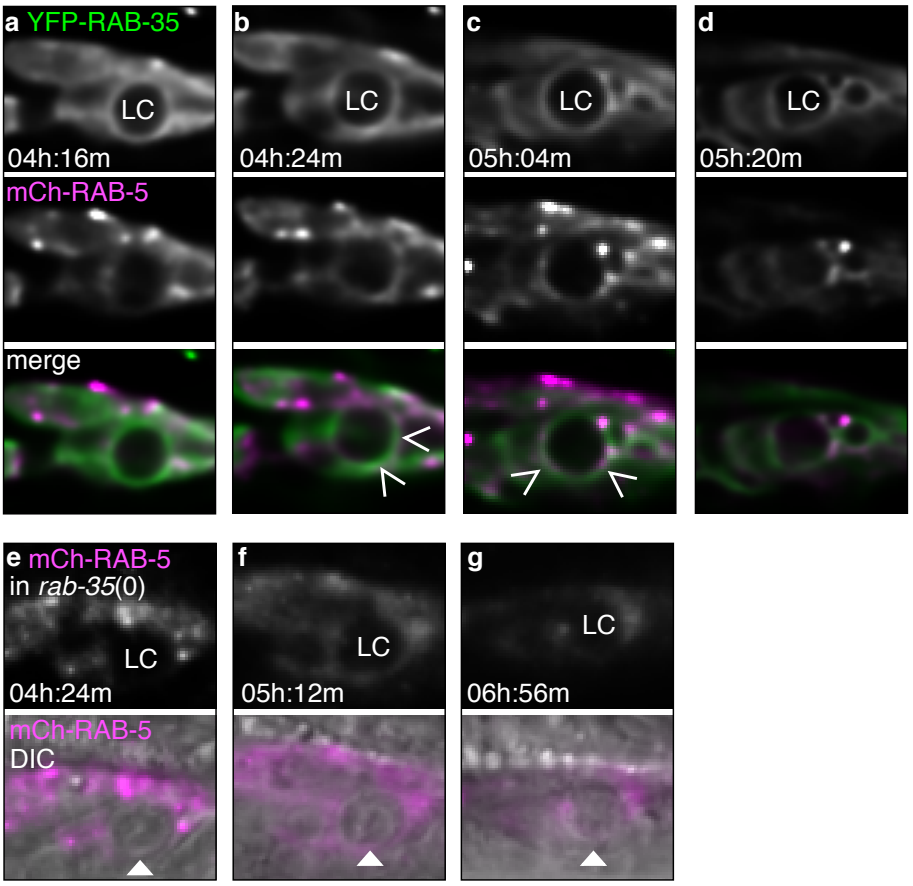

Figure 3-17. **RAB-5 and RAB-35 transiently colocalize around the phagosome.** (a-d) Localization of YFP-RAB-35 (top) and mCherry-RAB-5 (middle) within the U.l/rp cells examined during linker cell (LC) death and degradation in the wild type. Linker cell not fluorescently labeled. Caret, site of colocalization. LC, linker cell. (e-g) mCh-RAB-5 imaged in a *rab-35*(*b1013*) animal (top). Bottom: mCh-RAB-5 overlaid on DIC image. Arrowhead, linker cell. Scale bar, 5 µm.

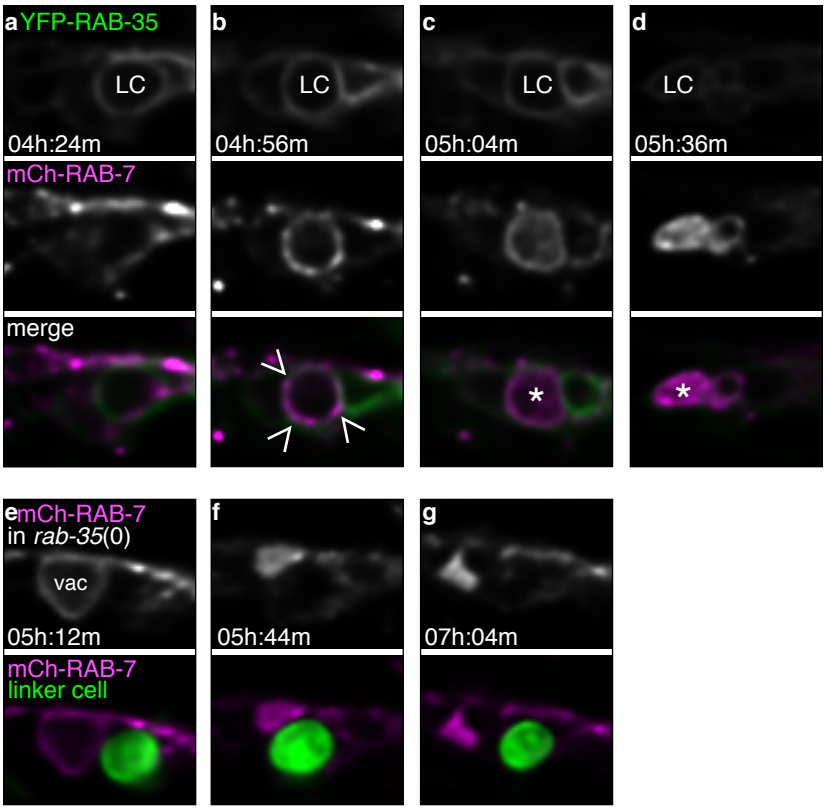

Figure 3-18. **RAB-7 and RAB-35 colocalize around the phagolysosome**.
(a-d) Localization of YFP-RAB-35 (top) and mCherry-RAB-7 (middle) within the U.l/rp cells examined during linker cell (LC) death and degradation in the wild type. Linker cell not fluorescently labeled. Caret, site of colocalization. LC, linker cell. Asterisk, accumulation within phagosome. (e-g) mCherry-RAB-7 (top) fails to surround linker cell in *rab-35*(*b1013*) mutant. Linker cell labeled in green. Scale bar, 5 µm.

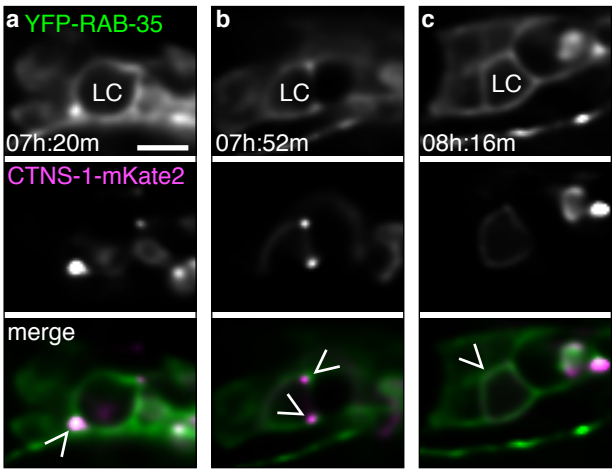

Figure 3-19. **CTNS-1 and RAB-35 have different localization patterns**.
(a-c) Localization of YFP-RAB-35 (top) and CTNS-1-mKate2 (middle) within the U.l/rp cells examined during linker cell (LC) death and degradation in the wild type. Bottom: merge, YFP-RAB-35, green; CTNS-mKate2, magenta. Scale bar, 5 µm. Caret, minimal colocalization between RAB-35 and CTNS-1.

3.5. ARF-6 pathway

3.5.1. The small GTPase ARF-6 blocks linker cell clearance

To delineate the molecular mechanism by which RAB-35 controls linker cell engulfment onset and degradation, I pursued studies of another mutant, *ns388*, isolated in the genetic screen. Animals carrying this lesion have similar linker cell defects to *rab-35* mutants (Figure 3-20a,b), but do not harbor mutations in *rab-35*, *tbc-10*, or *rme-4*.

Using whole genome sequencing and standard genetic mapping, I found that *ns388* animals contain a point mutation predicted to cause a D92N mutation in the small GTPase ARF-6 (Figure 3-21). Importantly, and unlike *rab-35* mutations, a single *arf-6*(*ns388*) allele is sufficient to block linker cell degradation. Thus, *arf-6*(*ns388*) is a dominant allele. The *arf-6*(*tm1447*) putative null allele, which lacks most of the

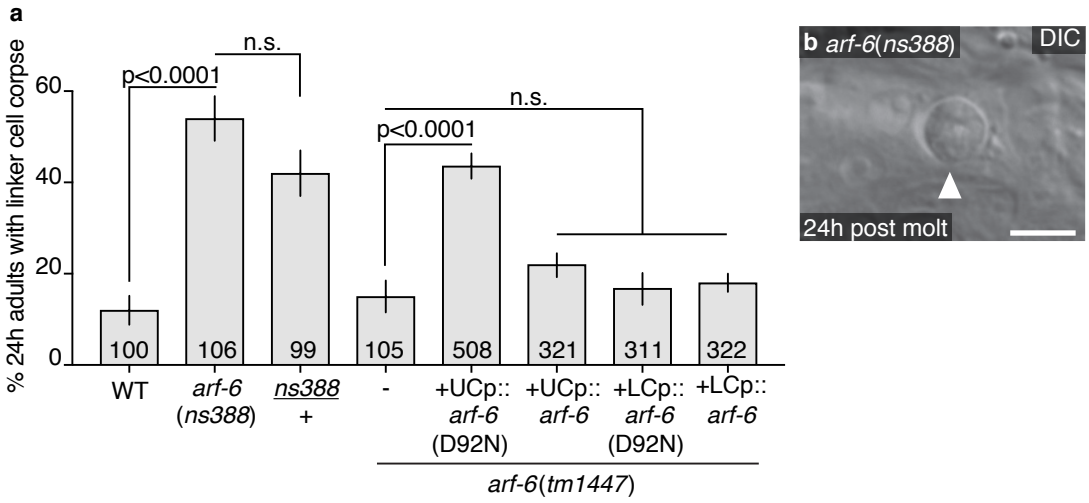

Figure 3-20. ***ns388* is a dominant allele of *arf-6*.**
(a) Linker cell degradation in indicated genotypes. Strains contain *lag-2*p::GFP linker cell reporter and *him-5*(*e1490*). UCp, *lin-48*p. LCp*, mig-24*p. Number of animals scored inside bars. Average of at least three independent lines. Error bars, standard error of the proportion or standard error of the mean. n.s., p>0.05, Fisher's exact test. (b) DIC image of persistent linker cell corpse (arrowhead) in *arf-6*(*ns388*) male. Scale bar, 5 µm.

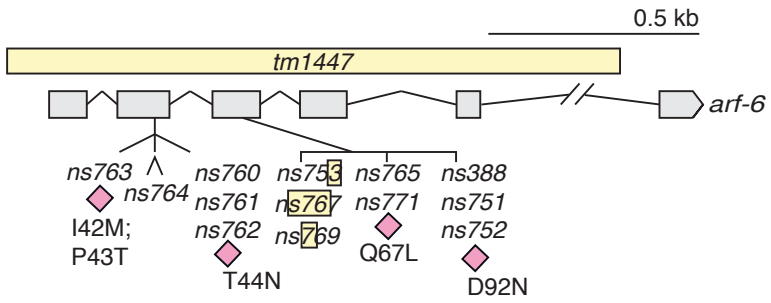

Figure 3-21. ***arf-6* genomic locus and mutant location**.
Yellow box, deletion alleles. Caret, single nucleotide insertion allele *ns764*. Pink diamonds, point mutations.

coding region, and has no ARF-6 expression by Western blot[207], exhibits normal linker cell clearance (Figure 3-20a, 3-21), suggesting that *arf-6*(*ns388*) is a gain-of-function and not a dominant-negative allele. To confirm that *arf-6* is indeed the relevant gene, I generated two independent CRISPR alleles, *ns751* and *ns752*, recreating the *arf-6*(*ns388*) lesion. Both promote linker cell defects similar to those of *arf-6*(*ns388*) mutants (Figure 3-22). Furthermore, while *arf-6* is widely expressed (Figure 3-23),

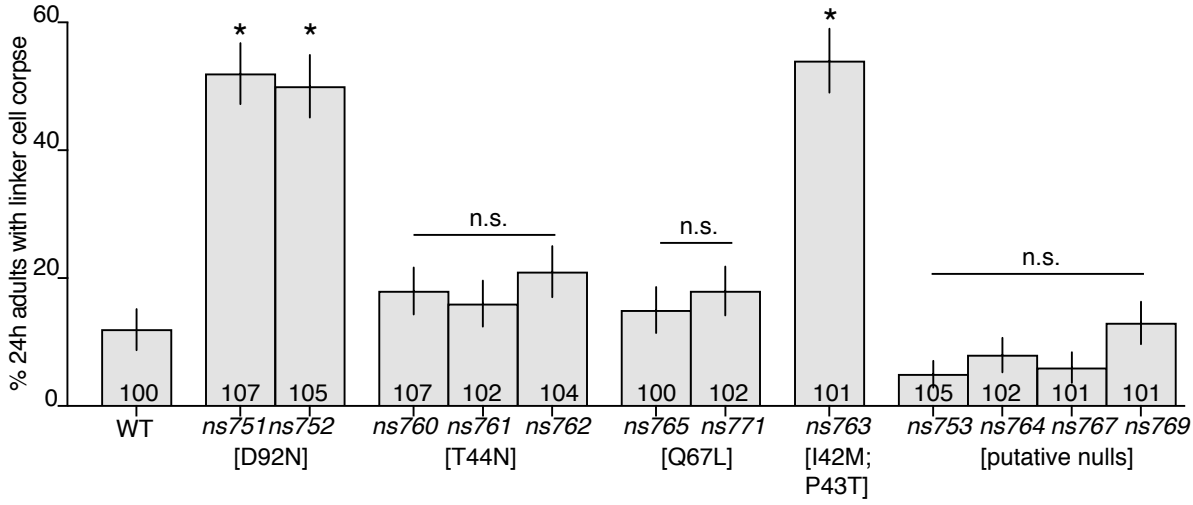

Figure 3-22. **CRISPR generated alleles of *arf-6*.**
Linker cell degradation in indicated genotypes. Strains contain *lag-2*p::GFP linker cell reporter and *him-5*(*e1490*). Number of animals scored inside bars. Error bars, standard error of the proportion. n.s., $p>0.05$; *, $p<0.05$; Fisher's exact test.

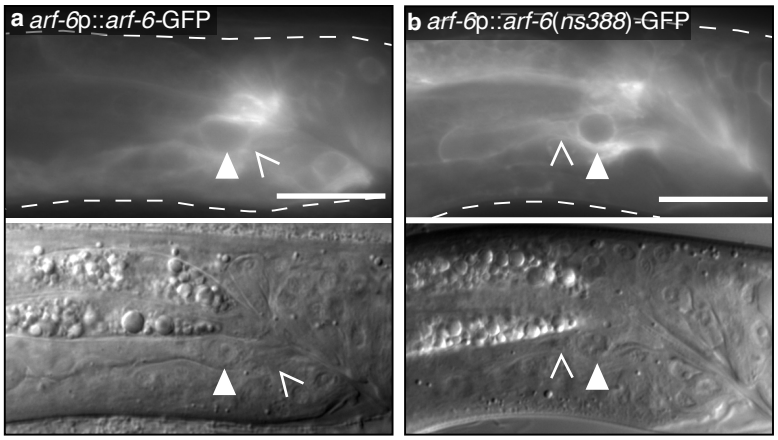

Figure 3-23. **Wild-type *arf-6* and *arf-6*(*ns388*) are broadly expressed**.
(a,b) Arrowhead, linker cell. Caret, U.lp or U.rp cell. Top: GFP; bottom: DIC. Scale bar, 10 µm. (a) *arf-6* translational reporter expression. (b) *arf-6*(*ns388*) translational reporter expression.

expression of an *arf-6*(*ns388*) cDNA in engulfing cells blocks linker cell clearance (Figure 3-20a). Wild-type *arf-6* expression in engulfing cells does not affect linker cell death, nor does expression of either *arf-6*(*ns388*) or *arf-6*(+) cDNAs in the linker cell (Figure 3-20a).

These results, therefore demonstrate that gain of ARF-6 function blocks linker cell clearance, and suggest that ARF-6 normally functions as a linker cell clearance inhibitor.

3.5.2. ARF-6(gf) promotes premature competitive phagocytosis onset and delays linker cell degradation

To understand how ARF-6(gf) interferes with linker cell clearance, I imaged *arf-6*(*ns388*) animals in the microfluidic device and followed hallmark linker cell death and degradation events (Table 3-1). Except for a slight advance in cuticle shedding, no defects in animal development or linker cell killing are seen in *arf-6*(*ns388*) mutants (Figure 3-14). However, as with *rab-35* mutants, premature onset of competitive phagocytosis is observed (Figure 3-24a,b), formation of a refractile linker cell corpse is delayed (Figure 3-24c), and the period of linker cell refractility is prolonged

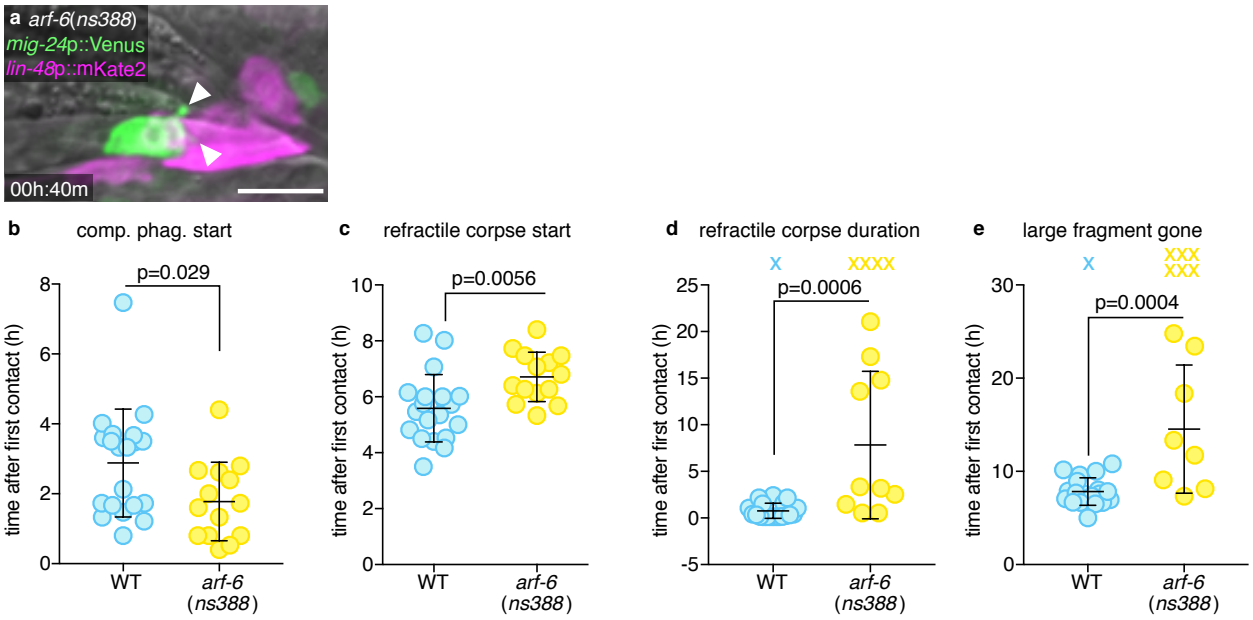

Figure 3-24. ***arf-6*(gf) causes premature competitive phagocytosis and delays large fragment degradation.**

(a) Arrowheads, premature competitive phagocytosis in *arf-6*(*ns388*). Scale bar, 10 µm. (b-e) Quantification of linker cell clearance events in *arf-6*(*ns388*). Strains contain linker cell reporter [*mig-24*p::Venus], U.l/rp cell reporter [*lin-48*p::mKate2], *him-5*(*e1490*). Bars, mean ± sd. Student's t-test. WT, wild-type. X, Event persisting or not observed by end of imaging; not included in statistical analysis.

(Figure 3-24d). Degradation of the large linker cell fragment is greatly delayed, if it occurs at all (Figure 3-24e).

The similar defects exhibited by *arf-6*(*ns388*) and *rab-35* mutants suggests that the proteins encoded by these genes may localize in a similar manner. To test this idea, I expressed ARF-6-YFP in the U.l/rp cells and followed its localization changes during linker cell death and degradation (Figure 3-25a-c). ARF-6-YFP localizes to U.l/rp pseudopods (Figure 3-25a), remains enriched on the phagosome membrane after cell splitting (Figure 3-25b), and then rapidly translocates to intracellular puncta (Figure 3-25c). Importantly, enrichment of mCherry-RAB-5 around the phagosome

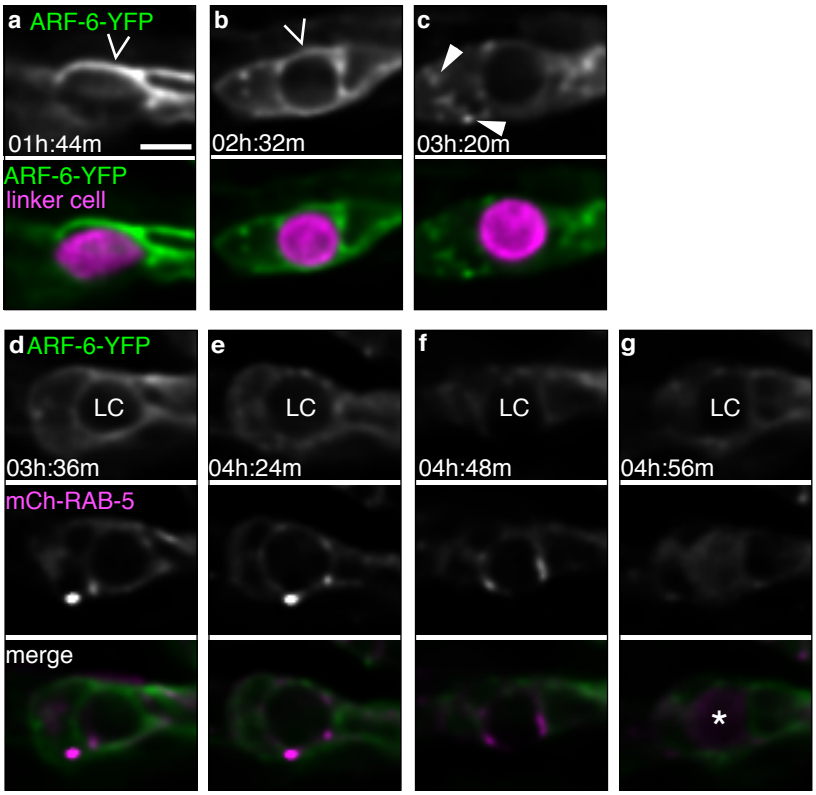

Figure 3-25. **ARF-6-YFP localizes to extending pseudopods, the nascent phagosome, and then translocates to intracellular puncta before RAB-5 enrichment**.
(a-c) Top: Localization of ARF-6-YFP within the U.l/rp cells. Caret, ARF-6 on phagosome membrane. Arrowhead, ARF-6 in intracellular puncta. Bottom: ARF-6-YFP (green), and linker cell (*mig-24*p::mKate2; magenta). (d-g) Localization of ARF-6-YFP (top) and mCherry-RAB-5 (middle). LC, linker cell. Asterisk, accumulation of RAB-5 within phagosome. Scale bar, 5 μm.

occurs after ARF-6-YFP removal (Figure 3-25d-g, 5/6 animals). As with RAB-7, I also observed RAB-5 accumulation in the phagosome interior (Figure 3-25g, 6/6 animals).

Thus, ARF-6 and RAB-35 localize to similar structures surrounding the dying linker cell. However, while RAB-35 normally promotes linker cell degradation, ARF-6 blocks this process.

3.5.3. ARF-6 function is regulated by CNT-1/ACAP2 and EFA-6/EFA6

To understand the dominant nature of the ARF-6(D92N) lesion, I attempted to assess the consequences of locking ARF-6 protein in the GTP or GDP bound states [211]. I used CRISPR to generate *arf-6* mutants encoding T44N and Q67L mutations (Figure 3-22), predicted to accumulate ARF-6[GDP] or ARF-6[GTP] proteins, respectively. Neither mutant, however, has linker cell defects, perhaps because they destabilize the protein. Consistent with this interpretation, the *arf-6*(Q67L) allele behaves as a null in genetic assays (see below). I did however, serendipitously isolate from the CRISPR mutagenesis an *arf-6*(I42M;P43T) double mutant with linker cell clearance defects. Based on an Arf6:Arf6GAP co-crystal protein structure [212], these lesions may interfere with GAP binding to ARF-6, and subsequent GTP hydrolysis. D92 of Arf6 forms intramolecular hydrogen bonds with R95 (Figure 3-26a). In the D92N mutant, these hydrogen bonds are lost (Figure 3-26b), which may result in loss of stability of adjacent interactions. Both P43 and I42 of Arf6 form hydrophobic interactions with W451 and I462 on the ArfGAP (Figure 3-26c). These interactions are lost in the P43T;I42M mutations (Figure 3-26d). Therefore, ARF-6[GTP] appears to inhibit

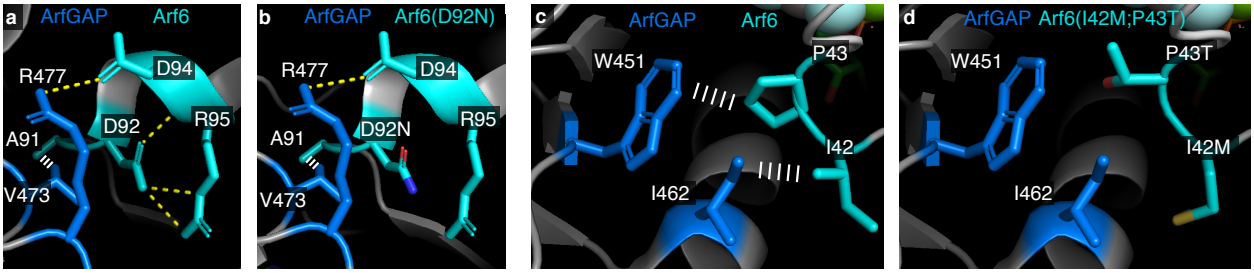

Figure 3-26. **Mutations in ARF-6 are predicted to disrupt ArfGAP binding**. (a) Protein structures of human Arf6 (teal) and ArfGAP (blue) from [209]. PDB: 3LVQ. Relevant amino acids indicated in white. Yellow dotted line, hydrogen bonds. White ladder, hydrophobic interactions. Amino acids shown are conserved in *C. elegans* ARF-6 and CNT-1. (b) D92N mutation mapped onto Arf6. Protein structure information as in (a). (c) Different region of Arf6 and ArfGAP. Protein structure information as in (a). (d) I42M, P43T mutations mapped onto Arf6.

phagosome maturation during linker cell clearance, and the mutants I isolated may hinder GAP binding.

To test this idea further, I reasoned that mutations in a relevant ARF-6 GAP would exhibit linker cell clearance defects, as they would lock ARF-6 in the GTP-bound state. From a screen of candidate mutations (Figure 3-27a, Table 3-3), we found that two independent putative null alleles of *cnt-1*, encoding a ubiquitously-expressed

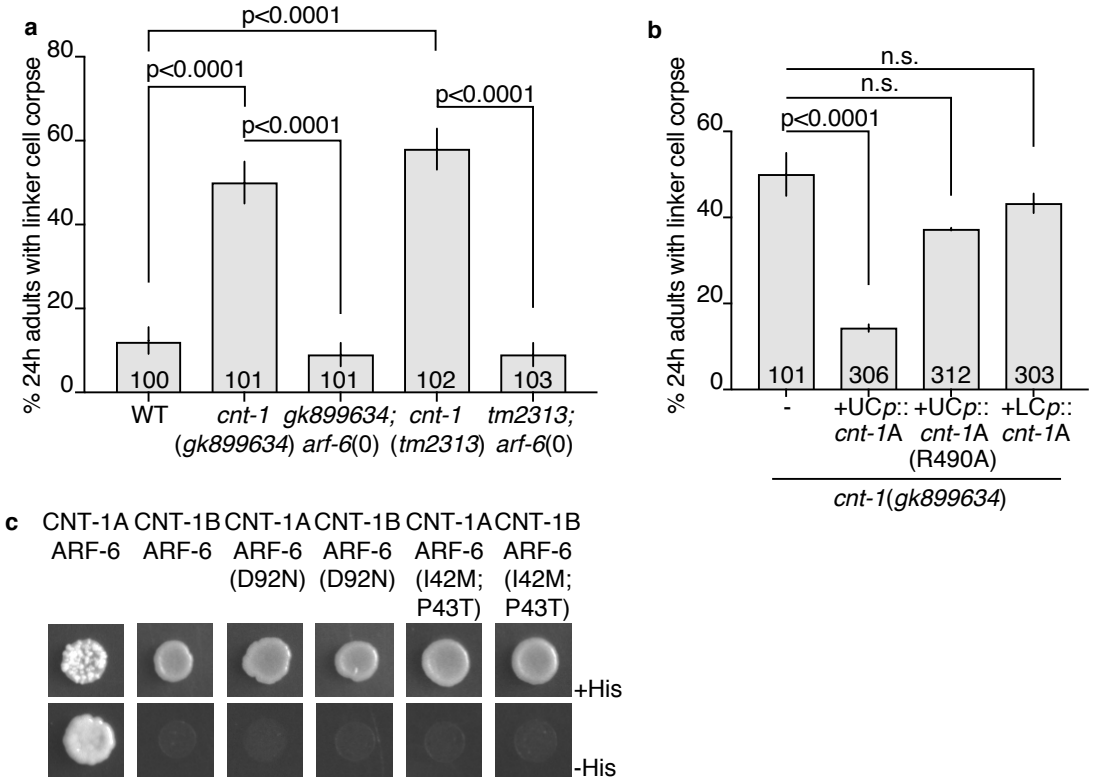

Figure 3-27. **CNT-1A is the relevant ARF-6 GTPase activating protein (GAP).** (a,b) Linker cell degradation in indicated genotypes. Strains contain *lag-2*p::GFP linker cell reporter and *him-5*(*e1490*). UCp, *lin-48*p. LCp*, mig-24*p. Number of animals scored inside bars. Average of at least three independent lines. Error bars, standard error of the proportion or standard error of the mean. n.s., p>0.05, Fisher's exact test. (c) Yeast two-hybrid assay with LexA-CNT-1A or LexA-CNT-1B as bait, GAD-ARF-6, GAD-ARF-6(D92N) or GAD-ARF-6(I42M,P43T) as prey. Top: histidine present. Bottom: histidine absence. Growth on -His plates indicates physical interaction.

Table 3-3. **Other putative ARF-6 GAPs have no linker cell defect** (mean ± SE of proportion).

Genotype	% linker cell corpses in 24h adults	N	homolog
WT	12 ± 3.2	100	
F23H11.4(*gk585084*)	8 ± 4.3	39	ARAP1-3/ ArfGAP
F23H11.4(*gk165637*)	13 ± 3.4	96	ARAP1-3/ ArfGAP
git-1(*ok1848*)	10 ± 3.9	59	GIT1
git-1(*gk392605*)	15 ± 5.6	41	GIT1
gap-2(*ok1001*)	10 ± 4.2	52	SynGAP/RasGAP
cnt-2(*gm377*)	12 ± 3.2	102	ArfGAP

All animals carried a *him-5*(*e1490*) mutation and *qIs56*[*lag-2*p::GFP] linker cell marker.

protein similar to vertebrate Acap2, block linker cell clearance (Figure 3-27a, 3-28a,b). Expression of the CNT-1A isoform in U.l/rp cells, but not the linker cell, fully rescues linker cell defects of *cnt-1* mutants (Figure 3-27b); whereas CNT-1B expression gives partial rescue (Figure 3-28c). Rescue is abolished by mutating the catalytic arginine of CNT-1A (Figure 3-27b). Importantly, ARF-6 is required for the linker cell defects of *cnt-1* mutants, as an *arf-6*(*tm1447*) loss-of-function mutation restores linker cell clearance to *cnt-1* mutants (Figure 3-27a). Consistent with the idea that the D92N and I42M;P43T mutations disrupt GAP binding, I found that while wild-type ARF-6 interacts with CNT-1A (but not CNT-1B) in a yeast two-hybrid assay; both ARF-6(D92N) and ARF-6(I42M;P43T) fail to interact with CNT-1A (Figure 3-27c). Thus, ARF-6[GTP] is likely the active form of the protein blocking linker cell removal, and CNT-1 is the ARF-6 GAP for linker cell clearance.

Similar reasoning used to identify TBC-10 as a RAB-35 GAP allowed me to identify EFA-6, homologous to the mammalian Arf6 GEF Efa6 [210], as the putative ARF-6 GEF for linker cell clearance. While the *efa-6*(*ok3533*) deletion allele has no linker cell degradation defect, this allele restores linker cell clearance to mutants carrying null alleles of *cnt-1* (Figure 3-29a; *cnt-1*(*tm2313*); *efa-6*(*ok3533*): 14 ± 3.4%, N = 102, $p<0.0001$ compared to *cnt-1*(*tm2313*), Fisher's exact test).

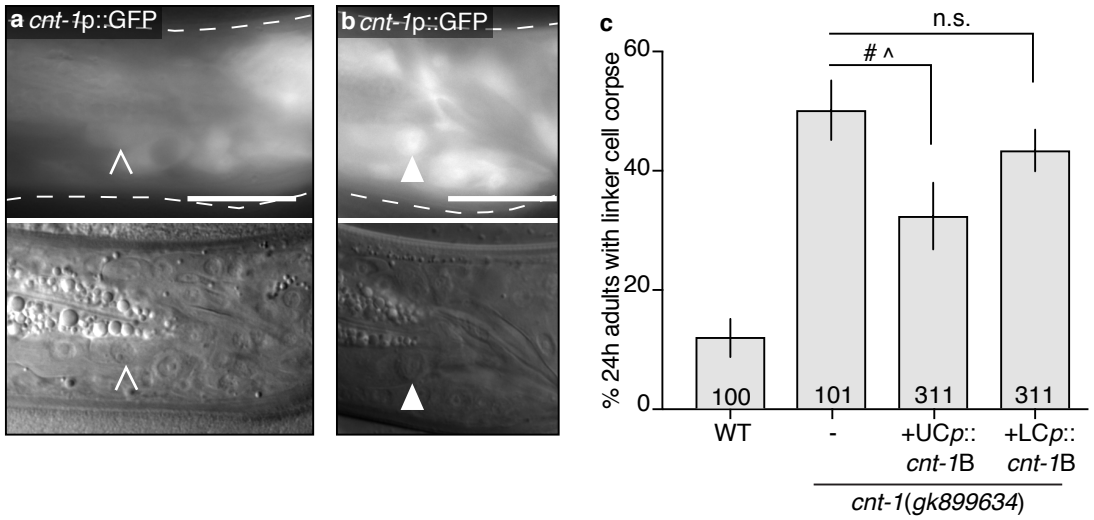

Figure 3-28. ***cnt-1* is ubiquitously expressed, and CNT-1B is not involved in linker cell corpse removal.**

(a,b) *cnt-1* transcriptional reporter expression. Caret, U.lp or U.rp cell. Arrowhead, linker cell. Top: GFP; bottom: DIC. Scale bar, 10 µm. (c) Linker cell degradation in indicated genotypes. Strains contain *lag-2*p::GFP linker cell reporter and *him-5*(*e1490*). UCp, *lin-48*p. LCp*, mig-24*p. Number of animals scored inside bars. Average of at least three independent lines. Error bars, standard error of the proportion or standard error of the mean. n.s., p>0.05, Fisher's exact test. #, significantly different from both *cnt-1*(*gk899634*) and wild type. ^, only two lines out of three show significant rescue.

Furthermore, *efa-6*(*ok3533*) also blocks the dominant defects of *arf-6*(*ns388*) and *arf-6*(*ns763*[I42M;P43T]) mutants, strengthening our assessment that ARF-6 GTP loading is required for the function of these ARF-6 gain-of-function proteins (Figure 3-29a,c). While EFA-6 is expressed in the linker cell and U.l/rp cells (Figure 3-29b), expression of EFA-6 isoforms in the U.l/rp cells partially restores linker cell clearance defects to *efa-6*(*ok3533*); *arf-6*(*ns388*) double mutants (Figure 3-29c). Furthermore, EFA-6 isoforms interact with ARF-6[GDP] in a yeast two-hybrid assay (Figure 3-29d).

Taken together, these results suggest that ARF-6 inhibits linker cell phagocytosis onset, and blocks linker cell degradation together with its regulators EFA-6/GEF and CNT-1A/GAP.

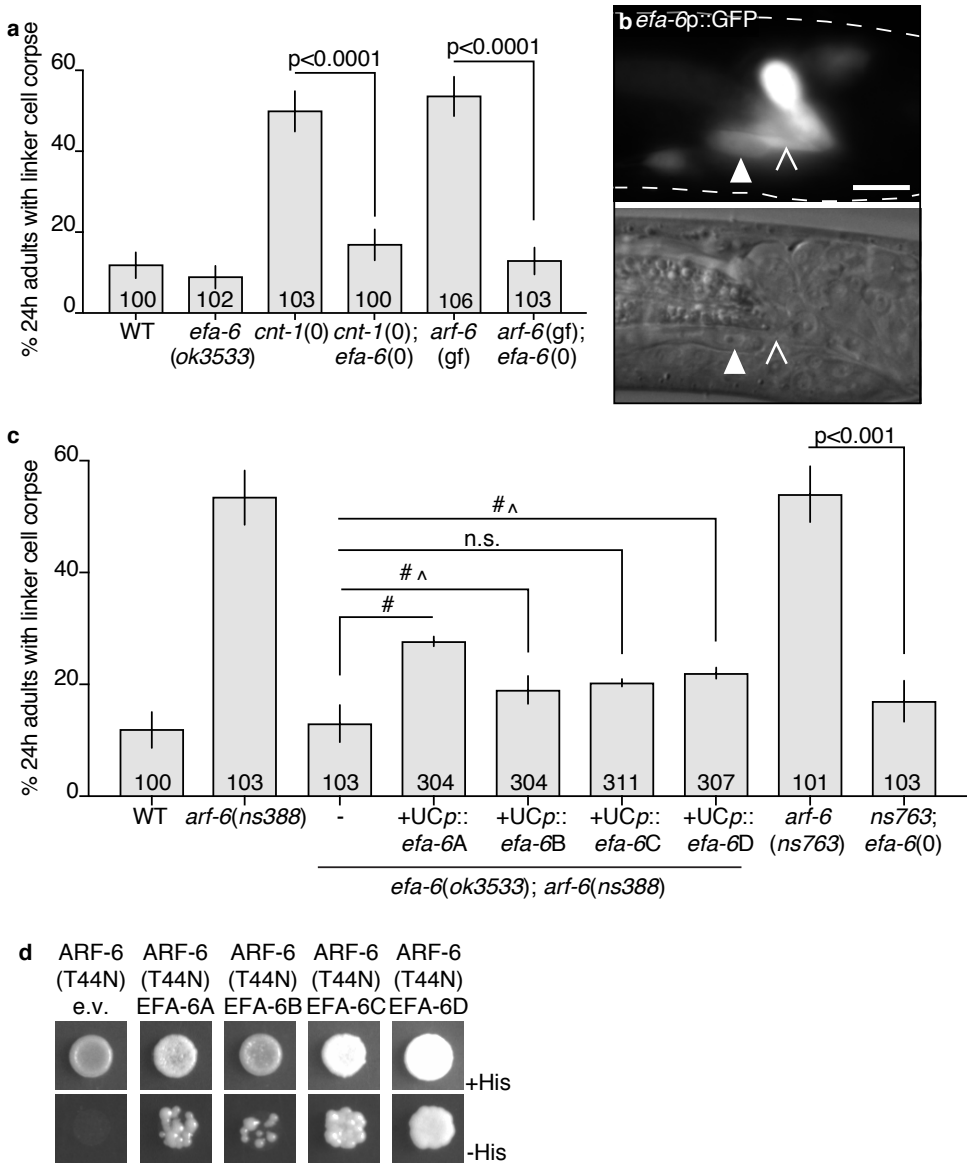

Figure 3-29. **EFA-6 is the relevant ARF-6 guanine nucleotide exchange factor.** (a) Linker cell degradation in indicated genotypes. Strains contain *lag-2*p::GFP linker cell reporter and *him-5*(*e1490*). Number of animals scored inside bars. Error bars, standard error of the proportion. Fisher's exact test. (b) *efa-6* transcriptional reporter. Caret, U.lp or U.rp cell. Arrowhead, linker cell. Top: GFP; bottom: DIC. Scale bar, 10 µm. (c) Histogram as in (a). UC*p* = *lin-48*p. Error bars represent standard error of the proportion or standard error of the mean. Average of at least three independent lines. #, significantly different from both *efa-6*(*ok3533*); *arf-6*(*ns388*) and *arf-6*(*ns388*). ^, only one line out of three show significant rescue. n.s., p>0.05. (d) Yeast two-hybrid assay with LexA-ARF-6[T44N] (GDP) as bait, GAD-EFA-6A-D as prey. Top: histidine present. Bottom: histidine absence. Growth on -His plates indicates physical interaction.

3.6. RAB-35 negatively regulates ARF-6 in linker cell corpse clearance

3.6.1. RAB-35 binds CNT-1A and drives ARF-6 removal from phagosome membranes

rab-35(0) and *arf-6*(gf) mutants exhibit similar linker cell clearance defects. I wondered, therefore, whether RAB-35 and ARF-6 proteins act in the same pathway. I found that putative null mutations in *arf-6* or *efa-6* almost fully restore linker cell clearance to *rab-35* mutants (Figure 3-30, 3-31a). The *arf-6*[Q67L] CRISPR mutant also suppresses *rab-35*(0) defects (Figure 3-31b), confirming this allele inactivates ARF-6 and is not an ARF-6[GTP] mimetic (see above). Linker cell clearance defects are restored to *rab-35*(*b1013*); *arf-6*(*tm1447*) double mutants by expressing wild-type *arf-6* in U.l/rp cells, but not in the linker cell (Figure 3-31c). Furthermore, neither mutations in *cnt-1* nor the dominant *arf-6* allele enhance the linker cell defects of *rab-35* mutants (Figure 3-31d). Finally, overexpression of YFP-RAB-35 in engulfing cells

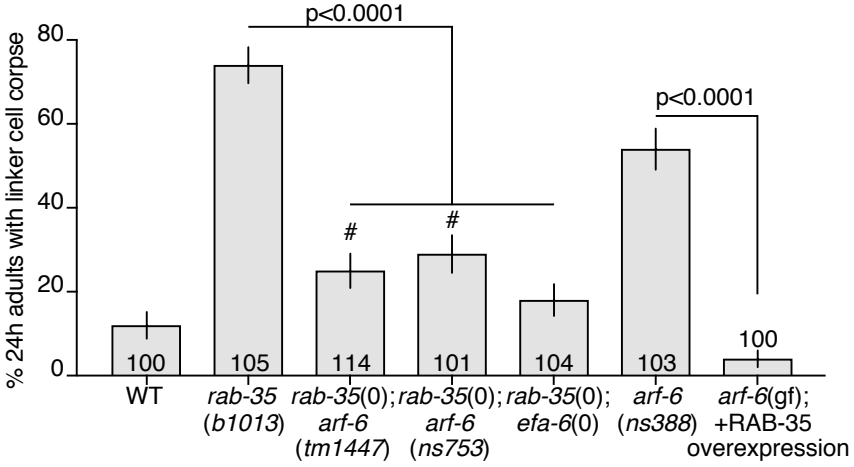

Figure 3-30. **RAB-35 inhibits ARF-6.**
Linker cell degradation in indicated genotypes. Strains contain *lag-2*p::GFP linker cell reporter and *him-5*(*e1490*). Number of animals scored inside bars. Error bars, standard error of the proportion. Fisher's exact test. #, significant difference compared to *rab-35*(*b1013*) and wild type.

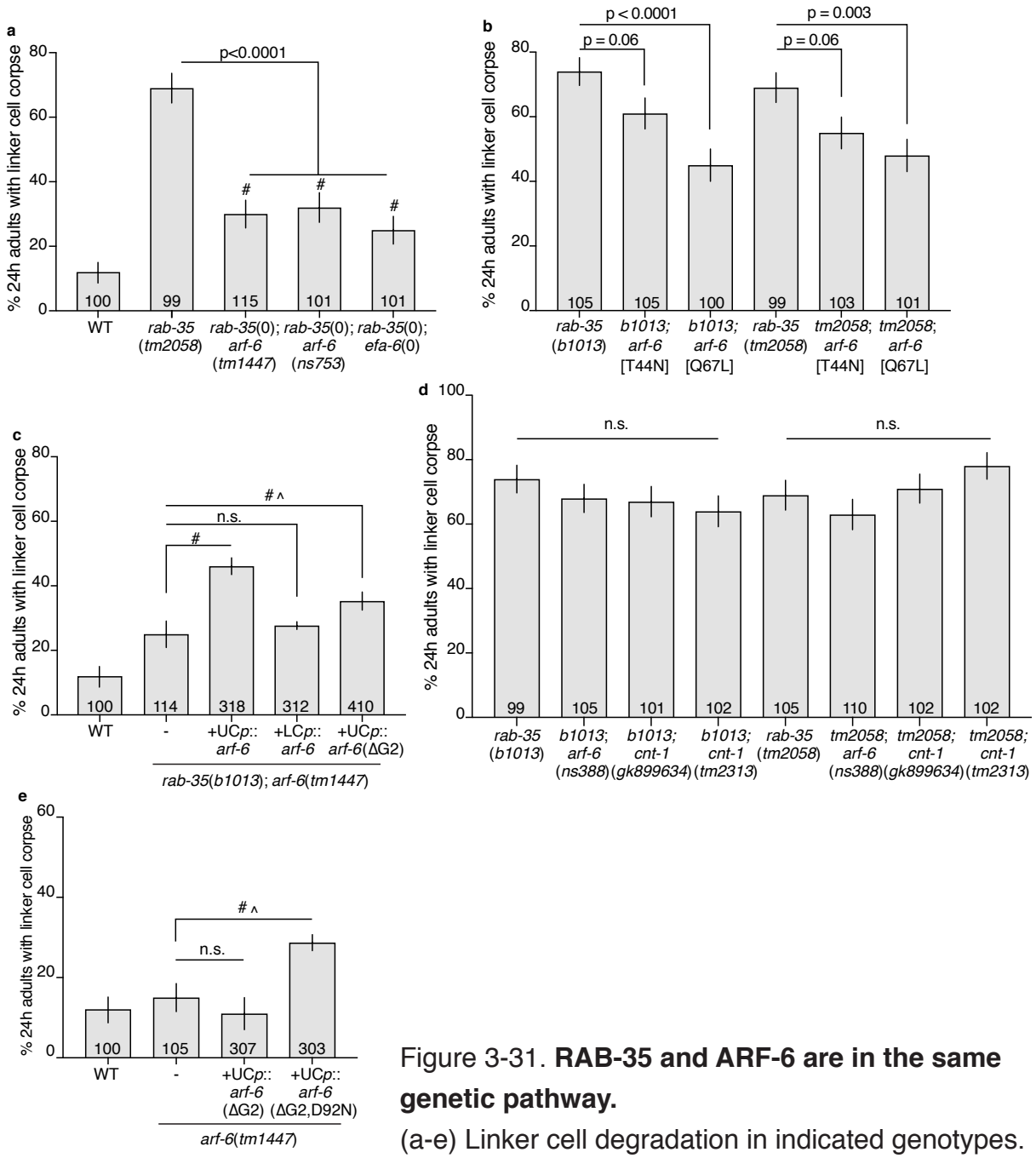

Figure 3-31. **RAB-35 and ARF-6 are in the same genetic pathway.**

(a-e) Linker cell degradation in indicated genotypes. Strains contain *lag-2*p::GFP linker cell reporter and *him-5*(*e1490*). UCp, *lin-48*p. LCp*, mig-24*p. Number of animals scored inside bars. Average of at least three independent lines. Error bars, standard error of the proportion or standard error of the mean. n.s., p>0.05, Fisher's exact test. ΔG2 = deletion of glycine2, necessary for myristoylation. #, (a) significantly different from single mutants, (c) significantly different from both *rab-35*(*b1013*); *arf-6*(*tm1447*) and *rab-35*(*b1013*), or (e) significantly different from both *arf-6*(*tm1447*) and *arf-6*(*ns388*). ^, only 2/4 lines showed significant rescue.

restores linker cell clearance to *arf-6*(*ns388*) mutants (Figure 3-30a). Taken together, these results suggest that RAB-35 normally functions to inactivate ARF-6.

To understand how RAB-35 inhibits ARF-6, I first imaged mKate2-RAB-35 and ARF-6-YFP localization in the same animal. Consistent with the other imaging studies, the two proteins initially co-localize to extending U.l/rp cell pseudopods (Figure 3-32a,b). RAB-35 then accumulates on the phagosome membrane, while ARF-6 enrichment fades (Figure 3-32c,d, 8/9 animals). Next, I examined ARF-6-YFP dynamics in *rab-35*(*b1013*) animals (Figure 3-32e-h). Remarkably, I found that ARF-6-YFP remains

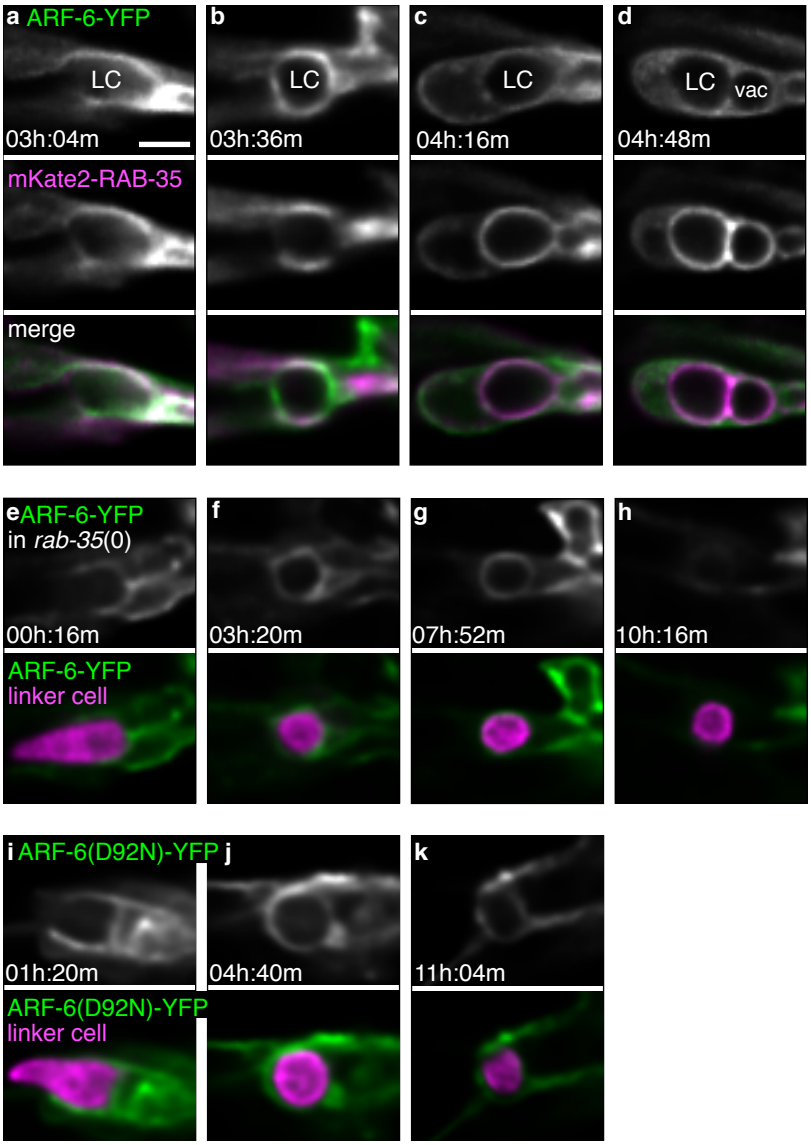

Figure 3-32. **RAB-35 removes ARF-6 from phagosome membranes**. (a-d) Localization of ARF-6-YFP (top) and mKate2-RAB-35 (middle) within the U.l/rp cells examined during linker cell (LC) death and degradation in the wild type. Bottom: merge, ARF-6-YFP, green; mKate2-RAB-35, magenta. Scale bar, 5 µm. (e-h) ARF-6-YFP localization in *rab-35*(*b1013*) mutant. LC labeled in magenta. Scale bar, 5 µm. (i-k) ARF-6(D92N)-YFP localization in otherwise wild-type animals. LC labeled in magenta. Scale bar, 5 µm.

on the membrane longer than in wild type animals (Figure 3-32g,h, 5/6 animals; ARF-6-YFP removed 4.6 ± 0.9h after first contact in wild type animals vs 15.4 ± 9.7 h in *rab-35*(*b1013*) where the corpse persists, p=0.023, Student's t-test). Furthermore, in wild-type animals, ARF-6(D92N) remains enriched on phagosome membranes longer than ARF-6-YFP (Figure 3-32i-k, 4/4 animals; 19.1 ± 11.4h after first contact, p=0.01 compared to WT, Student's t-test).

These results raise the possibility that RAB-35 promotes linker cell clearance, at least in part, by facilitating ARF-6 removal from the phagosome. Consistent with this notion, an ARF-6(D92N) gain-of-function protein is more effective in blocking linker cell clearance than ARF-6(D92N) lacking a myristoyl group addition sequence, required for membrane localization [214] (Figure 3-31e).

To determine whether ARF-6 localization is regulated by direct binding to RAB-35, I assessed their interactions in a yeast two-hybrid system. While I did not detect any interactions between these two proteins, I found that RAB-35[GTP], the active form of RAB-35, binds CNT-1A (and not CNT-1B) (Figure 3-33). Thus, RAB-35 may recruit CNT-1A to phagosome membranes, catalyzing conversion of active ARF-6[GTP] to inactive ARF-6[GDP].

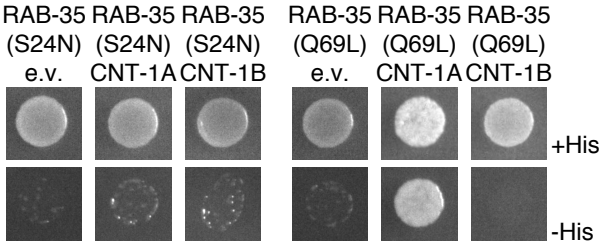

Figure 3-33. **RAB-35 interacts with the ARF-6 GAP, CNT-1A.**
Yeast two-hybrid assay with LexA-RAB-35[S24N] (GDP) or LexA-RAB-35[Q67L] (GTP) as bait, Gal4-AD (GAD)empty vector, GAD-CNT-1A, or GAD-CNT-1B as prey. Top: histidine present. Bottom: histidine absence. Growth on -His plates indicates physical interaction.

3.6.2. The RAB-35/ARF-6 module is not required for apoptotic cell clearance

Given the roles of RAB-35 and ARF-6 in the clearance of a cell dying by LCD, I wondered whether these proteins play similar roles in apoptotic cell clearance. To test this, I counted the number of persisting apoptotic cells in 3-fold embryos, after nearly all developmental cell death has taken place. In *him-5* mutant control animals, I counted 0.10 ± 0.30 persisting refractile corpses on average (N=21). In *arf-6*(*ns388*) mutants, 0.47 ± 0.60 corpses were observed (N=21, p=0.0131, Student's t-test). *rab-35*(*b1013*) mutants exhibited 0.81 ± 0.92 corpses, on average (N=21, p=0.0018, Student's t-test). These small defects pale in comparison to defects exhibited by mutants defective in canonical apoptotic engulfment genes (e.g. *ced-7; ced-10* double mutant: 16.8 ± 4.2 corpses, N = 11). Furthermore, *rme-4* mutant embryos I tested have no clearance defects (*ns410*: 0.14 ± 0.36 apoptotic corpses, N=14; *ns412*: 0.13 ± 0.33 apoptotic corpses, N=24). I also examined whether *rab-35* mutations exhibit genetic interactions with canonical apoptosis engulfment genes in linker cell death, but found no such interactions (Table 3-4).

Our results, therefore, demonstrate that the RAB-35/ARF-6 module plays specific roles in dismantling the linker cell that are not shared with clearance of apoptotic cells in *C. elegans*.

3.7. Discussion

3.7.1. A New Engulfment and Degradation Pathway for Non-Apoptotic Dying Cells

In this section, I demonstrate that the clearance machinery promoting the removal of the linker cell, which dies by LCD, differs from that used to clear apoptotic cells in *C. elegans*. These studies uncover a protein network promoting linker cell

Table 3-4. **Mutations in the canonical apoptotic engulfment genes *ced-1* and *ced-5* do not enhance mutations in *rab-35.***

(mean ± SE of proportion).

Genotype	% linker cell corpses in 24h adults	N
WT	12 ± 3.2	100
ced-1(*e1735*)	14 ± 3.4	103
ced-5(*n1812*)[a]	12 ± 2.9	125
rab-35(*b1013*)	74 ± 4.2	105
rab-35(*tm2058*)	69 ± 4.6	99
sand-1(*ok1963*)	58 ± 4.8	104
ced-1; *rab-35*(*b1013*)	77 ± 4.2	101
ced-5; *rab-35*(*b1013*)	63 ± 4.8	101
ced-1; *ced-5*; *rab-35*(*b1013*)	62 ± 4.8	103
ced-1; *rab-35*(*tm2058*)	56 ± 4.9	102
ced-5; *rab-35*(*tm2058*)	58 ± 4.9	102
ced-1; *ced-5*; *rab-35*(*tm2058*)	63 ± 4.7	104
sand-1; *rab-35*(*b1013*)[b]	95 ± 2.7	63

[a] = *nsIs1*[*lag-2*p::GFP, *rol-6*(+)]. [b] = animals scored at 36h post L4-adult transition to account for slow growth of double mutant. All animals carried a *him-5*(*e1490*) mutation and a GFP linker cell marker.

engulfment and degradation (Figure 3-34a). I find that RAB-35 and ARF-6 play key early roles, controlling the sequential loading of phagosome maturation factors onto the phagosome membrane (Figure 3-34b). These data are consistent with a model in which RAB-35[GTP] promotes elimination of dying cells by blocking the activity of an inhibitor of the process, ARF-6[GTP]. These studies are the first to implicate a RAB-35/ ARF-6 module in the engulfment and degradation of dying cells, define in detail multiple accessory factors, identify the relevant targets (e.g. RAB-7) and, importantly, explore the functions of these proteins in vivo in a living multicellular animal.

Although I identifed the LCD corpse engulfment pathway in *C. elegans*, a number of studies in other systems raise the possibility that this process may be conserved.

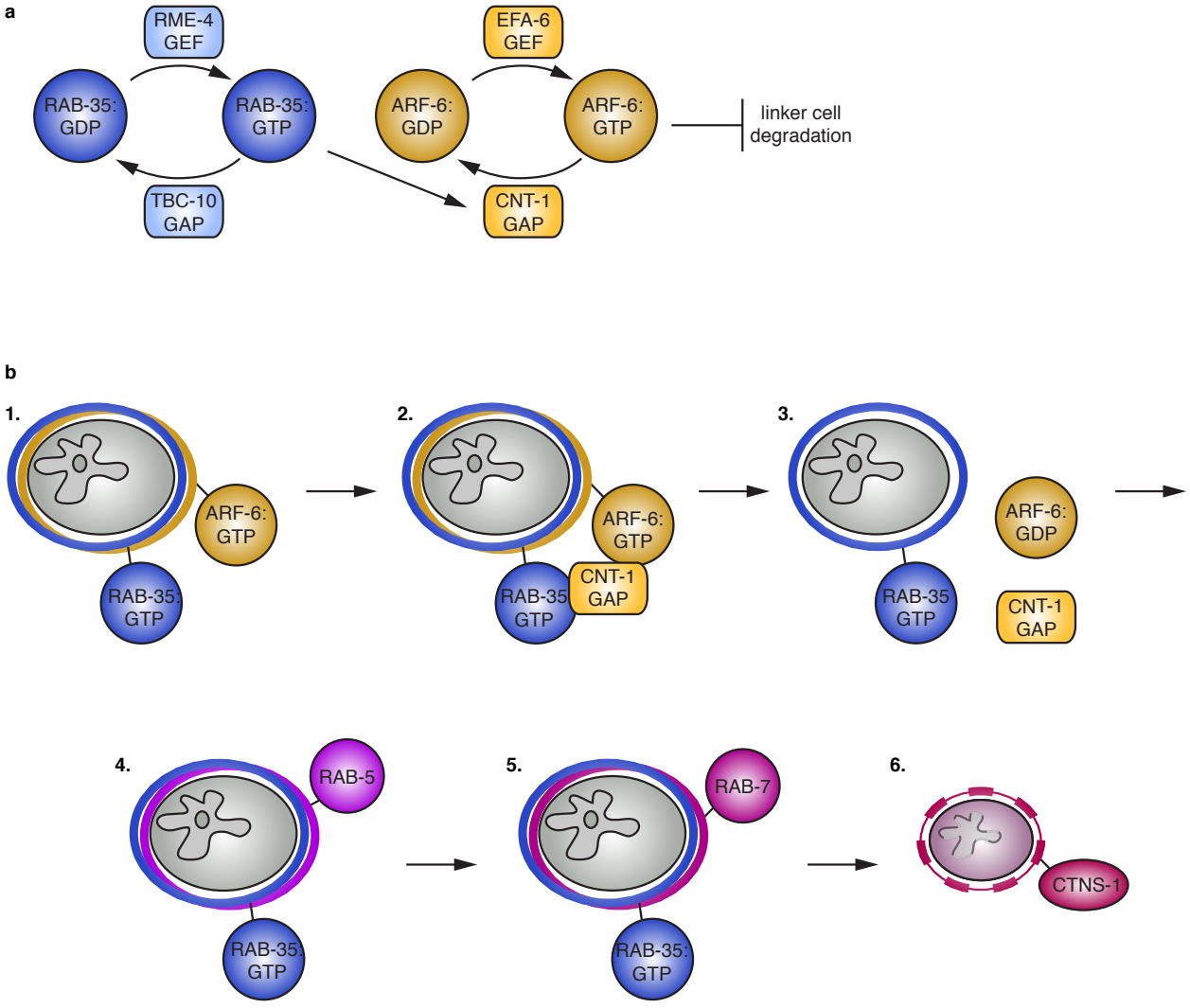

Figure 3-34. **A model for control of linker cell degradation by the RAB-35/ARF-6 module.**

(a) RAB-35:GTP promotes linker cell degradation by interacting with the ARF-6 GAP CNT-1. CNT-1 is required for turning ARF-6 off and removing it from the membrane. ARF-6:GTP inhibits linker cell degradation. GAP, GTPase activating protein. GEF, guanine nucleotide exchange factor. (b) 1. ARF-6 and RAB-35 surround the nascent phagosome. 2. RAB-35 recruits CNT-1. 3. CNT-1 turns off ARF-6, removing it from the phagosome membrane. RAB-35 remains on the membrane. 4. RAB-5 is recruited. 5. RAB-7 recruitment and RAB-5 loss. 6. RAB-35 is largely gone from the membrane once the lysosome (CTNS-1) fuses with the phagosome.

For example, in *Drosophila*, nurse cell death is thought to be caspase independent, and knockdown of RAB-35 results in persistent nurse cell nuclei [72]. While the role of RAB-35 was not further investigated, the involvement of this protein in a non-apoptotic setting is intriguing. Furthermore, concerted activities of RAB-35 and ARF-6 in other contexts have been described, including neurite outgrowth, cytokinesis, oligodendrocyte differentiation, maturation of recycling endosomes, and FcγR-mediated uptake of bacteria by macrophage [215-219]. In some of these cases, interactions between RAB-35 and putative ARF-6 GAPs are seen [220]. Additionally, ARF-6 is known to function in endocytosis of yolk proteins in *C. elegans* [221]. There it works with RAB-10 in a similar regulatory cascade as the one we have uncovered.

3.7.2. New Ways to Generate ARF[GTP] Mimics

My genetic analysis of linker cell engulfment yielded important reagents, likely to be of utility in studying ARF-family proteins. I found that a Q67L mutation in ARF-6, which is predicted to mimic the GTP-bound state of the protein, behaves instead as a functional null in our assay. This modification, effective in the context of other GTPases, may, therefore, result in protein instability, or loss of active conformation. However, I found that the ARF-6(D92N) mutant protein, or a protein carrying two lesions, ARF-6(I42M;P43T), appear to mimic ARF-6[GTP], and if anything, enhance protein stability. Based on the published structure of Arf6 binding to the ArfGAP ASAP3 [212], the D92N mutation is adjacent to a residue that coordinates to a key valine in the ArfGAP, whereas the I42M,P43T double mutations modify residues that directly coordinate to known GAP catalysis residues [212]. I propose that these lesions could keep the protein locked in the GTP-bound state, because they prevent GAP protein binding. This interpretation is bolstered by the protein interaction studies. I propose that introducing similar lesions into other ARF proteins, and perhaps into other GTPases, could allow for the development of new GTP-bound mimetics of these proteins.

3.7.3. Competitive Phagocytosis

In addition to unique molecular components, I found that the mechanics of linker cell engulfment are very different from engulfment of apoptotic cells. The imaging studies reveal a process of competitive phagocytosis, where two phagocytes compete to engulf portions of the linker cell, resulting in cell splitting. RAB-35 acting through ARF-6 prevents premature activation of this engulfment process. As with the molecular constitutes of linker cell engulfment and degradation, I believe that the process of competitive phagocytosis may also be conserved. In macrophage-less mice, for example, mesenchymal cells engulf dying neighbors during digit formation, and occasionally two mesenchymal cells can be seen engulfing the same dying cell in transmission electron microscopy images [222]. Consistent with this process involving new engulfment regulators, mesenchymal cells do not express the CED-7 homolog ABC1 [222]. Similarly, in developing rat cerebellum, more than one non-professional phagocyte can be seen engulfing a dying cell [223]. A related process has been documented during germ cell development in *C. elegans*. Primordial germ cells extend cytoplasm-containing lobes into the adjacent endoderm, and the lobe is excised from the remaining cell, in a process reminiscent of competitive phagocytosis [224].

The need for engulfment by more than one cell could be related to the size of the dying cell. For example, when macrophages attempt to engulf a particle that is too large, engulfment is stalled [225,226]. Engulfment by two or more cells could solve this problem. However, in this case, cytoplasmic spillage must be avoided. The new engulfment process I describe here accomplishes exactly that.

A process reminiscent of competitive phagocytosis can also be seen when cultured human peripheral blood monocytes engulf a *C. albicans* pathogen [227]. Similarly, cultured mouse monocytes simultaneously engulf a *Leishmania* parasite [227].

One cell engulfs the flagellum, while the other engulfs the posterior pole. In this context, roles for RAB-35 in pathogen clearance [178,215,220] are especially intriguing, and may suggest underlying mechanisms similar to linker cell clearance.

In summary, I demonstrate that engulfment and degradation of a cell that dies by LCD requires mechanics and machinery different from that used for apoptotic cell engulfment and degradation, and identify a molecular pathway governing this novel form of cell clearance. Given the conservation of LCD, I propose that this ancillary process may be conserved as well.

4. CED-3 is required for linker cell corpse degradation but not death

The linker cell dies independently of all known cell death genes, including members of the apoptotic pathway [82,83]. Knowing this, I was quite surprised when Holly Johnsen, a graduate student in Bob Horvitz's lab at MIT, came up to me at a meeting to let me know that she had seen *ced-3* transcripts in the linker cell while examining the role of caspase of other cells in the tail. I rechecked the surviving linker cell defects, and confirmed that the cells are still dying by the strict morphological defects to which we adhere. Interestingly, I noticed that *ced-3* and *ced-4* mutants instead had an increased number of cell corpses, suggesting that perhaps these genes are involved in corpse degradation, but not death.

4.1. CED-3 and CED-4 are required for efficient degradation

I reexamined the genes involved in apoptosis and found that the linker cell still dies, as evidenced by a crenellated nuclear envelope (Table 4-1). Instead, linker cell corpses in *ced-3* and *ced-4* animals persist, while corpses in *ced-9* or *egl-1* animals are largely cleared (Figure 4-1). To examine this further, I imaged *ced-3* animals using the microfluidic set up. I found no difference in development events compared to wild-

Table 4-1. **The linker cell dies in the absence of apoptotic genes.**

Genotype	% SLCs (N)
egl-1(*n1084n3082*)[a]	0 (47)
ced-9(*n1950*)[a]	6% (51)
ced-4(*n1162*)	0 (40)
ced-3(*n717*)	0 (47)
ced-3(*n2452*)	0 (45)

[a] = *nsIs1*[*lag-2*p::GFP, *rol-6*(+)]. All animals carried a *him-5*(*e1490*) mutation and a GFP linker cell marker.

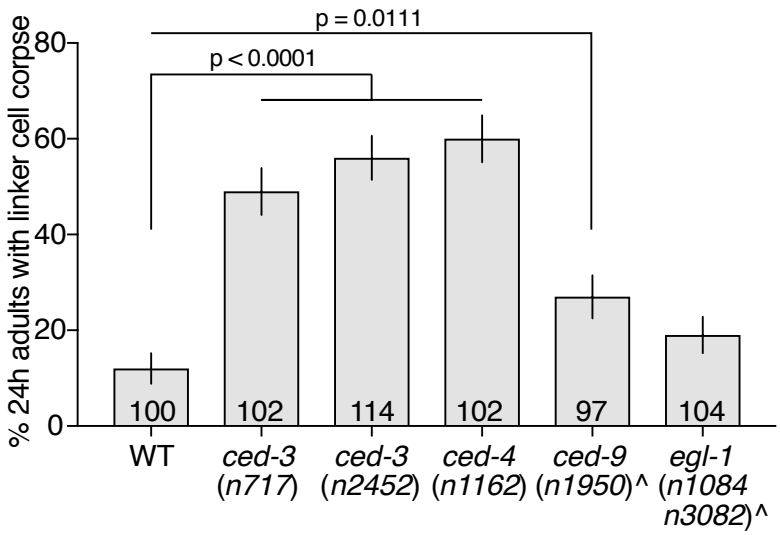

Figure 4-1. **Linker cell corpses in *ced-3* and *ced-4* mutant animals are not degraded**.
Linker cell degradation in indicated genotypes. Strains contain either *lag-2*p::GFP linker cell reporter or *nsIs1*[*lag-2*p::GFP, *rol-6*(+)] (denoted by ^) and *him-5*(*e1490*). Number of animals scored inside bars. Error bars, standard error of the proportion. Fisher's exact test.

type animals (*e.g.* tail tip retraction onset, Figure 4-2a-c). I also found no difference in onset of nuclear crenellation, suggesting that the death kinetics are similar between *ced-3* animals and wild-type animals (Figure 4-2e). I did notice, however, that *ced-3* animals lagged in most aspects of corpse degradation. There was a delay in linker cell corpse rounding, which sometimes never occurred (Figure 4-3a). This result suggests that *ced-3* corpses may have a delay in engulfment, which is corroborated by the observation that cell splitting is delayed in these animals (Figure 4-3b). There was also a delay in the formation and the duration of the refractile corpse (Figure 4-3c,d). Both the small fragment and the large fragment persisted longer than in wild type (Figure 4-3e,f), although the duration of the small fragment was unchanged (Figure 4-2f).

While there is a delay in phagocytosis, *ced-3* corpses are terminally engulfed 24h after the L4 to adult transition (Table 4-2). In agreement with this, *ced-3* mutant males

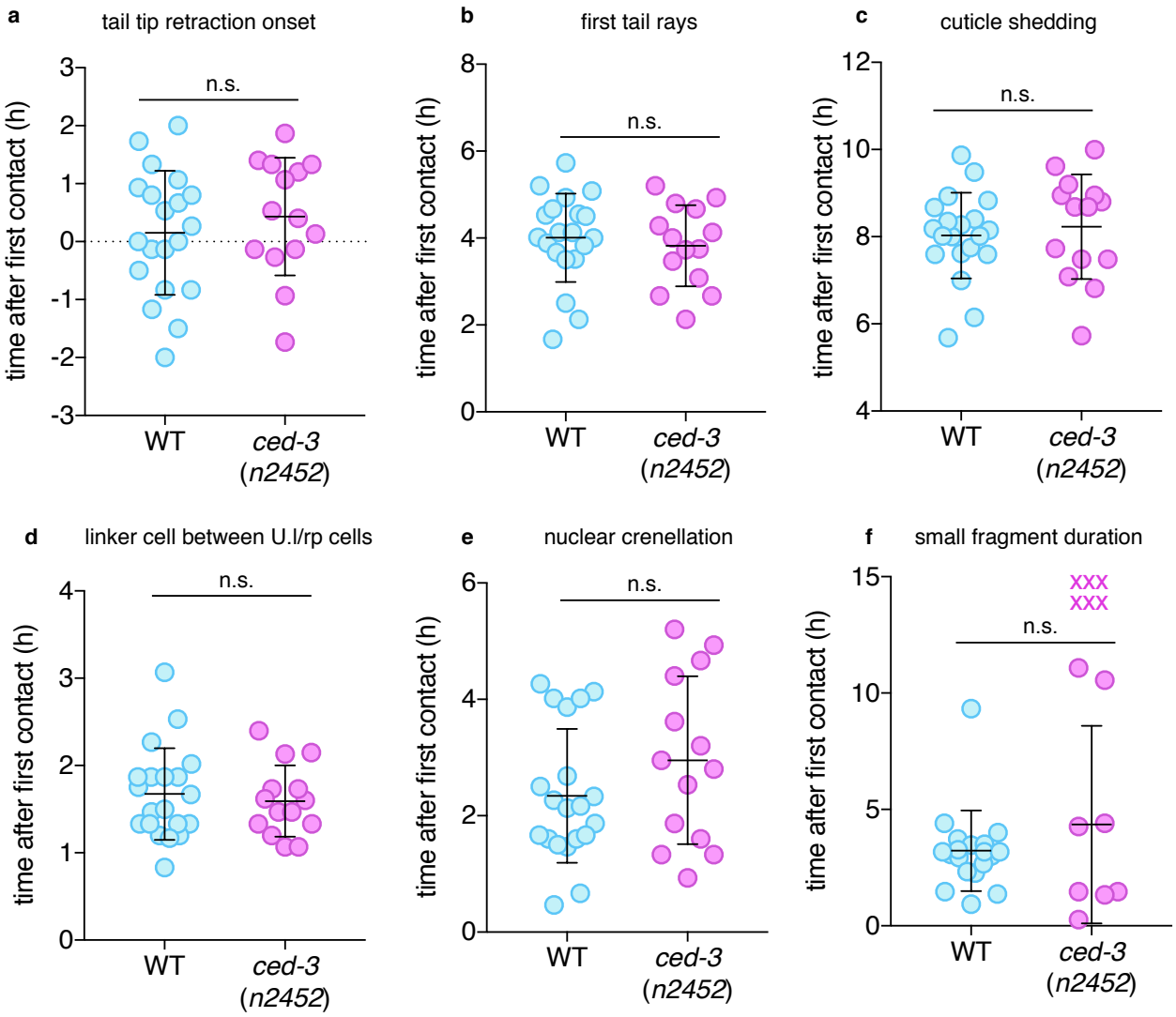

Figure 4-2. ***ced-3* mutations do not affect male developmental events**.
(a-f) Strains contain linker cell reporter [*mig-24*p::Venus], U.l/rp cell reporter [*lin-48*p::mKate2], and *him-5*(*e1490*) for males. Dots, individual events in single animals in hours with respect to first contact. X, event did not occur and was not factored into statistical analysis. Bars, mean ± std. n.s., p>0.05, Student's t-test. Wild type (WT) same animals as in Chapter 3.

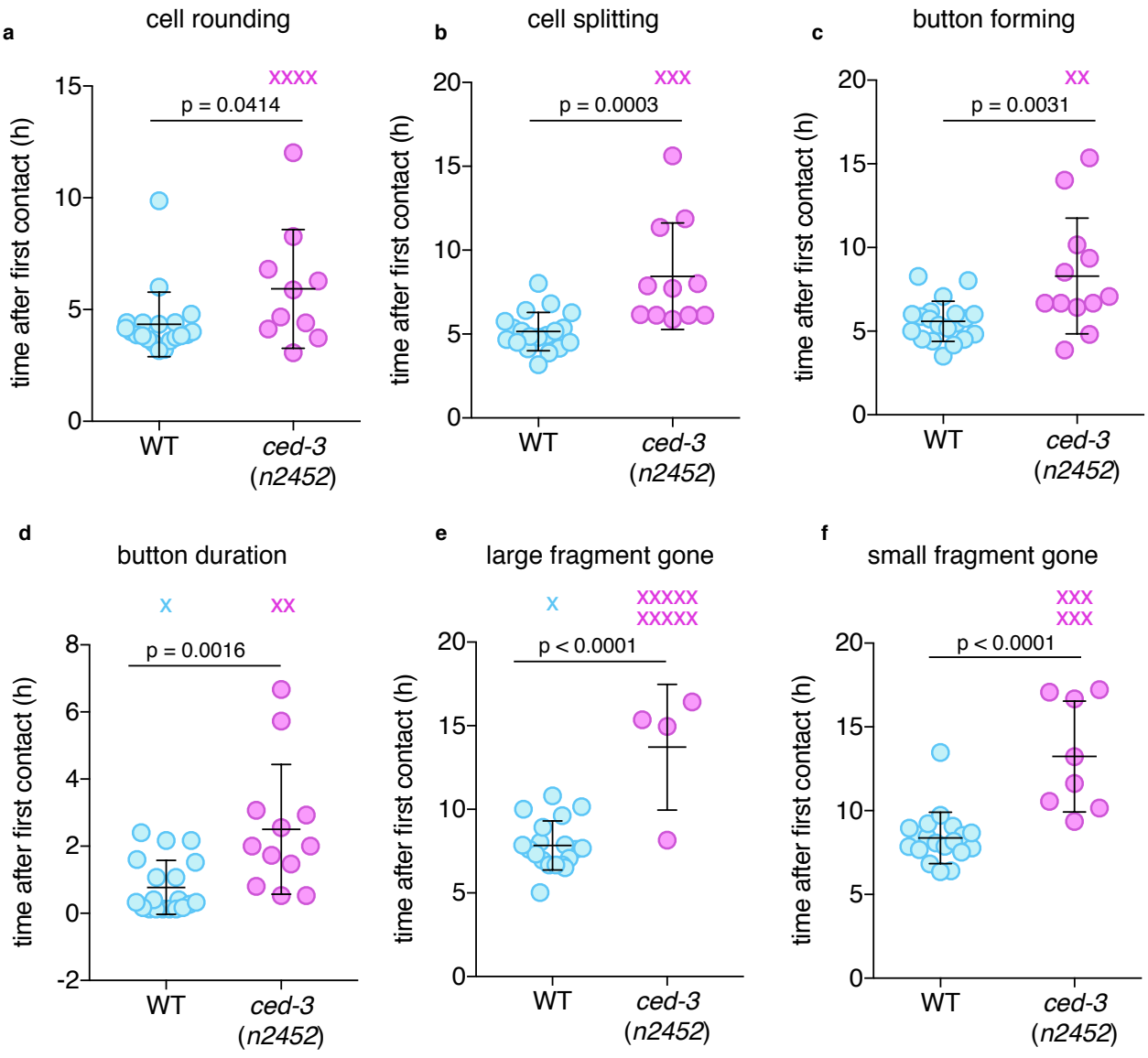

Figure 4-3. ***ced-3* mutations affect the majority of linker cell corpse degradation events**.

(a-f) details as in Figure 4-2.

are fertile, suggesting no interference between a lingering unengulfed linker cell and spermatid release [5].

To further bolster the hypothesis that CED-3 is involved in degradation rather than killing, I created *ced-3*; *pqn-41*(*ns294*) double mutants and found that loss-of-function mutations in *ced-3* did not enhance the surviving linker cell defects of *pqn-41* animals (Table 4-3).

4.2. ced-3 and *ced-4* act in the linker cell

Since corpses persist in both *ced-3* and *ced-4* mutants, I wanted to determine where these genes are expressed and where they function.

4.2.1. ced-3 expresses in the linker cell as it dies, but not as it migrates

I examined two transcriptional reporters, *nsIs25*[*ced-3*p::GFP] and *nsEx4944*[*ced-3*p::mCherry]. In both cases, I saw expression of fluorescent protein in the linker cell once it reached the cloaca, but not as it was migrating (Figure 4-4a,b). I noticed that expression in the linker cell was much fainter than other cells dying by apoptosis in the male tail (Figure 4-4a,b), suggesting that *ced-3* is not induced as strongly when required only for cell clearance. I also obtained *bcIs109*, a *ced-3* translational reporter, and found GFP puncta in the nucleus of the dying linker cell, consistent with a role in nuclear degradation (Figure 4-4c). I did not see expression in the U.l/rp cells from any of the reporters.

4.2.2. ced-4 is expressed in the linker cell

I created a *ced-4* transcriptional reporter and noticed expression in both the dying (Figure 4-5a) and migrating linker cell (Figure 4-5b). I also saw off-target overexpression artifacts in the intestine (Figure 4-5b). Nonetheless, perhaps this low-level expression in the migrating cell explains why *ced-3* must be transcriptionally induced, to prevent being

Table 4-2. **Linker cell corpses in degradation mutants are terminally engulfed.**

Genotype	% linker cell corpses engulfed in 24h adults	N
WT	100	3
arf-6(*ns388*)	92	97
rab-35(*b1013*)	99	119
rme-4(*ns410*)	99	102
ced-3(*n717*)	99	100
ced-3(*n2452*)	99	101
ced-4(*n1162*)	91	100
ced-9(*n1950*)	89	19
ced-3(*n2452*); *rab-35*(*tm2058*)	98	102
ced-3(*n2452*); *rab-35*(*b1013*)	100	107
ced-3(*n717*); *rab-35*(*tm2058*)	99	72
ced-3(*n717*); *rab-35*(*b1013*)	99	76

All animals carried a *him-5*(*e1490*) mutation, a GFP linker cell marker, and an mCherry U.l/rp cells marker.

Table 4-3. ***ced-3*(lf) does not enhance the surviving linker cell defects of *pqn-41*(*ns294*).**

Genotype	%SLC (N) 2h adults
Wild type	3% (157)
pqn-41(*ns294*)	20% (44)
pqn-41(*ns294*); *ced-3*(*n717*)	24% (50)
pqn-41(*ns294*); *ced-3*(*n2452*)	20% (114)

All animals carried a *him-5*(*e1490*) mutation and a GFP linker cell marker.

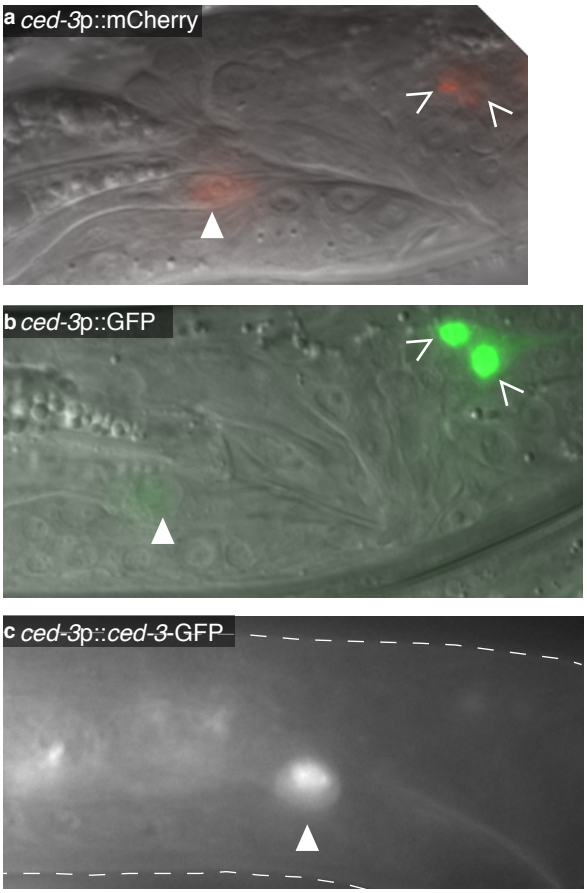

Figure 4-4. ***ced-3* is expressed in the dying linker cell**.
(a-c) Caret, cells dying by apoptosis. Arrowhead, linker cell. (a,b) *ced-3* transcriptional reporter expression. (c) *ced-3* translational reporter expression and localization.

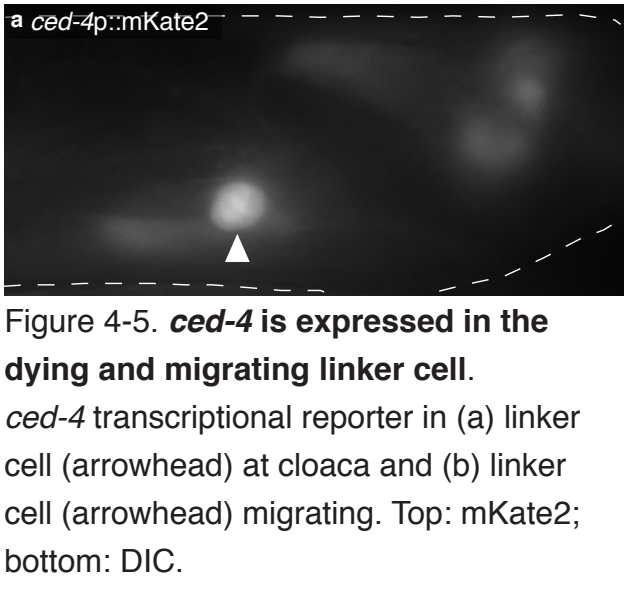

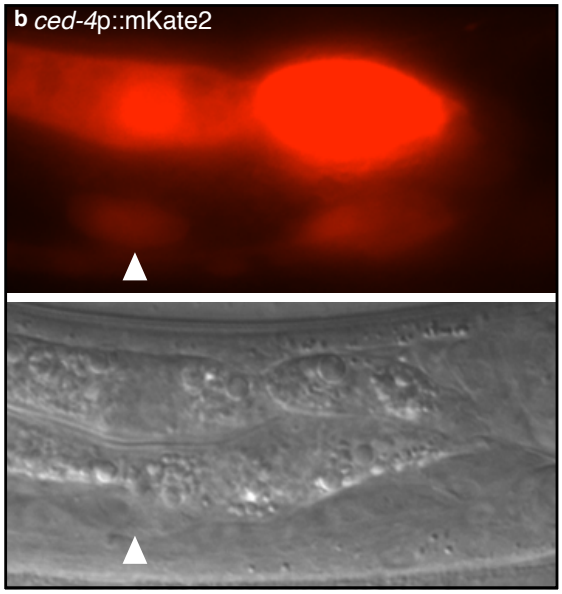

Figure 4-5. ***ced-4* is expressed in the dying and migrating linker cell**.
ced-4 transcriptional reporter in (a) linker cell (arrowhead) at cloaca and (b) linker cell (arrowhead) migrating. Top: mKate2; bottom: DIC.

activated by CED-4 prematurely. Together, these results suggest that CED-4 is present in the migrating linker cell, and *ced-3* is transcriptionally induced upon death initiation to begin its degradation function.

4.2.3. ced-4 functions in the linker cell, not the engulfing cell

Since both *ced-3* and *ced-4* are expressed in the linker cell, but not in the U.l/rp cells, I wanted to confirm that these proteins function within the linker cell. Because expression of *ced-3* ectopically in the linker cell may cause apoptotic cell death, I examined *ced-4* function instead. I expressed *ced-4* cDNA under a linker-cell-specific promoter (*mig-24*p) and a U.l/rp-promoter (*lin-48*p), and checked for rescue of the *ced-4*(*n1162*) defect. I found that expression in the linker cell, but not the engulfing cells rescued the phenotype (Figure 4-6), confirming that CED-4 functions in the linker cell to degrade it.

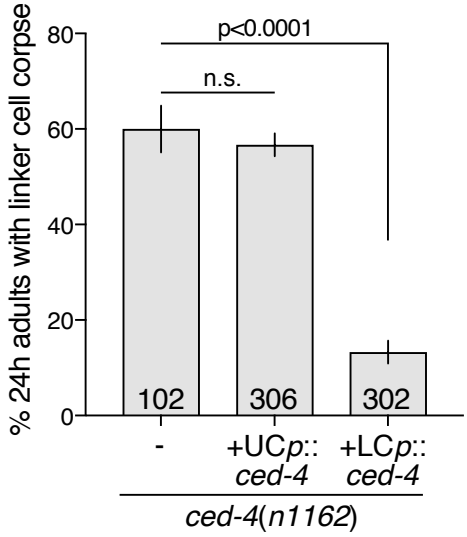

Figure 4-6. **CED-4 functions in the dying linker cell**.
Linker cell degradation in indicated genotypes. Strains contain *lag-2*p::GFP linker cell reporter and *him-5*(*e1490*). UCp, *lin-48*p. LCp*, mig-24*p. Number of animals scored inside bars. Average of at least three independent lines. Error bars, standard error of the proportion or standard error of the mean. n.s., p>0.05, Fisher's exact test.

4.3. Interactions between RAB-35/ARF-6 module and caspase

In the previous chapter, I described a RAB-35/ARF-6 module that is required for corpse degradation in the U.l/rp cells, and how it is necessary for proper phagosome maturation. CED-3 is also required in the linker cell to aid in its engulfment and degrade components of the nucleus. Because both are involved in some aspect of corpse degradation, I wanted to determine if and how these pathways interact.

4.3.1. ced-3 is still expressed when rab-35 and arf-6 are mutated

I wanted to determine if *ced-3* expression is affected when the RAB-35 or ARF-6 pathways are disrupted. To test this, I crossed the *ced-3* transcriptional reporter into *rab-35*(*b1013*) and *arf-6*(*ns388*) animals. In both cases, *ced-3* is still expressed (Figure 4-7). This result is consistent with the idea that *ced-3* is induced after cell death, but upstream of phagosome maturation.

4.3.2. ced-3 likely functions upstream of rab-35

To determine if there are any genetic interactions between the pathways, I created double mutants between *ced-3*, and *rab-35* and its GAP, *tbc-10*. I found no synergistic interactions (Figure 4-8), but these corpses more closely resembled *ce*d-3 corpses, suggesting it functions upstream of *rab-35*. I also wanted to determine if

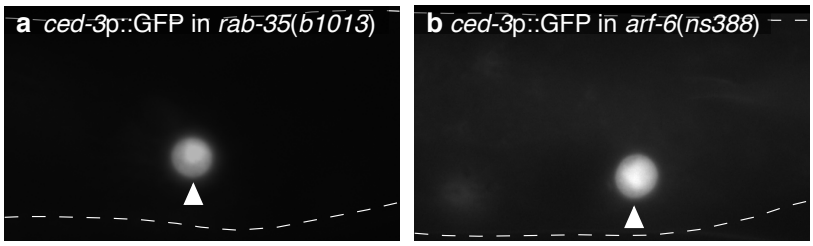

Figure 4-7. ***ced-3* is still expressed in *rab-35* and *arf-6* mutants**.
ced-3 transcriptional reporter in (a) *rab-35*(*b1013*) and (b) *arf-6*(*ns388*) animals. Arrowhead, linker cell.

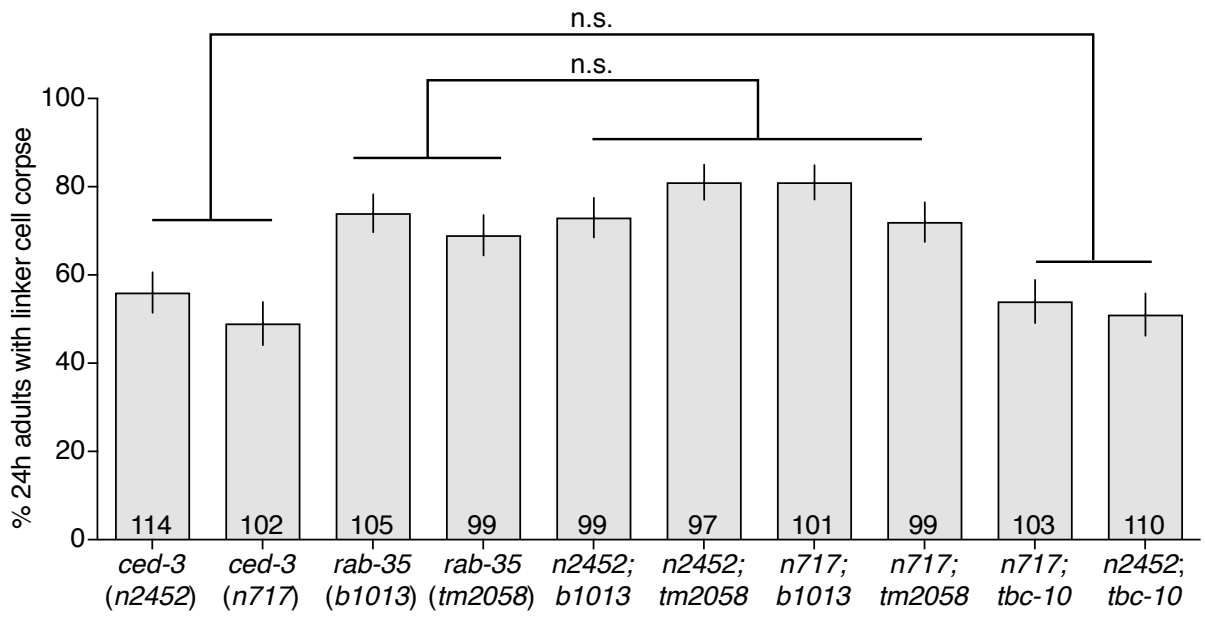

Figure 4-8. ***ced-3* and *rab-35* do not genetically interact**.
Linker cell degradation in indicated genotypes. Strains contain *lag-2*p::GFP linker cell reporter and *him-5*(*e1490*). Number of animals scored inside bars. Error bars, standard error of the proportion. n.s., p>0.05, Fisher's exact test.

recruitment of YFP-RAB-35 is defective in *ced-3* mutant animals using the microfluidic long-term imaging set up and imaging over the duration of linker cell clearance. I was unable to detect any consistent differences in YFP-RAB-35 localization or intensity between WT and *ced-3*, suggesting that RAB-35 function is unperturbed in *ced-3* animals.

4.3.3. ced-3 and arf-6(gf) are synergistic

Intriguingly, I found that *ced-3* and *arf-6* pathways interact. Double mutants between *arf-6*(gf) and *ced-3*(lf) are synergistic, while null mutations in *arf-6* do not affect the phenotype of *ced-3* animals (Figure 4-9).

As noted in Chapter 3, ARF-6-YFP localizes to either the dorsal or the ventral side of the engulfing cell. In *ced-3* animals, the intensity of ARF-6-YFP when

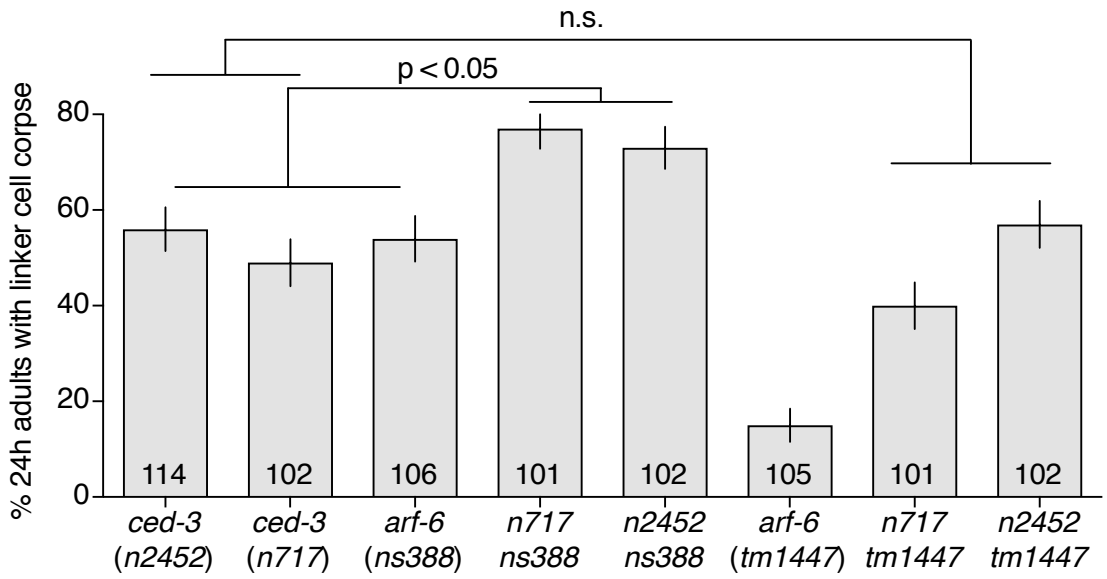

Figure 4-9. ***ced-3* and *arf-6* pathways interact**.
Linker cell degradation in indicated genotypes. Strains contain *lag-2*p::GFP linker cell reporter and *him-5*(*e1490*). Number of animals scored inside bars. Error bars, standard error of the proportion. n.s., p>0.05, Fisher's exact test.

localized to the ventral side of the cell, or to both the ventral and dorsal sides was unaffected (Figure 4-10). Intriguingly, when ARF-6-YFP localized to the dorsal side alone, both the intensity and duration was reduced in *ced-3* animals (Figure 4-11). Perhaps this result may have something to do with the role of *ced-3* in engulfment receptor presentation, and may hint at an additional function of ARF-6 in wild-type animals.

4.4. Discussion

I found that the caspase CED-3 and its upstream activator CED-4 are required for linker cell corpse degradation, perhaps having a role in engulfment receptor presentation and nuclear degradation. Neither of the proteins are required for death, as the linker cell corpse displays nuclear crenellation and is eventually engulfed in the absence of these genes.

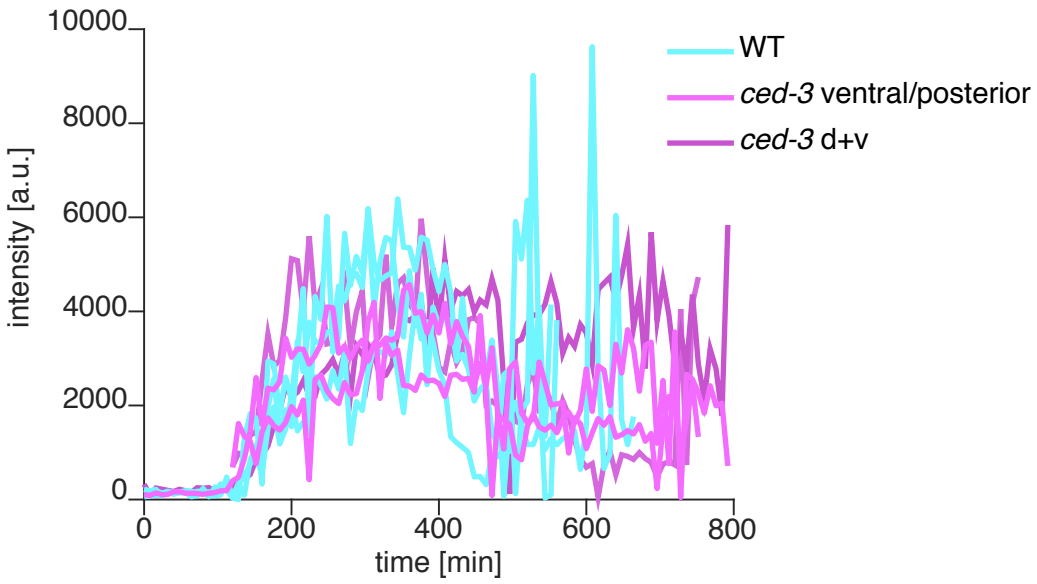

Figure 4-10. **ARF-6-YFP intensity is unaffected when localized only on the ventral arm of the pseudopod or on both arms in *ced-3* mutants**.
The intensity of ARF-6-YFP around the linker cell during linker cell death and degradation was monitored in the microfluidic device over at least 20 h. Total intensity values were plotted as a function of time. Wild type (WT) localization (ventral/posterior localization) in blue, ventral/posterior localization in *ced-3*(*n2452*) in light pink, and dorsal+ventral localization in *ced-3*(*n2452*) in dark pink.

I noticed that the majority of corpses in *ced-3* animals were small, consisting solely of a crenellated nucleus with little cytoplasm remaining. Based on the long-term imaging studies, I know that this small cell is the larger fragment, where the cytoplasm has been removed, and only the nucleus remains. Perhaps CED-3 is responsible for presentation of engulfment receptors and degradation of the nucleus, but not nuclear envelope changes or bulk cytoplasmic degradation. Further investigation is necessary to determine how CED-3 is affecting cell splitting and cell engulfment. Intriguingly, the *ced-3* linker cell corpse morphology is reminiscent to that of dying motoneurons in the absence of the pro-apoptotic Bax [112]. Those cells are also small with shriveled nuclei and do not maintain synaptic connections, suggesting they are dead, but not degraded. Perhaps in that system, LCD is the main driver of cell death, and caspase is required to

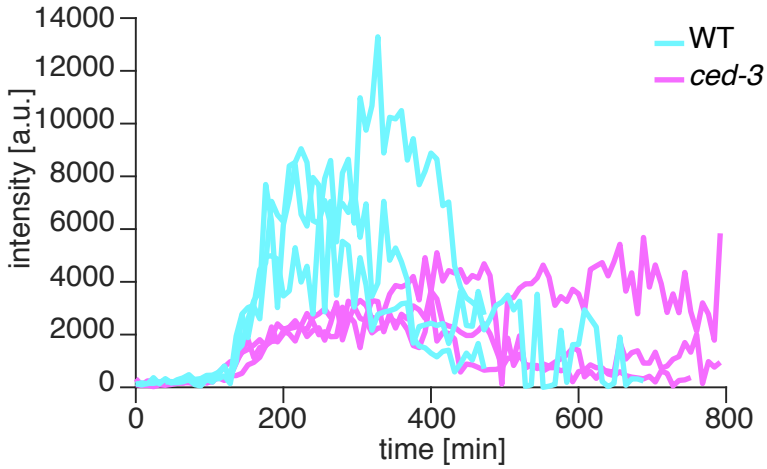

Figure 4-11. **ARF-6-YFP intensity and duration is affected when localized only on the dorsal arm of the pseudopod in *ced-3* mutants**.
The intensity of ARF-6-YFP around the linker cell during linker cell death and degradation was monitored in the microfluidic device over at least 20 h. Total intensity values were plotted as a function of time. Wild type (WT) localization (dorsal localization) in blue, dorsal localization in *ced-3*(*n2452*) animals in pink.

clear the corpse debris.

A role of *ced-3* in degradation rather than killing is also supported from its known targets. The majority of caspase targets identified could actually be required mostly for corpse cleanup, instead of death. For example, in apoptosis in *C. elegans*, CED-3 cleaves DCR-1 to convert it from an RNase to a DNase and degrade DNA in dying cells [228]. In mammalian cells, effector caspases activate a DNase to degrade the DNA as well [111]. While bulk cleavage of DNA would presumably lead to cell death, the primary function could actually be nuclear clearance after phagocytosis. Determining the exact timing of death, caspase activation, DNA degradation, and corpse removal will be key in determining the primary, likely extremely nuanced function of caspase in dying cells.

The ability of caspases to carry out nuanced cell function is well-documented. Controlled expression of caspase either by levels or location can have a wide variety of consequences in development. For example, in *C. elegans*, CED-3 is known to cleave LIN-14, LIN-28, and DISL-2, which are key regulators of developmental

timing [229,230]. These cleavage events allow for robust development of the worm. In Drosophila, controlled activation of caspase is required for proper sperm development [231]. Based on these examples, the idea that caspase is a bulk killing machine is likely incorrect, but that its activation in cell death, degradation, and other proteolytic events is likely distinct and very well-controlled.

5. Discussion and future directions

5.1. A model for linker cell death and degradation

During my graduate studies, I discovered components required for both linker cell death and degradation. I found that HPK-1, a homeodomain protein kinase, interacts with the polyglutamine protein PQN-41C. This interaction may disrupt the positive interactions between HPK-1 and the heat shock function of HSF-1, perhaps allowing HSF-1 to undertake its linker cell killing role. After linker cell death, I found that the U.l/rp cells simultaneously engulf the dying cell, eventually leading to cell splitting and internalization. Precocious competitive phagocytosis occurs in animals lacking the small GTPase *rab-35*, or in a gain-of-function mutant of *arf-6*. In these animals, phagosome maturation fails to proceed, although engulfment itself is unaffected. Linker cell corpse degradation also requires the caspase *ced-3* from within the linker cell for efficient removal.

The linker cell requires both external (*i.e.* RAB-35) and internal (*i.e.* CED-3) proteins for proper corpse elimination. Perhaps these extra layers of degradation ensure that the linker cell is properly cleared, as removal of the linker cell from the gonadal tube is absolutely essential for male fertility. Multiple avenues of corpse removal would therefore be prudent to guaranteeing male fertility and propagation of genetic material.

One of the few pro-survival factors targeted by CED-3 in *C. elegans* is CNT-1 [232]. In apoptosis, CNT-1 interacts with Akt signaling to promote cell survival, and cleavage of CNT-1 by CED-3 removes this function [228]. It is quite interesting that I also found a role for CNT-1, although in a different context. In linker cell phagosome maturation, CNT-1 is required to turn off ARF-6 through recruitment by RAB-35. Given that *ced-3* and *arf-6*(gf) genetically interact, one might suspect that CNT-1 is the link. A few pieces of evidence dispute this, however. First, CNT-1 acts in the engulfing cell, while CED-4, and by proxy, CED-3, act in the linker cell. Second, using CRISPR, I

removed the CED-3 cleavage site in the endogenous *cnt-1* locus, and I found no effect on linker cell degradation, suggesting that CED-3 cleavage of CNT-1 is dispensable for linker cell corpse removal.

The use of caspase to degrade the linker cell, but not to kill it, shows the fine line between death and degradation, and how difficult it may be to distinguish between these phenotypes. In linker cell death, however, I think caspase is involved in downstream degradation events, because persistent linker cell corpses in *ced-3* mutant animals have lost a majority of their cytoplasmic volume and are much smaller than typical surviving cells. In addition, the nuclear envelope is crenellated. This phenotype has been confirmed by scientists in external laboratories, and is even the case in quadruple caspase mutants [83].

Instead *ced-3* mutant animals have difficulty with internalization of the cell corpse, as evidenced by the delay in cell splitting. They also have trouble in digesting the fragments after internalization, especially the larger nuclear fragment. While these animals also have a delay in removal of the small, cytoplasmic piece, the actual duration of this piece is unaffected. This means that it takes longer for the animal to generate the smaller fragment, but this piece is degraded efficiently once it is. Intriguingly, *ced-3* persistent linker cell corpses resemble dying motoneurons in the absence of apoptosis [112]. Perhaps these cells are dying by LCD and are then being degraded via caspase activation. Another alternative is that both cell death forms are used to kill and degrade the cell of interest, depending on developmental stage, signaling pathways, and the local environment.

5.2. A new function of caspase and an alternative explanation of published results

Caspase-dependent apoptosis does not account for many cell death events that occur during animal development. Indeed, mice homozygous for knockout alleles of key

apoptotic genes, including caspase-3, caspase-9, Apaf1, or Bax and Bak, can survive to adulthood [33,36,233], a surprising observation given the prevalence of cell death in murine development. Inactivation of apoptosis genes also only weakly interferes with degenerative disease progression [234]. LCD, a non-apoptotic cell death process, is prevalent in vertebrates [235] and may account for a significant fraction of cell deaths that take place during development and in disease.

From our studies, it is apparent that caspase is instead needed for bulk cell degradation, as well as a more specific function in engulfment. Perhaps some of present apoptotic data could also be explained by this alternative function of caspases. For example, in $Bax^{-}Bak^{-}$ mice, cell death between the digits is greatly delayed [38]. However, since the morphology of these dying cells was not examined by electron microscopy, one could imagine a scenario where caspase activation is needed only after LCD has commenced in these cells.

Indeed, in collaboration with Sarit Larisch and Dana Mamriev at the University of Haifa, we noticed that mouse embryonic fibroblasts (MEFs) display LCD-like morphology only 8 min after treatment with the cell-death-inducing drug staurosporine (STS) (M. Alam, *unpubl. data*). In HeLa cells treated with STS, the initiator caspase-9 is activated 30 min after treatment, and the effector caspase-3 is induced 3h after treatment [236]. Caspase-3 activation peaks 12h after STS treatment in human corneal endothelial cells, and the cells adopt apoptotic morphology 12h after treatment [237]. These results suggest that LCD could be the main killing function, with caspase responsible for clearing cellular debris.

The LCD-like crenellations still occur in treated MEF cells with mutated apoptotic genes (D. Mamriev, M. Alam, *unpubl. data*). We also noticed induction of components of the ubiquitin proteasome system 30 min after treatment (L. Kutscher, D. Mamriev, *unpubl. data*). While the research is still early, this system mimics what we see with the death of the linker cell.

Perhaps there are other pathways that were initially thought to be exclusively apoptotic that instead rely on apoptotic genes for efficient corpse clearance, and not for death. Given the diversity of non-apoptotic functions for caspase [238], then perhaps it is not so far-fetched that caspase has a nuanced role in cell death.

5.2.1. Suggestions for classifying cell death in vivo

How then should we classify apoptosis versus LCD, especially given that molecules between the two may be shared but have distinct functions? First, I would argue that ultrastructural morphology is important for identifying the relevant pathway. LCD and apoptosis have distinct morphology by electron microscopy (EM), and this could be used as a first step in identifying the cell death process at play. As EM methods require specialized training and equipment, it may not always be available. Perhaps in this case, nuclear morphology is the best indication of LCD vs. apoptotic. Expression of fluorescently tagged lamin in cells dying by LCD revealed that the crenellations are visible with light microscopy (M. Alam, *unpubl. data*).

The presence of cleaved caspase-3 should no longer be considered a proxy for apoptosis, given the role of CED-3 in corpse clearance of cells dying by LCD. Determining exactly how to differentiate between these cell death pathways will hopefully become clearer as we learn more about the relative contributions each makes to eliminate a dying cell.

5.2.2. LCD and apoptosis as parallel pathways?

One possibility is that LCD drives cell death in development, while caspases perform a cell degradation role. Another possibility is that the two pathways work in parallel, each functioning in certain developmental stages and contexts. Perhaps LCD is the main cell death program in vertebrate systems, especially since mutations in apoptotic genes only affect certain tissues. Finding the molecules conserved across

species will be crucial in testing these hypotheses. Many of the LCD genes isolated so far, including the ones described in this thesis, may be nematode-specific, as most of the upstream regulatory genes isolated tell the linker cell exactly when and where to die. The key will be identifying the genes targeted by the ubiquitin proteasome system, and determining if those molecules are conserved across systems.

5.3. Future directions

While my graduate work revealed a substantial amount about the genes and mechanisms involved in linker cell death and degradation, many pertinent questions remain. Discussed below are some that I consider most pressing in relation to my work.

5.3.1. Linker cell death future questions

Chapter two of my thesis focused on the role of PQN-41C interacting proteins in cell death. I recovered many interesting candidate genes that warrant additional investigation, including the aconitase *aco-2*, the zinc finger protein *zfp-1*, two additional polyglutamine-containing genes *pqn-59* and *pqn-85*, and the cell death inhibitor *hpk-1*. I am especially interested in how these interactions with PQN-41C contribute to cell death, especially since neurodegenerative diseases associated with polyglutamine expansion proteins may result from a developmental cell death program gone awry [94].

5.3.1.1. Does PQN-41C bind HPK-1 to prevent it from activating HSF-1?

I isolated the homeodomain protein kinase HPK-1 as an interacting partner of PQN-41C. Genetic experiments placed HPK-1 with HSF-1, and additional preliminary experiments showed that loss of *hpk-1* affects HSF-1 heat shock function and abrogates the heat-related cell death defect of the linker cell. A positive regulatory interaction between HPK-1 and HSF-1 in modulating the stress response is bolstered by previously published data in *C. elegans* [186,196,197] and other organisms [188,239].

Because loss of *hpk-1* allows cell death to occur more robustly, I hypothesized that HPK-1 normally promotes the stress-related, pro-survival role of HSF-1, and that an interaction with PQN-41C is necessary to disrupt this interaction. This would then allow HSF-1 to function in its pro-death capacity instead. However, it seems necessary for HPK-1 to function prior to death, as loss of *hpk-1* affects male fertility. Further work should directly test this hypothesis. Ideally, this would be tested biochemically, as discussed in Chapter 2. Another, perhaps simpler way to test this hypothesis, would be to mutate putative Ser/Thr phosphorylation residues to alanines on HSF-1 and test for rescue in *hsf-1*(*sy441*) animals. By doing this as a single copy insertion under the endogenous promoter, one could test these residues for their role in both the heat shock response globally, as well as their role in linker cell death specifically.

5.3.1.2. How does HPK-1 regulate HSF-1 in its heat shock role?

One added benefit to the above method is that we could simultaneously identify amino acid residues necessary for both functions of HSF-1 in a single experiment. In other systems, HPK-1 inhibits the ability of HSF-1 to become sumoylated, which bolsters its heat shock response [196]. Alternatively, in response to increased levels of reactive oxygen species (ROS), the HPK-1 homolog, HIPK2, is desumoylated, which drives downstream gene expression changes [239]. Perhaps in linker cell death, when HPK-1 is inhibited, HSF-1 becomes sumoylated, pushing HSF-1 towards its cell death role. Identifying sumoylation sites computationally and attempting to rescue *hsf-1*(*sy441*) with lysine to alanine mutations at these residues may help identify putative sumoylation sites on HSF-1. The role of sumoylation in modifying and modulating HSF-1 and HPK-1 in linker cell death definitely deserves closer inspection.

Adding to the intrigue, Jennifer Malin identified the E3 sumo-conjugating enzyme UBC-9 as a putative substrate of the E3 ligase BTBD-2 in linker cell death. Perhaps selective removal of a sumoylation-promoting enzyme is required to kill the linker cell.

Identifying the post-translation modifications necessary to modulate the different roles of HSF-1 is crucial to fully understanding the interactions between these proteins, and learning how the cell decides between life and death.

5.3.2. Linker cell degradation future questions

Chapters 3 and 4 of my thesis focused on the events that occur after linker cell death, namely how is the dying linker cell cleared from the organism. I discovered a core genetic network involving the two small GTPases ARF-6 and RAB-35, whose interplay is required for proper phagosome maturation and cell degradation. I also discovered that caspase is required in the linker cell to be properly engulfed by the U.l/rp cells and for the nucleus of the linker cell to be properly degraded. While I uncovered quite a bit about the dismantling of the cell corpse, some questions remain and are discussed below.

5.3.2.1. How is the cell specificity of ARF-6 and RAB-35 function conferred?

One puzzling piece remaining is the fact that the U.l/rp cells seem specifically equipped to dismantle the linker cell, yet both *arf-6*, *rab-35*, and many of their regulators are expressed throughout the entire animal. Overall, animals harboring mutations in these genes do not have major issues in viability, although these genes have additional endocytic and membrane trafficking functions [207,210]. Perhaps one aspect of specificity could be downstream effectors of these genes that have yet to be identified, which equip the U.l/rp cells with specialized phagocytosis and degradation functions.

5.3.2.2. How is the dying linker cell corpse recognized?

Both RAB-35 and ARF-6 have roles in phagocytosis onset and phagosome maturation. It is still unknown, however, what the exact signaling molecules and engulfment receptors displayed on the linker cell membrane are. We know that

canonical apoptotic genes are not involved, and PS exposure was also not readily detected. I think the linker cell is emitting a “find me” signal though, as I occasionally witnessed dying cells that had a slight migration defect, where the U.l/rp cells extended processes and appeared to pull the linker cell into its proper place. At the same time, it also must have highly regulated “eat me” and “don’t eat me” signals, as competitive phagocytosis and internalization should not take place before the linker cell is completely sandwiched between the two engulfing cells and the gonad contents are protected. What these signals are should be a future area of active investigation.

What is the best way to go about finding these molecules? I would suggest revisiting my forward genetic screen, but this time carrying out the screen in animals carrying both a U.l/rp marker (*nsIs589*) and a linker cell marker (*nsIs65*). I would suggest picking off young adult males with intact linker cells under low magnification (dissecting microscope), but then immediately mounting these males on a slide for examination under high magnification (compound microscope). By doing so, it will be easier to identify surviving cells based on DIC morphology, and perhaps also cells that remain sandwiched but unengulfed within the U.l/rp cells (but still display a crenellated nuclear envelope, indicating death). After recovery, I would suggest isolating each male with a single wild-type hermaphrodite for 24h, to ensure that these males are infertile (because a surviving or unengulfed linker cell will block spermatid exit). Only then would I suggest attempting the artificial insemination (AI) procedure with these 24h old males, noting also whether the linker cell is still around prior to AI. By more carefully conducting the forward genetic screen can we find genes specifically involved in death or dying cell recognition.

5.3.2.3. What other genes are involved in corpse degradation?

We discovered that RAB-35 seems to be required to remove ARF-6 from the nascent phagosome, and RAB-35 also has downstream functions involving RAB-5

and RAB-7 recruitment. Based on *sand-1*; *rab-35* double mutants, which have nearly all cell corpses remaining even 36h after the L4 to adult transition, I think that RAB-35 is required in parallel to *sand-1*, at the RAB-5 to RAB-7 transition. This hypothesis is bolstered additionally by the fact that while in the majority of *rab*-35(b1*013*) animals, mCh-RAB-5 was never recruited to the phagosome, there was one animal where mCh-RAB-5 persisted around the phagosome for nearly the entire experiment, suggesting that RAB-35 is necessary for its removal. This is especially surprising for RAB-5, as it is usually only enriched around the phagosome for a single frame in wild-type animals. For mCh-RAB-7 localization in *rab-35* mutant animals, I never saw such persistent localization, despite screening more animals.

To pinpoint the ARF-6-independent function of RAB-35 more precisely, I should examine mCh-RAB-5 and mCh-RAB-7 localization in persistent cell corpses in *arf-6*(*tm1447*); *rab-35*(*b1013*) double mutant animals. These animals have a small but significant increase in the number of cell corpses compared to wild type, so that such analysis would be possible. If my above idea is true, I should see persistent mCh-RAB-5 recruitment around these lingering corpses, and never see mCh-RAB-7 recruitment.

5.3.2.4. What are the target proteins of CED-3?

I also determined that CED-3 is required for proper corpse degradation, especially of the nucleus-containing fragment, and perhaps also plays a role in timely engulfment. The latter could be investigated using the genetic screen I described, but the former could be investigated by a candidate screen. As previously mentioned, in apoptosis in the *C. elegans* embryo, CED-3 is required to convert the RNase DCR-1 to a DNase tDCR-1 to efficiently remove DNA from the dying cell [224]. To investigate whether something similar could be occurring here, I tested a mutant of *dcr-1*. While the research is still preliminary, there was a slight delay in corpse removal at 2h after the L4 to adult transition. The nuclease *nuc-1*, also a CED-3 target, has a small but significant

corpse removal defect at 24h. Perhaps a *nuc-1*; *dcr-1* double mutant would resemble the *ced-3* mutant animals and hint at the role of CED-3 in removing nuclear DNA from a dead cell.

5.4. Concluding remarks

The studies described here suggest how linker cell death may be inhibited when opposing cell survival signals are present. Additional studies are needed to determine the exact molecular mechanism by which this inhibition occurs, but may provide much needed clues to understanding how the HSF-1 switch is controlled in linker cell death. These studies also provide clear mechanistic insight to how the linker cell corpse is removed and degraded following cell death, which is controlled by two small GTPases, RAB-35 and ARF-6, and their regulators. RAB-35 and ARF-6 have been previously implicated in phagocytosis of pathogens, suggesting that the insights provided here are well-conserved in many modes of phagocytosis. The finding that CED-3 is involved in cell degradation and not cell death perhaps answers the question as to why many mouse models of apoptotic knockout genes are viable: those genes are involved in the degradation of cells that are dying by LCD. Investigating the role of LCD in mammalian development is thus an urgent and exciting avenue of research in the near future.

6. Materials and Methods

6.1. Reagents

6.1.1. C. elegans strains

C. elegans strains were raised at 20°C on nematode growth medium (NGM) seeded with OP50 bacteria [240], unless otherwise indicated. Wild-type animals were of the Bristol N2 strain. All strains have one of two mutations that generate a high incidence of male progeny, *him-8*(*e1489*) IV or *him-5*(*e1490*) V. Mutants recovered by EMS mutagenesis were outcrossed five times before use. Transgenic lines were generated by injection of plasmid DNA mixes into the hermaphrodite gonad. Integrated transgenic strains were generated with UV/trioxalen treatment [241] (Sigma, T6137) and were outcrossed at least four times before imaging experiments. Most strains also had one of three integrated linker cell markers *qIs56*[*lag-2*p::GFP] V, *nsIs65*[*mig-24*p::Venus] X, or *nsIs650*[*mig-24*p::mKate2] X. Other alleles and transgenes are as follows:

LGI: *chd-7*(*tm6138*), *chd-7*(*tm6139*), *chd-7*(*gk290*), *chd-7*(*gk306*), *rab-2*(*n3263*), *ced-1*(*e1735*), *cep-1*(*gk138*), *dpy-5*(*e907*)

LGII: *rrf-3*(*pk1426*), *pqn-85*(*tm2334*), *pqn-85*(*tm2338*), *hsf-1*(*sy441*), *cnt-1*(*gk899634*), *cnt-1*(*tm2313*)

LGIII: *zfp-1*(*ok554*), *rab-35*(*b1013*), *rab-35*(*tm2058*), *tbc-10*(*gk388086*), *unc-119*(*ed3*), *ttr-52*(*tm2003*), *ttr-52*(*tm2078*), *F23H11.4*(*gk585084*), *F23H11.4*(*gk165637*), *cnt-2*(*gm377*), *ced-9*(*n1950*), *ced-4*(*n1162*)

LGIV: *pqn-41*(*ns294*), *pqn-41*(*ns807*), *egl-20*(*n585*), *arf-6*(*tm1447*), *arf-6*(*ns388*), *arf-6*(*ns751*[D92N]), *arf-6*(*ns752*[D92N]), *arf-6*(*ns753*), *arf-6*(*ns760*[T44N]), *arf-6*(*ns761*[T44N]), *arf-6*(*ns762*[T44N]), *arf-6*(*ns763*[I42M;P43T]), *arf-6*(*ns765*[Q67L]), *arf-6*(*ns771*[Q67L]), *arf-6*(*ns753*), *arf-6*(*ns764*), *arf-6*(*ns767*), *arf-6*(*ns769*), *sand-1*(*or552*), *sand-1*(*ok1963*), *efa-6*(*ok3533*), *ced-10*(*n1993*), *ced-5*(*n1812*),

psr-1(*ok714*), *psr-1*(*tm469*), *ced-3*(*n717*), *ced-3*(*n2452*)

LGV: *rde-1*(*ne219*), *egl-1*(*n1084n3082*)

LGX: *hpk-1*(*pk1393*), *sek-1*(*ag1*), *bar-1*(*ga80*), *rme-4*(*ns410*), *rme-4*(*ns412*), *rme-4*(*b1001*), *rme-4*(*tm1865*), *tbc-13*(*ok1812*), *piki-1*(*ok2346*), *him-4*(*e1267*), *git-1*(*ok1848*), *git-1*(*gk392605*), *gap-2*(*ok1001*)

6.1.2. Transgenes generated or used in present study

Transgene	Constructs
nsIs387	UV/TMP integration of *nsEx3148*[*mig-24*p::*rde-1*-SL2-mCherry + *lag-2*p::mCherry]
drSi13 II	*hsf-1*p::*hsf-1*-GFP::unc-54 3'UTR + Cbr-unc-119(+) single copy insertion [189]
nsIs653	UV/TMP integration of *nsEx5304*[pLMK10[*lin-48*p::mKate2-PH] (10 ng/ul)+ *unc-119*(+) (25 ng/ul) + pBluescript (65 ng/ul)]
nsEx4770,-71,-88,-89 *nsEx4361,4618,4668*	*rme-4* fosmid (WRM0615bE09) 10 ng/ul + *lin-48*p::*mCh* (25 ng/ul) + pBluescript (65 ng/ul)
nsEx4721,-22,-16	pLMK11[*lin-48*p::*rme-4a cDNA-SL2-mCh*](20 ng/ul) + *odr-1*p::RFP(+) (20 ng/ul) + pBluescript (60 ng/ul)
nsEx4559,-60,4748	pLMK12[*mig-24*p::*rme-4a cDNA*](20 ng/ul) + *odr-1*p::RFP(+) (20 ng/ul) + pEB30[*lag-2*p::mCh] (25 ng/ul) + pBluescript (35 ng/ul)
nsEx4669,-64,4742	pLMK13[*lin-48*p::*rme-4b cDNA-SL2-mCh*](20 ng/ul) + *odr-1*p::RFP(+) (20 ng/ul) + pBluescript (60 ng/ul)
pwIs268	*rme-4* translational reporter, gift from B. Grant [207]
nsEx4658,-66,-91	pLMK14[*lin-48*p::*rab-35 cDNA-SL2-mCh*](20 ng/ul) + *odr-1*p::RFP(+) (20 ng/ul) + pBluescript (60 ng/ul)
nsEx4654,-89,-90	pLMK15[*mig-24*p::*rab-35 cDNA*](20 ng/ul) + *odr-1*p::RFP(+) (20 ng/ul) + pEB30 (25 ng/ul) + pBluescript (35 ng/ul)
nsEx4813,-16,-47	pLMK16[*mig-24*p::*rab-35*(*Q69L*) *cDNA*](20 ng/ul) + *odr-1*p::RFP(+) (20 ng/ul) + pEB30 (25 ng/ul) + pBluescript (35 ng/ul)

nsEx4799,4821,-31, -29,20	pLMK17[*mig-24*p::*rab-35*(*S24N*) *cDNA*](20 ng/ul) + *odr-1*p::RFP(+) (20 ng/ul) + pEB30 (25 ng/ul) + pBluescript (35 ng/ul)
pwIs357	*rab-35* translational reporter, gift from B. Grant [207]
nsEx4741,-49,-86, 4937,-81,-82	pLMK18[*lin-48*p::*tbc-10 cDNA-SL2-mCh*](20 ng/ul) + *odr-1*p::RFP(+) (20 ng/ul) + pBluescript (60 ng/ul)
nsEx5703,-04,-05	pLMK19[*lin-48*p::*tbc-10*(R225A) *cDNA-SL2-mCh*](20 ng/ul) + *odr-1*p::RFP(+) (20 ng/ul) + pBluescript (60 ng/ul)
nsIs493	UV/TMP integration of *sEx10170*[rCes R06B10.5::GFP + pCeh361]. Strain BC10170 from CGC.
nsIs595 V	UV/TMP integration of *nsEx5132*[pLMK20[*lin-48*p::YFP-RAB-35 cDNA] (10 ng/ul)+ *unc-119*(+) (25 ng/ul) + pBluescript (65 ng/ul)]
nsIs713	UV/TMP integration of [pLMK21[*lin-48*p::mKate2-RAB-35 cDNA] (10 ng/ul)+ *unc-119*(+) (25 ng/ul) + pBluescript (65 ng/ul)]
nsIs60	*mig-24*p::Venus + *unc-119*(+), a gift from M. Abraham
nsIs622 X	UV/TMP integration of *nsEx4724*[pLMK22[*lin-48*p::mCherry-RAB-5 cDNA] (1 ng/ul)+ *unc-119*(+) (25 ng/ul) + pBluescript (74 ng/ul)]
nsIs592 V	UV/TMP integration of *nsEx5610*[pLMK23[*lin-48*p::mCherry-RAB-7 cDNA] (1 ng/ul)+ *unc-119*(+) (25 ng/ul) + pBluescript (74 ng/ul)]
nsIs586 V	UV/TMP integration of *nsEx5798*[pLMK24[*lin-48*p::CTNS-1-mKate2 cDNA] (10 ng/ul)+ *unc-119*(+) (25 ng/ul) + pBluescript (65 ng/ul)]
nsEx4717,-38,4848, 4564,-82,-83	pLMK25[*lin-48*p::*arf-6 cDNA-SL2-mCh*](20 ng/ul) + *odr-1*p::RFP(+) (20 ng/ul) + pBluescript (60 ng/ul)
nsEx4657,-60, 4753,-85,-50	pLMK26[*lin-48*p::*arf-6(D92N) cDNA-SL2-mCh*](20 ng/ul) + *odr-1*p::RFP(+) (20 ng/ul) + pBluescript (60 ng/ul)
nsEx4825,-44,-45, 4815,-46,-49	pLMK27[*mig-24*p::*arf-6 cDNA*](20 ng/ul) + *odr-1*p::RFP(+) (20 ng/ul) + pEB30 (25 ng/ul) + pBluescript (35 ng/ul)
nsEx4787,-94, 4814	pLMK28[*mig-24*p::*arf-6(D92N) cDNA*](20 ng/ul) + *odr-1*p::RFP(+) (20 ng/ul) + pEB30 (25 ng/ul) + pBluescript (35 ng/ul)
nsEx4595	pLMK29[*arf-6*p*::arf-6* genomic DNA-GFP-*unc-54* 3'UTR] (10 ng/ul) + *unc-119*(+) (25 ng/ul) + pBluescript (65 ng/ul)

nsEx4602	pLMK30[*arf-6*p*::arf-6*(*ns388*) genomic DNA-GFP-*unc-54* 3'UTR] (10 ng/ul) + *unc-119*(+) (25 ng/ul) + pBluescript (65 ng/ul)
nsEx4953,-48, 5612, 5106,-10,-14,-59	pLMK31[*lin-48*p::*arf-6(ΔG2) cDNA-SL2-mCh*](20 ng/ul) + *odr-1*p::RFP(+) (20 ng/ul) + pBluescript (60 ng/ul)
nsEx4954,-67,5696	pLMK32[*lin-48*p::*arf-6(ΔG2, D92N) cDNA-SL2-mCh*](20 ng/ul) + *odr-1*p::RFP(+) (20 ng/ul) + pBluescript (60 ng/ul)
nsEx5694,-95	pLMK33[*lin-48*p::*cnt-1a cDNA-SL2-mCh*](20 ng/ul) + *odr-1*p::RFP(+) (20 ng/ul) + pBluescript (60 ng/ul)
nsEx4951,-52,-5692	pLMK34[*mig-24*p::*cnt-1a cDNA*](20 ng/ul) + *odr-1*p::RFP(+) (20 ng/ul) + pEB30 (25 ng/ul) + pBluescript (35 ng/ul)
nsEx5740,-42,-58	pLMK35[*lin-48*p::*cnt-1a(R490A) cDNA-SL2-mCh*](20 ng/ul) + *odr-1*p::RFP(+) (20 ng/ul) + pBluescript (60 ng/ul)
nsEx5741,-44,-60	pLMK36[*lin-48*p::*cnt-1b cDNA-SL2-mCh*](20 ng/ul) + *odr-1*p::RFP(+) (20 ng/ul) + pBluescript (60 ng/ul)
nsEx4938,-49,-50	pLMK37[*mig-24*p::*cnt-1b cDNA*](20 ng/ul) + *odr-1*p::RFP(+) (20 ng/ul) + pEB30 (25 ng/ul) + pBluescript (35 ng/ul)
nsEx5757	pLMK38[*cnt-1*p::GFP] (10 ng/ul) + *unc-119*(+) (25 ng/ul) + pBluescript (65 ng/ul)
nsEx5743,-56,-59	pLMK39[*lin-48*p::*efa-6a cDNA-SL2-mCh*](20 ng/ul) + *odr-1*p::RFP(+) (20 ng/ul) + pBluescript (60 ng/ul)
nsEx5133,-51,-52	pLMK40[*lin-48*p::*efa-6b cDNA-SL2-mCh*](20 ng/ul) + *odr-1*p::RFP(+) (20 ng/ul) + pBluescript (60 ng/ul)
nsEx5139,-47,-5140	pLMK41[*lin-48*p::*efa-6c cDNA-SL2-mCh*](20 ng/ul) + *odr-1*p::RFP(+) (20 ng/ul) + pBluescript (60 ng/ul)
nsEx5134,-35,-40	pLMK42[*lin-48*p::*efa-6d cDNA-SL2-mCh*](20 ng/ul) + *odr-1*p::RFP(+) (20 ng/ul) + pBluescript (60 ng/ul)
nsEx5100	pLMK43[*efa-6p*::GFP] (25 ng/ul) + *unc-119*(+) (25 ng/ul) + pBluescript (50 ng/ul)
nsIs625	UV/TMP integration of *nsEx5136*[pLMK44[*lin-48*p::ARF-6-YFP cDNA] (10 ng/ul)+ *unc-119*(+) (25 ng/ul) + pBluescript (65 ng/ul)]
nsIs636	UV/TMP integration of *nsEx5130*[pLMK45[*lin-48*p::ARF-6(D92N)-YFP cDNA] (10 ng/ul)+ *unc-119*(+) (25 ng/ul) + pBluescript (65 ng/ul)]

nsEx4620,-31,-45, -48,-49	pLMK64[*lin-48*p::MFGe8-GFP] (10 ng/ul) + *unc-119*(+) (25 ng/ul) + pBluescript (65 ng/ul), gift from Z. Zhou [151]
nsIs25	*ced-3*p::GFP, *rol-6*(+), gift from C. Maurer
nsEx4944,-5	pPG08[*ced-3*p::mCherry], a gift from P. Ghose (10 ng/ul) + *unc-119*(+) (25 ng/ul) + pBluescript (65 ng/ul)]
bcIs109	*ced-3*p::*ced-3-GFP*, *rol-6*(+), gift from B. Conradt
nsEx5307	pLMK65[*ced-4*p::mKate2] (25 ng/ul) + *unc-119*(+) (25 ng/ul) + pBluescript (50 ng/ul)]
nsEx5627,-8,-9,	pLMK66[*mig-24*p::*ced-4a* cDNA] (20 ng/ul) + *odr-1*p::RFP(+) (20 ng/ul) + pEB30 (20 ng/ul) + pBluescript (40 ng/ul)
nsEx5619,-20,-81	pLMK67[*lin-48*p::*ced-4a* cDNA-SL2-mCh] (20 ng/ul) + *odr-1*p::RFP(+) (20 ng/ul) + pBluescript (60 ng/ul)

6.1.3. Additional Plasmids generated or used in present study

Plasmid	Details
pLMK46	LexA-CNT-1A, Yeast two-hybrid (Y2H)
pLMK47	LexA-CNT-1B, Y2H
pLMK48	GAD-ARF-6, Y2H
pLMK49	GAD-ARF-6(D92N), Y2H
pLMK50	GAD-ARF-6(I42M,P43T), Y2H
pLMK51	LexA-ARF-6(T44N), Y2H
pLMK52	GAD-EFA-6A, Y2H
pLMK53	GAD-EFA-6B, Y2H
pLMK54	GAD-EFA-6C, Y2H
pLMK55	GAD-EFA-6D, Y2H
pLMK56	LexA-RAB-35(S24N), [GDP], Y2H
pLMK57	LexA-RAB-35(Q69L), [GTP], Y2H
pLMK58	GAD-CNT-1A, Y2H
pLMK59	GAD-CNT-1B, Y2H
pLMK60	GAD-RME-4A, Y2H
pLMK61	GAD-RME-4B, Y2H
pLMK62	*arf-6*[D92N] CRISPR targeting vector, pDD162 backbone
pLMK63	*arf-6*[T44N] CRISPR targeting vector, pDD162 backbone
pLMK64	*arf-6*[Q67L] CRISPR targeting vector, pDD162 backbone

6.2. C. elegans methods

6.2.1. Forward genetic screen and artificial insemination

Young L4 hermaphrodites containing *qIs56* [*lag-2*p::GFP] and *him-5*(*e1490*) were mutagenized with 75 mM ethylmethanesulfonate (EMS, Sigma M0880) for 4h at 20°C. Animals were synchronized twice by bleaching, and male animals were enriched by passing through a 40 µm cell strainer (BD Falcon) passively for 20 min [242]. Male animals fit more readily through the mesh than hermaphrodites and were enriched to ~88%. Animals were then scored under a fluorescent dissecting microscope (Leica) for presence of a linker cell by GFP 24h after the L4 to adult transition. GFP-expressing animals were isolated away from hermaphrodites for 24h after that to accumulate spermatids within the gonad. Mutant males were immobilized on a dried agar pad under immersion oil, and spermatids removed with a needle containing SM buffer (50 mM HEPES, pH 7, 50 mM NaCl, 25 mM KCl, 5 mM $CaCl_2$, 1 mM $MgSO_4$, 1 mg/ml BSA) [206]. An N2 hermaphrodite with a single row of eggs was then immobilized on the same dried agar pad and gently injected with the collected sperm through the vulva. We typically tried to insert all spermatids into a single hermaphrodite. GFP^+ heterozygous progeny were collected, allowed to self fertilize, and linker cell persistence confirmed under a dissecting microscope.

6.2.2. Gene identification

A combination of Hawaiian Snip-SNP mapping [243] and whole genome sequencing [244] was used to identify *rme-4*(*ns410*), *rme-4*(*ns412*), and *arf-6*(*ns388*) using output from galign [245]. *rme-4* was confirmed by fosmid rescue using WRM0615bE09, and *arf-6* identification was confirmed by mutant cDNA expression and CRISPR alleles.

6.2.3. Linker cell survival and corpse persistence assays

Linker cell death was scored as previously described [87]. Briefly, unstarved gravid hermaphrodites were bleached to isolate embryos, which were allowed to hatch overnight in M9. Synchronized L1 animals were released on 9-cm NGM plates seeded with OP50 or HT115 *E. coli* containing the RNAi construct of interest on IPTG-RNAi plates. Male animals were isolated onto a new plate prior to the L4-to-adult transition based on full retraction of the male tail tip with rays visible under the unshed L4 cuticle. 2h or 24h later, these animals were mounted onto 2% agarose-water pads, anaesthetized in 25 mM sodium azide, and examined on an Axioplan 2 fluorescence microscope (Zeiss) with a 63x/1.4NA objective (Zeiss) and Nomarski optics. The linker cell was identified by location, morphology, and fluorescence from reporter transgenes. Cells were then scored as surviving, dead, or gone based on DIC morphology and fluorescence. For heat shock experiments, animals were subjected to brief heat shock 4h prior to the L4 to adult transition [85].

6.2.4. Germline transformation and rescue experiments

Plasmid mixes containing the plasmid of interest, co-injection markers, and pBluescript were injected into both gonads of young adult hermaphrodites [246]. Injected animals were singled onto NGM plates and allowed to grow for two generations. Transformed animals based on co-injection markers were picked onto single plates, and screened for stable inheritance of the extrachromosomal array. Only lines from different P0 injected hermaphrodites were considered independent. For cell-specific rescue experiments, animals expressing mCherry in either the linker cell or the U.l/rp cells were picked to a new plate at the early L4 stage, before linker cell death, to avoid bias. Isolated animals were then staged based on tail morphology under a white light microscope for appropriate linker cell scoring.

6.2.5. RNAi assay

pL4440 RNAi plasmids containing coding sequence to genes of interest were isolated from the Ahringer Library [247] (Source BioScience) and the coding sequence was confirmed by sequencing. Additional targeting plasmids were generated by cloning in the Y2H hit to the pL4440 vector. All plasmids were grown at 37°C in HT115 bacteria, which have a plasmid containing an inducible promoter driving T7 RNA polymerase. The bacteria were plated on NGM plates that had been supplemented with the antibiotic carbomycin and IPTG. One day later, synchronized L1 animals were plated on the RNAi plates and grown for two days before assaying for linker cell corpse persistence.

6.2.6. Apoptotic corpse assay

Strain and vectors used in assay were from the DUALHybrid Kit (Dualsystem Biotech). Bait cDNA was cloned into the pLexA plasmid and prey cDNA was cloned into pGAD vectors. These plasmids were cotransformed into NMY51 yeast strain using the lithium acetate method described in the DualHybrid manual. Selection was performed on SD plates lacking the amino acids leucine, tryptophan, and histidine.

6.3. Molecular biology methods

6.3.1. Yeast two-hybrid screen

Strain and vectors used in assay were from the DUALHybrid Kit (Dualsystem Biotech). Bait cDNA was cloned into the pLexA plasmid and prey cDNA was cloned into pGAD vectors, or a *C. elegans* cDNA library tagged to GAD was used as bait, in the case of the screen. These plasmids were cotransformed into NMY51 yeast strain using the lithium acetate method described in the DualHybrid manual. Selection was performed on SD plates lacking at least the amino acids leucine, tryptophan, and histidine, and occasionally adenine, where noted.

6.3.2. Generation of arf-6 alleles using CRISPR-Cas9 genome editing

Alleles of *arf-6* were generated using the co-CRISPR-based genome editing method as previously described [248]. pDD162 was used as a vector backbone, and the following sgRNA sequences were added for each individual CRISPR attempt (D92N: 5' CTAAAAACCTGTCTCTATCAG 3'; T44N: 5' TCAGTGACCACAATGACGA 3'; Q67L 5' CTTCAGGACGTCGGCGGAC 3') to generate *arf-6* targeting vectors. A *dpy-10* sgRNA-pDD162-based vector was also generated (5' GCTACCATAGGCAC CACGAG 3'). Single-stranded repair oligos were PAGE purified and ordered from Sigma (D92N: 5' aggaaaaaaaccaatttttccgcatttttcgcctaaaaacCTGTCTCTATtAGCaG CGTCCATCACAAAAATGAGCGCCTGAGTTCCTGTGTAATAATGTC 3'; T44N: 5' agCAATTCTGTACAAACTGAAGCTCGGGCAATCAGTGACCACAATTCCGAacGT GGGCTTCAATGTGGAGACTGTCACGTATAAAAATATCAAATTCAACGT 3'; Q67L 5' ggcctaaaaacccccaaaaaccccaatttttcttcagGACGTCGGCGGACttGACAAAATTCGAC CCCTCTGGCGACATTATTACACAGGAACTCAGGCGCT 3', *dpy-10*(*cn64*): 5' CACTT GAACTTCAATACGGCAAGATGAGAATGACTGGAAACCGTACCGCATGCGGTG CCTATGGTAGCGGAGCTTCACATGGCTTCAGACCAACAGCCTAT 3' [248]. N2 animals were injected with the following mix: 50 ng/µl dpy-10 sgRNA, 50 ng/µl *arf-6* targeting vector, 20 ng/µl *dpy-10*(*cn64*) repair oligo, 20 ng/µl *arf-6* repair oligo in 1x injection buffer (20mM potassium phosphate, 3mM potassium citrate, 2% PEG, pH 7.5). F1 animals with Dpy or Rol phenotypes were picked to individual plates, indicating a CRISPR-based editing event had occurred. F1 animals were allowed to lay eggs, and then genotyped for successful co-conversion of the *arf-6* locus using PCR and restriction enzyme screening or Cel1 digestion of heteroduplex DNA [249]. Non-Rol, non-Dpy F2 animals were then singled and homozygosed for the *arf-6* mutation.

6.3.3. Plasmid construction

Plasmids containing *lin-48*p, *mig-24*p, or transcriptional reporters were cloned

using multi-piece one-step cloning into a modified pPD95.75 backbone lacking GFP. For CRISPR-related vectors, plasmids were generated using a site-directed plasmid mutagenesis protocol on pDD162 [250,251]. Yeast vectors were generated using traditional cloning from either a pLexA-N-terminus vector or a pGAL4AD-N-terminus vector (Dualsystems Biotech), and single amino acid change variants were generated using QuikChange (Agilent).

6.4. Cell biology methods

6.4.1. Long-term imaging and movie generation

Early L4 male animals were imaged in a microfluidic device described in detail in [201]. Animals were fed a constant flow of NA22 bacteria in S medium, supplemented with kanamycin (50 ng/µl) to prevent bacterial overgrowth. Animals were immobilized and imaged every 8 minutes for at least 20h. Mutant animals were typically imaged for > 30h. Exposure time and light intensity was held constant across strains when the same integrated transgene was imaged. Occasionally tail development was perturbed by the flow of medium and repeated immobilization procedures, and these animals were not included in subsequent analyses.

6.4.2. Deconvolution

Images were cropped to a region of interest surrounding the linker cell. We measured the point-spread function (PSF) of our optical setup using red (580/605nm) and green (505/515nm) fluorescent 200nm beads (ThermoFisher Scientific). Using these PSFs, we deconvolved the cropped fluorescence z-stacks using the classic maximum likelihood estimation (CMLE) algorithm with standard parameters (refractive index of imaging medium: 1.338) in the Huygens Essential software (Huygens Essential 3.7.1) by Scientific Volume Imaging (SVI).

6.4.3. Image Analysis

Image analysis was performed using custom-written Matlab R2016b (Mathworks) scripts by Wolfgang Keil. To overlay imaging frames, I straightened each three-dimensional image stack using a previously published algorithm [201,252] based on a manually selected worm backbone in the DIC channel. To correct for small residual animal movements during multi-channel acquisition, obvious landmarks visible in the fluorescence channels, such as the cloaca, fluorescently labeled cells in the animal's tail, or vesicles within the U-cell descendants were then manually aligned to the DIC channel in each frame. Time-lapse movies were generated by centering all straightened, aligned images on the linker cell and cropping the entire movie to an appropriate size.

6.4.4. Protein structures

The co-crystal structure of human Arf6 with the ArfGAP ASAP3 (PDB 3LVQ) was examined in Pymol (The PyMOL Molecular Graphics System, Version 1.2r3pre, Schrödinger, LLC.) in silico mutagenesis for D92N and I42M;P43T was performed and hydrophilic interactions tested within Pymol. Key residues in ASAP3 are conserved in *C. elegans* CNT-1, and those for Arf6 are conserved in *C. elegans* ARF-6.

6.5. Data analysis

Statistical analysis was performed using GraphPad Prism. Statistical parameters including mean ± standard error of the proportion, mean ± SEM, and N are reported in the main text, figures and figure legends. Data is judged to be statistically significant when $p < 0.05$ by Fisher's exact test, χ^2-test, or student's t-test, where appropriate.

When comparing a transgenic line to the parental strain, a minimum of three independent lines was scored. Approximately 100 animals from each of these lines were examined for linker cell defects, and compared to the parental strain using a Fisher's exact test to determine significance. For ease of presentation, I pooled the lines from

a given experiment and displayed them on the relevant figure using mean ± SEM (N = 3, 4, or 5 lines). If only a subset of the three lines showed significance using a Fisher's exact test, I indicated this on the figure and figure legend.

7. Appendix: A list of mutants from the genetic screen.

Category explanations:

I. weakly surviving: Animals have a small but significant increase in the number of surviving cells.

II. relatively healthy: There are no surviving cells by our strict classifications, but the cells look pretty good overall. May represent a timing defect.

III. odd death: Cells are still dying, but are doing so in an atypical manner. May represent an aberration in engulfment or degradation.

IV. delayed death: There is an increase in the number of cell corpses at 2h after the adult molt, but not at 24h.

V. persistent corpse: There is an increase in the number of cell corpses at both 2h and 24h after the molt.

FP. may represent a false positive.

Strain/Allele	Category	% SLCs	% RH	%GFP 2h	%GFP 24h	Notes
Wild-type (OS238)		3%	6%	40% (157)	12% (100)	
ns414	I	26%		51% (35)	29% (14)	
ns417	I	17%	9%	63% (35)	33% (50)	Likely on LGV
ns575	I	15%	17%	60% (53)	20% (55)	
ns570	I	13%	17%	64% (47)	19% (58)	
ns427	I	11%	0	39% (28)	7% (30)	
ns578	I	10%	14%	52% (50)	12% (51)	
ns425	II	0	36%	80% (36)	20% (45)	
ns574	II	7%	25%	52% (56)	18% (39)	
ns389	II	5%	21%	83% (58)	51% (53)	Likely on LGIII
ns428	II	3%	23%	50% (26)	n.d.	
ns426	III	0	n.d.	71% (21)	11% (37)	33% OD
ns587	III	2%	4%	46% (46)	10% (29)	24% OD
ns485	III	0	9%	45% (47)	20% (35)	15% OD
ns580	III	2%	2%	59% (46)	5% (56)	16% OD
ns573	III	0	25%	70% (38)	9% (43)	25% OD
ns579	III	9%	n.d.	47% (34)	n.d.	18% OD
ns594	III	2%	12%	41% (49)	11% (44)	8% OD
ns435	IV	0	6%	78% (18)	24% (59)	
ns483	IV	0	0	74% (38)	19% (37)	29% OD
ns581	IV	9%	2%	84% (45)	13% (38)	
ns416	IV	3%	3%	73% (37)	20% (25)	11% OD
ns544	IV	12%	8%	65% (49)	29% (42)	
ns431	IV	14%	8%	61% (49)	2% (45)	
ns432	IV	4%	4%	56% (45)	21% (43)	

ns545	IV	8%	6%	59% (49)	20% (13)	
ns598	IV	7%	7%	74% (43)	12% (5)	Likely *col-108*
ns388	V	2%	0	95% (37)	60% (38)	*arf-6*
ns412	V	3%	2%	88% (42)	57% (28)	*rme-4*
ns576	V	12%	21%	85% (33)	30% (46)	
ns410	V	0%	13%	95% (41)	67% (33)	*rme-4*
ns430	V	0	9%	61% (46)	30% (54)	
ns434	V	4%	8%	52% (50)	27% (26)	
ns421	FP	2%	14%	55% (42)	13% (38)	
ns429	FP	2%	12%	52% (50)	11% (134)	
ns586	FP	2%	11%	40% (53)	16% (70)	
ns568	FP	2%	10%	56% (62)	12% (50)	
ns577	FP	2%	13%	53% (50)	9% (34)	
ns584	FP	0	5%	57% (37)	17% (35)	
ns411	FP	0	0	38% (21)	21% (24)	
ns566	FP	8%	9%	41% (46)	8% (52)	
ns419	FP	9%	0	40% (23)	6% (18)	
ns418	FP	8%	0	33% (24)	40% (10)	
ns433	FP	7%	9%	38% (45)	10% (42)	
ns415	FP?	0	n.d.	38% (45)	11% (45)	11% OD
ns575	FP	7%	10%	54% (41)	21% (39)	9% OD

8. Bibliography

[1] Lockshin RA, Williams CM. Programmed cell death—II. Endocrine potentiation of the breakdown of the intersegmental muscles of silkmoths. J Insect Physiol 1964;10:643–9.

[2] Lockshin RA, Zakeri Z. Programmed cell death and apoptosis: origins of the theory. Nat Rev Mol Cell Biol 2001;2:545–50.

[3] Kerr JFR, Wyllie AH, Currie AR. Apoptosis: A Basic Biological Phenomenon with Wide-ranging Implications in Tissue Kinetics. Br J Cancer 1972;26:239–57.

[4] Wyllie AH, Kerr JF, Currie AR. Cell death: the significance of apoptosis. Int Rev Cytol 1980;68:251–306.

[5] Ellis H, Horvitz HR. Genetic control of programmed cell death in the nematode *C. elegans*. Cell 1986;44:817–29.

[6] Xue D, Shaham S, Horvitz HR. The *Caenorhabditis elegans* cell-death protein CED-3 is a cysteine protease with substrate specificities similar to those of the human CPP32 protease. Genes Dev 1996;10:1073–83.

[7] Song Z. DCP-1, a Drosophila Cell Death Protease Essential for Development. Science 1997;275:536–40.

[8] Chinnaiyan AM, Chaudhary D, O'Rourke K, Koonin EV, Dixit VM. Role of CED-4 in the activation of CED-3. Nature 1997;388:728–9.

[9] Li P, Nijhawan D, Budihardjo I, Srinivasula SM, Ahmad M, Alnemri ES, et al. Cytochrome c and dATP-Dependent Formation of Apaf-1/Caspase-9 Complex Initiates an Apoptotic Protease Cascade. Cell 1997;91:479–89.

[10] Conradt B, Horvitz HR. The C. elegans Protein EGL-1 Is Required for Programmed Cell Death and Interacts with the Bcl-2–like Protein CED-9. Cell 1998;93:519–29.

[11] Hengartner MO, Ellis R, Horvitz R. Caenorhabditis elegans gene ced-9 protects cells from programmed cell death. Nature 1992;356:494–9.

[12] White K, Grether ME, Abrams JM, Young L, Farrell K, Steller H. Genetic control of programmed cell death in Drosophila. Science 1994;264:677–83.

[13] Kuida K, Zheng TS, Na S, Kuan C-Y, Yang D, Karasuyama H, et al. Decreased apoptosis in the brain and premature lethality in CPP32-deficient mice. Nature 1996;384:368–72.

[14] Goyal L, McCall K, Agapite J, Hartwieg E, Steller H. Induction of apoptosis by Drosophila reaper, hid and grim through inhibition of IAP function. Embo J 2000;19:589–97.

[15] Yoo SJ, Huh JR, Muro I, Yu H, Wang L, Wang SL, et al. Hid, Rpr and Grim negatively regulate DIAP1 levels through distinct mechanisms. Nat Cell Biol 2002;4:416–24.

[16] Sandu C, Ryoo HD, Steller H. Drosophila IAP antagonists form multimeric complexes to promote cell death. J Cell Biol 2010;190:1039–52.

[17] Hay BA, Wassarman DA, Rubin GM. Drosophila homologs of baculovirus inhibitor of apoptosis proteins function to block cell death. Cell 1995;83:1253–62.

[18] Roy N, Mahadevan MS, McLean M, Shutter G, Yaraghi Z, Farahani R, et al. The gene for neuronal apoptosis inhibitory protein is partially deleted in individuals with spinal muscular atrophy. Cell 1995;80:167–78.

[19] Yu X, Wang L, Acehan D, Wang X, Akey CW. Three-dimensional structure of a double apoptosome formed by the Drosophila Apaf-1 related killer. J Mol Biol 2006;355:577–89.

[20] Chew SK, Akdemir F, Chen P, Lu W-J, Mills K, Daish T, et al. The apical caspase dronc governs programmed and unprogrammed cell death in Drosophila. Dev Cell 2004;7:897–907.

[21] Quinn LM, Dorstyn L, Mills K, Colussi PA, Chen P, Coombe M, et al. An essential role for the caspase dronc in developmentally programmed cell death in Drosophila. J Biol Chem 2000;275:40416–24.

[22] Xu D, Wang Y, Willecke R, Chen Z, Ding T, Bergmann A. The effector caspases drICE and dcp-1 have partially overlapping functions in the apoptotic pathway in Drosophila. Cell Death Differ 2006;13:1697–706.

[23] Laundrie B, Peterson JS, Baum JS, Chang JC, Fileppo D, Thompson SR, et al. Germline cell death is inhibited by P-element insertions disrupting the dcp-1/pita nested gene pair in Drosophila. Genetics 2003;165:1881–8.

[24] Bouillet P, Strasser A. BH3-only proteins - evolutionarily conserved proapoptotic Bcl-2 family members essential for initiating programmed cell death. J Cell Sci 2002;115:1567–74.

[25] Sattler M, Liang H, Nettesheim D, Meadows RP, Harlan JE, Eberstadt M, et al. Structure of Bcl-xL-Bak peptide complex: recognition between regulators of apoptosis. Science 1997;275:983–6.

[26] Wolter KG, Hsu YT, Smith CL, Nechushtan A, Xi XG, Youle RJ. Movement of Bax from the cytosol to mitochondria during apoptosis. J Cell Biol 1997;139:1281–92.

[27] Wei MC, Lindsten T, Mootha VK, Weiler S, Gross A, Ashiya M, et al. tBID, a membrane-targeted death ligand, oligomerizes BAK to release cytochrome c. Genes Dev 2000;14:2060–71.

[28] Zong WX, Lindsten T, Ross AJ, MacGregor GR, Thompson CB. BH3-only proteins that bind pro-survival Bcl-2 family members fail to induce apoptosis in the absence of Bax and Bak. Genes Dev 2001;15:1481–6.

[29] Qiu X-B, Goldberg AL. The membrane-associated inhibitor of apoptosis protein, BRUCE/Apollon, antagonizes both the precursor and mature forms of Smac and caspase-9. J Biol Chem 2005;280:174–82.

[30] Zhou L, Chang DC. Dynamics and structure of the Bax-Bak complex responsible for releasing mitochondrial proteins during apoptosis. J Cell Sci 2008;121:2186–96.

[31] Jürgensmeier JM, Xie Z, Deveraux Q, Ellerby L, Bredesen D, Reed JC. Bax directly induces release of cytochrome c from isolated mitochondria. Proc Natl Acad Sci USA 1998;95:4997–5002.

[32] Hakem R, Hakem A, Duncan GS, Henderson JT, Woo M, Soengas MS, et al. Differential Requirement for Caspase 9 in Apoptotic Pathways In Vivo. Cell 1998;94:339–52.

[33] Kuida K, Haydar TF, Kuan CY, Gu Y, Taya C, Karasuyama H, et al. Reduced apoptosis and cytochrome c-mediated caspase activation in mice lacking caspase 9. Cell 1998;94:325–37.

[34] Cecconi F, Alvarez-Bolado G, Meyer BI, Roth KA, Gruss P. Apaf1 (CED-4 Homolog) Regulates Programmed Cell Death in Mammalian Development. Cell 1998;94:727–37.

[35] Yoshida H, Kong Y-Y, Yoshida R, Elia AJ, Hakem A, Hakem R, et al. Apaf1 Is Required for Mitochondrial Pathways of Apoptosis and Brain Development. Cell 1998;94:739–50.

[36] Lindsten T, Ross AJ, King A, Zong W-X, Rathmell JC, Shiels HA, et al. The Combined Functions of Proapoptotic Bcl-2 Family Members Bak and Bax Are Essential for Normal Development of Multiple Tissues. Mol Cell 2000;6:1389–99.

[37] Leonard JR, Klocke BJ, D'sa C, Flavell RA, Roth KA. Strain-Dependent Neurodevelopmental Abnormalities in Caspase-3-Deficient Mice. J Neuropath Exp Neurol 2002;61:673–7.

[38] Honarpour N, Gilbert SL, Lahn BT, Wang X, Herz J. Apaf-1 deficiency and neural tube closure defects are found in fog mice. Proc Natl Acad Sci USA 2001;98:9683–7.

[39] Okamoto H, Shiraishi H, Yoshida H. Histological analyses of normally grown, fertile Apaf1-deficient mice. Cell Death Differ 2005;13:668–71.

[40] Woo M, Hakem R, Soengas MS, Duncan GS, Shahinian A, Kagi D, et al. Essential contribution of caspase 3/CPP32 to apoptosis and its associated nuclear changes. Genes Dev 1998;12:806–19.

[41] Lindsten T, Thompson CB. Cell death in the absence of Bax and Bak. Cell Death Differ 2006;13:1272–6.

[42] Pajni-Underwood S, Wilson CP, Elder C, Mishina Y, Lewandoski M. BMP signals control limb bud interdigital programmed cell death by regulating FGF signaling. Development 2007;134:2359–68.

[43] Oppenheim RW. Cell Death During Development of the Nervous System. Annu Rev Neurosci 1991;14:453–501.

[44] Nonomura K, Yamaguchi Y, Hamachi M, Koike M, Uchiyama Y, Nakazato K, et al. Local Apoptosis Modulates Early Mammalian Brain Development through the Elimination of Morphogen-Producing Cells. Dev Cell 2013;27:621–34. .

[45] Miura M, Chen X-D, Allen MR, Bi Y, Gronthos S, Seo B-M, et al. A crucial role of caspase-3 in osteogenic differentiation of bone marrow stromal stem cells. J Clin Invest 2004;114:1704–13.

[46] Fuchs Y, Steller H. Live to die another way: modes of programmed cell death and the signals emanating from dying cells. Nat Rev Mol Cell Biol 2015;16:329–44.

[47] Clarke PGH. Developmental cell death: morphological diversity and multiple mechanisms. Anat Embryol 1990;181:195–213.

[48] Yacobi-Sharon K, Namdar Y, Arama E. Alternative germ cell death pathway in Drosophila involves HtrA2/Omi, lysosomes, and a caspase-9 counterpart. Dev Cell 2013;25:29–42.

[49] Vercammen D, Beyaert R, Denecker G, Goossens V, Van Loo G, Declercq W, et al. Inhibition of Caspases Increases the Sensitivity of L929 Cells to Necrosis Mediated by Tumor Necrosis Factor. J Exp Med 1998;187:1477–85.

[50] Strauss KM, Martins LM, Plun-Favreau H, Marx FP, Kautzmann S, Berg D, et al. Loss of function mutations in the gene encoding Omi/HtrA2 in Parkinson's disease. Hum Mol Genet 2005;14:2099–111.

[51] Suzuki Y, Imai Y, Nakayama H, Takahashi K, Takio K, Takahashi R. A Serine Protease, HtrA2, Is Released from the Mitochondria and Interacts with XIAP, Inducing Cell Death. Mol Cell 2001;8:613–21.

[52] Fehrenbacher N, Gyrd-Hansen M, Poulsen B, Felbor U, Kallunki T, Boes M, et al. Sensitization to the lysosomal cell death pathway upon immortalization and transformation. Cancer Res 2004;64:5301–10.

[53] Kreuzaler PA, Staniszewska AD, Li W, Omidvar N, Kedjouar B, Turkson J, et al. Stat3 controls lysosomal-mediated cell death *in vivo*. Nat Cell Biol 2011;13:303–9.

[54] Allan DJ, Harmon BV, Roberts SA. Spermatogonial apoptosis has three morphologically recognizable phases and shows no circadian rhythm during normal spermatogenesis in the rat. Cell Prolif 1992;25:241–50.

[55] Lee B, Park I, Jin S, Choi H, Kwon JT, Kim J, et al. Impaired Spermatogenesis and Fertility in Mice Carrying a Mutation in the *Spink2* Gene Expressed Predominantly in Testes. J Biol Chem 2011;286:29108–17. .

[56] Knudson CM, Tung KSK, Tourtellotte WG, Brown GAJ, Korsmeyer SJ. Bax-Deficient Mice with Lymphoid Hyperplasia and Male Germ Cell Death. Science 1995;270:96–9.

[57] Rodriguez I, Ody C, Araki K, Garcia I, Vassalli P. An early and massive wave of germinal cell apoptosis is required for the development of functional spermatogenesis. Embo J 1997;16:2262–70.

[58] Jenkins VK, Timmons AK, McCall K. Diversity of cell death pathways: insight from the fly ovary. Trends Cell Biol 2013;23:567–74.

[59] Cavaliere V, Taddei C, Gargiulo G. Apoptosis of nurse cells at the late stages of oogenesis of *Drosophila melanogaster*. Dev Genes Evol 1998;208:106–12.

[60] Bass BP, Tanner EA, Mateos San Martín D, Blute T, Kinser RD, Dolph PJ, et al. Cell-autonomous requirement for *DNaseII* in nonapoptotic cell death. Cell Death Differ 2009;16:1362–71.

[61] Nezis IP, Shravage BV, Sagona AP, Lamark T, Bjørkøy G, Johansen T, et al. Autophagic degradation of dBruce controls DNA fragmentation in nurse cells during late *Drosophila melanogaster* oogenesis. J Cell Biol 2010;190:523–31.

[62] Peterson JS, Barkett M, McCall K. Stage-specific regulation of caspase activity in *drosophila* oogenesis. Dev Biol 2003;260:113–23.

[63] Mazzalupo S, Cooley L. Illuminating the role of caspases during Drosophila oogenesis. Cell Death Differ 2006;13:1950–9.

[64] Bass BP, Cullen K, McCall K. The axon guidance gene *lola* is required for programmed cell death in the *Drosophila* ovary. Dev Biol 2007;304:771–85.

[65] Foley K, Cooley L. Apoptosis in late stage Drosophila nurse cells does not require genes within the H99 deficiency. Development 1998;125:1075–82.

[66] Peterson JS, Bass BP, Jue D, Rodriguez A, Abrams JM, McCall K. Noncanonical cell death pathways act during *Drosophila* oogenesis. Genesis 2007;45:396–404.

[67] Baum JS, Arama E, Steller H, McCall K. The Drosophila caspases Strica and Dronc function redundantly in programmed cell death during oogenesis. Cell Death Differ 2007;14:1508–17.

[68] Xu D, Li Y, Arcaro M, Lackey M, Bergmann A. The CARD-carrying caspase Dronc is essential for most, but not all, developmental cell death in Drosophila. Development 2005;132:2125–34.

[69] Nezis IP, Stravopodis DJ, Margaritis LH, Papassideri IS. Chromatin condensation of ovarian nurse and follicle cells is regulated independently from DNA fragmentation during Drosophila late oogenesis. Differentiation 2006;74:293–304.

[70] Mukae N, Yokoyama H, Yokokura T, Sakoyama Y, Nagata S. Activation of the innate immunity in Drosophila by endogenous chromosomal DNA that escaped apoptotic degradation. Genes Dev 2002;16:2662–71.

[71] Peterson JS, McCall K. Combined Inhibition of Autophagy and Caspases Fails to Prevent Developmental Nurse Cell Death in the Drosophila melanogaster Ovary. PLoS ONE 2013;8:e76046.

[72] Timmons AK, Mondragon AA, Schenkel CE, Yalonetskaya A, Taylor JD, Moynihan KE, et al. Phagocytosis genes nonautonomously promote developmental cell death in the Drosophila ovary. Proc Natl Acad Sci USA 2016;113:E1246–55.

[73] Jiang C, Baehrecke EH, Thummel CS. Steroid regulated programmed cell death during Drosophila metamorphosis. Development 1997;124:4673–83.

[74] Berry DL, Baehrecke EH. Growth Arrest and Autophagy Are Required for Salivary Gland Cell Degradation in Drosophila. Cell 2007;131:1137–48.

[75] Lee CY, Baehrecke EH. Steroid regulation of autophagic programmed cell death during development. Development 2001;128:1443–55.

[76] Martin DN. Caspases function in autophagic programmed cell death in Drosophila. Development 2003;131:275–84.

[77] Gorski SM, Chittaranjan S, Pleasance ED, Freeman JD, Anderson CL, Varhol RJ, et al. A SAGE Approach to Discovery of Genes Involved in Autophagic Cell Death. Curr Biol 2003;13:358–63.

[78] Lee C-Y, Clough EA, Yellon P, Teslovich TM, Stephan DA, Baehrecke EH. Genome-Wide Analyses of Steroid- and Radiation-Triggered Programmed Cell Death in Drosophila. Curr Biol 2003;13:350–7.

[79] Muro I. The Drosophila caspase Ice is important for many apoptotic cell deaths and for spermatid individualization, a nonapoptotic process. Development 2006;133:3305–15.

[80] McPhee CK, Logan MA, Freeman MR, Baehrecke EH. Activation of autophagy during cell death requires the engulfment receptor Draper. Nature 2010;465:1093–6.

[81] Wu YC, Stanfield GM, Horvitz HR. NUC-1, a *Caenorhabditis elegans* DNase II homolog, functions in an intermediate step of DNA degradation during apoptosis. Genes Dev 2000;14:536–48.

[82] Abraham MC, Lu Y, Shaham S. A morphologically conserved nonapoptotic program promotes linker cell death in *Caenorhabditis elegans*. Dev Cell 2007;12:73–86.

[83] Denning DP, Hatch V, Horvitz HR. Both the caspase CSP-1 and a caspase-independent pathway promote programmed cell death in parallel to the canonical pathway for apoptosis in *Caenorhabditis elegans*. PLoS Genet 2013;9:e1003341.

[84] Kimble J. Alterations in cell lineage following laser ablation of cells in the somatic gonad of *Caenorhabditis elegans.* Dev Biol 1981;87:286–300.

[85] Kinet MJ, Malin JA, Abraham MC, Blum ES, Silverman MR, Lu Y, et al. HSF-1 activates the ubiquitin proteasome system to promote non-apoptotic

developmental cell death in *C. elegans*. Elife 2016;5:73.

[86] Malin JA, Kinet MJ, Abraham MC, Blum ES, Shaham S. Transcriptional control of non-apoptotic developmental cell death in *C. elegans*. Cell Death Differ 2016;23:1985–94.

[87] Blum ES, Abraham MC, Yoshimura S, Lu Y, Shaham S. Control of nonapoptotic developmental cell death in *Caenorhabditis elegans* by a polyglutamine-repeat protein. Science 2012;335:970–3.

[88] Horvitz HR, Sternberg PW, Greenwald IS, Fixsen W, Ellis HM. Mutations That Affect Neural Cell Lineages and Cell Fates during the Development of the Nematode *Caenorhabditis elegans*. Cold Spring Harb Symp Quant Biol 1983;48:453–63.

[89] Lunn ER, Perry VH, Brown MC, Rosen H, Gordon S. Absence of Wallerian Degeneration does not Hinder Regeneration in Peripheral Nerve. Eur J Neurosci 1989;1:27–33.

[90] Mack TG, Reiner M, Beirowski B, Mi W, Emanuelli M, Wagner D, et al. Wallerian degeneration of injured axons and synapses is delayed by a Ube4b/Nmnat chimeric gene. Nat Neurosci 2001;4:1199–206.

[91] Osterloh JM, Yang J, Rooney TM, Fox AN, Adalbert R, Powell EH, et al. dSarm/Sarm1 Is Required for Activation of an Injury-Induced Axon Death Pathway. Science 2012;337:481–4.

[92] Gerdts J, Summers DW, Sasaki Y, DiAntonio A, Milbrandt J. Sarm1-mediated axon degeneration requires both SAM and TIR interactions. J Neurosci 2013;33:13569–80.

[93] Summers DW, DiAntonio A, Milbrandt J. Mitochondrial dysfunction induces Sarm1-dependent cell death in sensory neurons. J Neurosci 2014;34:9338–50.

[94] Blum ES, Schwendeman AR, Shaham S. PolyQ disease: misfiring of a developmental cell death program? Trends Cell Biol 2013;23:168–74.

[95] Davies SW, Turmaine M, Cozens BA, DiFiglia M, Sharp AH, Ross CA, et al. Formation of Neuronal Intranuclear Inclusions Underlies the Neurological Dysfunction in Mice Transgenic for the HD Mutation. Cell 1997;90:537–48.

[96] Turmaine M, Raza A, Mahal A, Mangiarini L, Bates GP, Davies SW. Nonapoptotic neurodegeneration in a transgenic mouse model of Huntington's disease. Proc Natl Acad Sci USA 2000;97:8093–7.

[97] Bots GTAM, Bruyn GW. Neuropathological changes of the nucleus accumbens

in Huntington's chorea. Acta Neuropathologica 1981;55:21–2.

[98] Skinner PJ, Koshy BT, Cummings CJ, Klement IA, Helin K, Servadio A, et al. Ataxin-1 with an expanded glutamine tract alters nuclear matrix-associated structures. Nature 1997;389:971–4.

[99] Evert BO. High level expression of expanded full-length ataxin-3 in vitro causes cell death and formation of intranuclear inclusions in neuronal cells. Hum Mol Genet 1999;8:1169–76.

[100] Takahashi H, Egawa S, Piao Y-S, Hayashi S, Yamada M, Shimohata T, et al. Neuronal nuclear alterations in dentatorubral-pallidoluysian atrophy: ultrastructural and morphometric studies of the cerebellar granule cells. Brain Res 2001;919:12–9.

[101] Zander C. Similarities between spinocerebellar ataxia type 7 (SCA7) cell models and human brain: proteins recruited in inclusions and activation of caspase-3. Hum Mol Genet 2001;10:2569–79.

[102] Maat-Schieman MLC, Dorsman JC, Smoor MA, Siesling S, Van Duinen SG, Verschuuren JJGM, et al. Distribution of Inclusions in Neuronal Nuclei and Dystrophic Neurites in Huntington Disease Brain. J Neuropath Exp Neurol 1999;58:129–37.

[103] Schwartz LM, Smith SW, Jones ME, Osborne BA. Do all programmed cell deaths occur via apoptosis? Proc Natl Acad Sci USA 1993;90:980–4.

[104] Schwartz LM, Myer A, Kosz L, Engelstein M, Maier C. Activation of polyubiquitin gene expression during developmentally programmed cell death. Neuron 1990;5:411–9.

[105] Haas AL, Baboshina O, Williams B, Schwartz LM. Coordinated Induction of the Ubiquitin Conjugation Pathway Accompanies the Developmentally Programmed Death of Insect Skeletal Muscle. J Biol Chem 1995;270:9407–12.

[106] Kelliher MA, Grimm S, Ishida Y, Kuo F, Stanger BZ, Leder P. The Death Domain Kinase RIP Mediates the TNF-Induced NF-κB Signal. Immunity 1998;8:297–303.

[107] Li P, Allen H, Banerjee S, Franklin S, Herzog L, Johnston C, et al. Mice deficient in IL-1β-converting enzyme are defective in production of mature IL-1β and resistant to endotoxic shock. Cell 1995;80:401–11.

[108] Schweichel JU, Merker HJ. The morphology of various types of cell death in prenatal tissues. Teratology 1973;7:253–66.

[109] Candi E, Schmidt R, Melino G. The cornified envelope: a model of cell death in the skin. Nat Rev Mol Cell Biol 2005;6:328–40.

[110] Oppenheim RW, Flavell RA, Vinsant S, Prevette D, Kuan CY, Rakic P. Programmed cell death of developing mammalian neurons after genetic deletion of caspases. J Neurosci 2001;21:4752–60.

[111] Enari M, Sakahira H, Yokoyama H, Okawa K, Iwamatsu A, Nagata S. A caspase-activated DNase that degrades DNA during apoptosis, and its inhibitor ICAD. Nature 1998;391:43–50.

[112] Sun W, Gould TW, Vinsant S, Prevette D, Oppenheim RW. Neuromuscular development after the prevention of naturally occurring neuronal death by Bax deletion. J Neurosci 2003;23:7298–310.

[113] Oppenheim RW, Blomgren K, Ethell DW, Koike M, Komatsu M, Prevette D, et al. Developing Postmitotic Mammalian Neurons *In Vivo* Lacking Apaf-1 Undergo Programmed Cell Death by a Caspase-Independent, Nonapoptotic Pathway Involving Autophagy. J Neurosci 2008;28:1490–7.

[114] Hamburger V, Levi-montalcini R. Proliferation, differentiation and degeneration in the spinal ganglia of the chick embryo under normal and experimental conditions. J Exp Zool 1949;111:457–501.

[115] O'Connor TM. Cell death in the embryonic chick spinal cord. J Cell Biol 1974;60:448–59.

[116] Chu-Wang IW, Oppenheim RW. Cell death of motoneurons in the chick embryo spinal cord. I. A light and electron microscopic study of naturally occurring and induced cell loss during development. J Comp Neurol 1978;177:33–57.

[117] Borsello T, Mottier V, Castagné V, Clarke PGH. Ultrastructure of retinal ganglion cell death after axotomy in chick embryos. J Comp Neurol 2002;453:361–71.

[118] Pilar G. Ultrastructural differences during embryonic cell death in normal and peripherally deprived ciliary ganglia. J Cell Biol 1976;68:339–56.

[119] Brunet N, Tarabal O, Portero-Otín M, Oppenheim RW, Esquerda JE, Calderó J. Survival and death of mature avian motoneurons in organotypic slice culture: Trophic requirements for survival and different types of degeneration. J Comp Neurol 2007;501:669–90.

[120] Yaginuma H, Shiraiwa N, Shimada T, Nishiyama K, Hong J, Wang S, et al. Caspase Activity Is Involved in, but Is Dispensable for, Early Motoneuron Death in the Chick Embryo Cervical Spinal Cord. Mol Cell Neurosci 2001;18:168–82.

[121] Pampfer S, Donnay I. Apoptosis at the time of embryo implantation in mouse and rat. Cell Death Differ 1999;6:533–45.

[122] El-Shershaby AM, Hinchliffe JR. Cell redundancy in the zona-intact preimplantation mouse blastocyst: a light and electron microscope study of dead cells and their fate. J Embryol Exp Morphol 1974;31:643–54.

[123] Zhang Q, Paria BC. Importance of Uterine Cell Death, Renewal, and Their Hormonal Regulation in Hamsters that Show Progesterone-Dependent Implantation. Endocrinology 2006;147:2215–27.

[124] Leidenfrost S, Boelhauve M, Reichenbach M, Güngör T, Reichenbach H-D, Sinowatz F, et al. Cell Arrest and Cell Death in Mammalian Preimplantation Development: Lessons from the Bovine Model. PLoS ONE 2011;6:e22121.

[125] Parr EL, Tung HN, Parr MB. Apoptosis as the Mode of Uterine Epithelial Cell Death during Embryo Implantation in Mice and Rats. Biol Reprod 1987;36:211–25.

[126] El-Shershaby AM, Hinchliffe JR. Epithelial autolysis during implantation of the mouse blastocyst: an ultrastructural study. J Embryol Exp Morphol 1975;33:1067–80.

[127] Li Y, Sun X, Dey SK. Entosis Allows Timely Elimination of the Luminal Epithelial Barrier for Embryo Implantation. Cell Rep 2015;11:358–65.

[128] Overholtzer M, Mailleux AA, Mouneimne G, Normand G, Schnitt SJ, King RW, et al. A nonapoptotic cell death process, entosis, that occurs by cell-in-cell invasion. Cell 2007;131:966–79.

[129] Mullen RD, Behringer RR. Molecular genetics of Müllerian duct formation, regression and differentiation. Sex Dev 2014;8:281–96.

[130] Dyche WJ. A comparative study of the differentiation and involution of the Mullerian duct and Wolffian duct in the male and female fetal mouse. J Morphol 1979;162:175–209.

[131] Cate RL, Mattaliano RJ, Hession C, Tizard R, Farber NM, Cheung A, et al. Isolation of the bovine and human genes for müllerian inhibiting substance and expression of the human gene in animal cells. Cell 1986;45:685–98.

[132] Kobayashi A, Stewart CA, Wang Y, Fujioka K, Thomas NC, Jamin SP, et al. β-Catenin is essential for Mullerian duct regression during male sexual differentiation. Development 2011;138:1967–75.

[133] Price JM, Donahoe PK, Ito Y, Hendren WH. Programmed cell death in the Müllerian duct induced by Müllerian inhibiting substance. Am J Anat 1977;149:353–75.

[134] Djehiche B, Segalen J, Chambon Y. Ultrastructure of mullerian and wolffian ducts of fetal rabbit in vivo and in organ culture. Tissue Cell 1994;26:323–32.

[135] Price JM, Donahoe PK, Ito Y. Involution of the female mullerian duct of the fetal rat in the organ-culture assay for the detection of mullerian inhibiting substance. Am J Anat 1979;156:265–83.

[136] Allard S, Adin P, Gouédard L, di Clemente N, Josso N, Orgebin-Crist MC, et al. Molecular mechanisms of hormone-mediated Müllerian duct regression: involvement of beta-catenin. Development 2000;127:3349–60.

[137] Parr BA, McMahon AP. Sexually dimorphic development of the mammalian reproductive tract requires Wnt-7a. Nature 1998;395:707–10.

[138] Behringer RR, Finegold MJ, Cate RL. Müllerian-inhibiting substance function during mammalian sexual development. Cell 1994;79:415–25.

[139] Mishina Y, Rey R, Finegold MJ, Matzuk MM, Josso N, Cate RL, et al. Genetic analysis of the Müllerian-inhibiting substance signal transduction pathway in mammalian sexual differentiation. Genes Dev 1996;10:2577–87.

[140] Orvis GD, Jamin SP, Kwan KM, Mishina Y, Kaartinen VM, Huang S, et al. Functional Redundancy of TGF-beta Family Type I Receptors and Receptor-Smads in Mediating Anti-Müllerian Hormone-Induced Müllerian Duct Regression in the Mouse1. Biol Reprod 2008;78:994–1001.

[141] Roberts LM, Visser JA, Ingraham HA. Involvement of a matrix metalloproteinase in MIS-induced cell death during urogenital development. Development 2002;129:1487–96.

[142] Itoh T, Ikeda T, Gomi H, Nakao S, Suzuki T, Itohara S. Unaltered secretion of beta-amyloid precursor protein in gelatinase A (matrix metalloproteinase 2)-deficient mice. J Biol Chem 1997;272:22389–92.

[143] Blelloch R, Kimble J. Control of organ shape by a secreted metalloprotease in the nematode *Caenorhabditis elegans*. Nature 1999;399:586–90.

[144] Garlena RA, Lennox AL, Baker LR, Parsons TE, Weinberg SM, Stronach BE. The receptor tyrosine kinase Pvr promotes tissue closure by coordinating corpse removal and epidermal zippering. Development 2015;142:3403–15.

[145] Poon IKH, Lucas CD, Rossi AG, Ravichandran KS. Apoptotic cell clearance: basic biology and therapeutic potential. Nat Rev Immunol 2014;14:166–80.

[146] Ellis RE, Jacobson DM, Horvitz HR. Genes required for the engulfment of cell corpses during programmed cell death in *Caenorhabditis elegans*. Genetics 1991;129:79–94.

[147] Kinchen JM, Doukoumetzidis K, Almendinger J, Stergiou L, Tosello-Trampont A, Sifri CD, et al. A pathway for phagosome maturation during engulfment of apoptotic cells. Nat Cell Biol 2008;10:556–66.

[148] Kinchen JM, Ravichandran KS. Identification of two evolutionarily conserved genes regulating processing of engulfed apoptotic cells. Nature 2010;464:778–82.

[149] Yu X, Lu N, Zhou Z. Phagocytic receptor CED-1 initiates a signaling pathway for degrading engulfed apoptotic cells. PLoS Biol 2008;6:e61.

[150] Guo P, Hu T, Zhang J, Jiang S, Wang X. Sequential action of *Caenorhabditis elegans* Rab GTPases regulates phagolysosome formation during apoptotic cell degradation. Proc Natl Acad Sci USa 2010;107:18016–21.

[151] Mangahas PM, Yu X, Miller KG, Zhou Z. The small GTPase Rab2 functions in the removal of apoptotic cells in *Caenorhabditis elegans*. J Cell Biol 2008;180:357–73.

[152] Franc NC, Heitzler P, Ezekowitz RA, White K. Requirement for croquemort in phagocytosis of apoptotic cells in Drosophila. Science 1999;284:1991–4.

[153] Park S-Y, Kim I-S. Engulfment signals and the phagocytic machinery for apoptotic cell clearance. Exp Mol Med 2017;49:e331.

[154] Tosello-Trampont AC, Brugnera E, Ravichandran KS. Evidence for a conserved role for CRKII and Rac in engulfment of apoptotic cells. J Biol Chem 2001;276:13797–802.

[155] Robertson AMG, Thomson JN. Morphology of programmed cell death in the ventral nerve cord of *Caenorhabditis elegans* larvae. J Embryol Exp Morphol 1982;67:89–100.

[156] Sulston JE, Schierenberg E, White JG, Thomson JN. The embryonic cell lineage of the nematode Caenorhabditis elegans. Dev Biol 1983;100:64–119.

[157] Hedgecock EM, Sulston JE, Thomson JN. Mutations affecting programmed cell deaths in the nematode Caenorhabditis elegans. Science 1983;220:1277–9.

[158] Zhou Z, Hartwieg E, Horvitz HR. CED-1 is a transmembrane receptor that mediates cell corpse engulfment in C. elegans. Cell 2001;104:43–56.

[159] Liu QA, Hengartner MO. Candidate adaptor protein CED-6 promotes the engulfment of apoptotic cells in C. elegans. Cell 1998;93:961–72.

[160] Wu YC, Horvitz HR. The C. elegans cell corpse engulfment gene ced-7 encodes a protein similar to ABC transporters. Cell 1998;93:951–60.

[161] Li Z, Venegas V, Nagaoka Y, Morino E, Raghavan P, Audhya A, et al. Necrotic Cells Actively Attract Phagocytes through the Collaborative Action of Two Distinct PS-Exposure Mechanisms. PLoS Genet 2015;11:e1005285.

[162] Reddien PW, Horvitz HR. CED-2/CrkII and CED-10/Rac control phagocytosis and cell migration in Caenorhabditis elegans. Nat Cell Biol 2000;2:131–6.

[163] Wu YC, Horvitz HR. C. elegans phagocytosis and cell-migration protein CED-5 is similar to human DOCK180. Nature 1998;392:501–4.

[164] Gumienny TL, Brugnera E, Tosello-Trampont AC, Kinchen JM, Haney LB, Nishiwaki K, et al. CED-12/ELMO, a novel member of the CrkII/Dock180/Rac pathway, is required for phagocytosis and cell migration. Cell 2001;107:27–41.

[165] Wu YC, Tsai MC, Cheng LC, Chou CJ, Weng NY. C. elegans CED-12 acts in the conserved crkII/DOCK180/Rac pathway to control cell migration and cell corpse engulfment. Dev Cell 2001;1:491–502.

[166] Nichols ALA, Meelkop E, Linton C, Giordano-Santini R, Sullivan RK, Donato A, et al. The Apoptotic Engulfment Machinery Regulates Axonal Degeneration in C. elegans Neurons. Cell Rep 2016;14:1673–83.

[167] Ruggiero L, Connor MP, Chen J, Langen R, Finnemann SC. Diurnal, localized exposure of phosphatidylserine by rod outer segment tips in wild-type but not Itgb5-/- or Mfge8-/- mouse retina. Proc Natl Acad Sci USa 2012;109:8145–8.

[168] Shen Q, He B, Lu N, Conradt B, Grant BD, Zhou Z. Phagocytic receptor signaling regulates clathrin and epsin-mediated cytoskeletal remodeling during apoptotic cell engulfment in C. elegans. Development 2013;140:3230–43.

[169] Freeman MR, Delrow J, Kim J, Johnson E, Doe CQ. Unwrapping glial biology: Gcm target genes regulating glial development, diversification, and function. Neuron 2003;38:567–80.

[170] Manaka J, Kuraishi T, Shiratsuchi A, Nakai Y, Higashida H, Henson P, et al. Draper-mediated and phosphatidylserine-independent phagocytosis of apoptotic cells by Drosophila hemocytes/macrophages. J Biol Chem

2004;279:48466–76.

[171] Suzuki E, Nakayama M. The mammalian Ced-1 ortholog MEGF10/KIAA1780 displays a novel adhesion pattern. Exp Cell Res 2007;313:2451–64.

[172] Lanot R, Zachary D, Holder F, Meister M. Postembryonic hematopoiesis in Drosophila. Dev Biol 2001;230:243–57.

[173] Huang S, Jia K, Wang Y, Zhou Z, Levine B. Autophagy genes function in apoptotic cell corpse clearance during C. elegans embryonic development. Autophagy 2013;9:138–49.

[174] He B, Yu X, Margolis M, Liu X, Leng X, Etzion Y, et al. Live-cell imaging in Caenorhabditis elegans reveals the distinct roles of dynamin self-assembly and guanosine triphosphate hydrolysis in the removal of apoptotic cells. Mol Biol Cell 2010;21:610–29.

[175] Lu N, Shen Q, Mahoney TR, Neukomm LJ, Wang Y, Zhou Z. Two PI 3-kinases and one PI 3-phosphatase together establish the cyclic waves of phagosomal PtdIns(3)P critical for the degradation of apoptotic cells. PLoS Biol 2012;10:e1001245.

[176] Lu N, Shen Q, Mahoney TR, Liu X, Zhou Z. Three sorting nexins drive the degradation of apoptotic cells in response to PtdIns(3)P signaling. Mol Biol Cell 2011;22:354–74.

[177] Nieto C, Almendinger J, Gysi S, Gómez-Orte E, Kaech A, Hengartner MO, et al. ccz-1 mediates the digestion of apoptotic corpses in C. elegans. J Cell Sci 2010;123:2001–7.

[178] Yeo JC, Wall AA, Luo L, Stow JL. Sequential recruitment of Rab GTPases during early stages of phagocytosis. Cell Logist 2016;6:e1140615.

[179] Gutierrez MG. Functional role(s) of phagosomal Rab GTPases. Small GTPases 2013;4:148–58.

[180] Vieira OV, Bucci C, Harrison RE, Trimble WS, Lanzetti L, Gruenberg J, et al. Modulation of Rab5 and Rab7 recruitment to phagosomes by phosphatidylinositol 3-kinase. Mol Cell Biol 2003;23:2501–14.

[181] Maderna P, Godson C. Phagocytosis of apoptotic cells and the resolution of inflammation. Biochim Biophys Acta 2003;1639:141–51.

[182] Gillingham AK, Munro S. Long coiled-coil proteins and membrane traffic. Biochim Biophys Acta 2003;1641:71–85.

[183] Schaefer MH, Wanker EE, Andrade-Navarro MA. Evolution and function of CAG/polyglutamine repeats in protein-protein interaction networks. Nucleic Acids Res 2012;40:4273–87.

[184] Bernier R, Golzio C, Xiong B, Stessman HA, Coe BP, Penn O, et al. Disruptive CHD8 mutations define a subtype of autism early in development. Cell 2014;158:263–76.

[185] Albert TK, Lemaire M, van Berkum NL, Gentz R, Collart MA, Timmers HT. Isolation and characterization of human orthologs of yeast CCR4-NOT complex subunits. Nucleic Acids Res 2000;28:809–17.

[186] Berber S, Llamosas E, Thaivalappil P, Boag PR, Crossley M, Nicholas HR. Homeodomain interacting protein kinase (HPK-1) is required in the soma for robust germline proliferation in C. elegans. Dev Dyn 2013;242:1250–61.

[187] Malin JA. Components of the Ubiquitin Proteasome System are Required for the Nonapoptotic Death of the *C. elegans* Linker Cell. The Rockefeller University. Ph.D. Thesis. 2015.

[188] Lee P, Cho B-R, Joo H-S, Hahn J-S. Yeast Yak1 kinase, a bridge between PKA and stress-responsive transcription factors, Hsf1 and Msn2/Msn4. Mol Microbiol 2008;70:882–95.

[189] Morton EA, Lamitina T. Caenorhabditis elegans HSF-1 is an essential nuclear protein that forms stress granule-like structures following heat shock. Aging Cell 2013;12:112–20.

[190] Martius C, Kuoop F. Der physiologische Abbau der Citronensäure. Hoppe-Seyler´S Zeitschrift Für Physiologische Chemie 1937;246.

[191] Juang H-H. Modulation of mitochondrial aconitase on the bioenergy of human prostate carcinoma cells. Mol Genet Metab 2004;81:244–52.

[192] Chen C-M, Wu Y-R, Chang K-H. Altered Aconitase 2 Activity in Huntington's Disease Peripheral Blood Cells and Mouse Model Striatum. Int J Mol Sci 2017;18:2480.

[193] Chaplin T, Ayton P, Bernard OA, Saha V, Valle Della V, Hillion J, et al. A novel class of zinc finger/leucine zipper genes identified from the molecular cloning of the t(10;11) translocation in acute leukemia. Blood 1995;85:1435–41.

[194] Singh A, Kumar N, Matai L, Jain V, Garg A, Mukhopadhyay A. A chromatin modifier integrates insulin/IGF-1 signalling and dietary restriction to regulate longevity. Aging Cell 2016;15:694–705.

[195] Hartley AD, Ward MP, Garrett S. The Yak1 protein kinase of Saccharomyces cerevisiae moderates thermotolerance and inhibits growth by an Sch9 protein kinase-independent mechanism. Genetics 1994;136:465–74.

[196] Das R, Melo JA, Thondamal M, Morton EA, Cornwell AB, Crick B, et al. The homeodomain-interacting protein kinase HPK-1 preserves protein homeostasis and longevity through master regulatory control of the HSF-1 chaperone network and TORC1-restricted autophagy in Caenorhabditis elegans. PLoS Genet 2017;13:e1007038.

[197] Hietakangas V, Anckar J, Blomster HA, Fujimoto M, Palvimo JJ, Nakai A, et al. PDSM, a motif for phosphorylation-dependent SUMO modification. Proc Natl Acad Sci USA 2006;103:45–50.

[198] Berber S, Wood M, Llamosas E, Thaivalappil P, Lee K, Liao BM, et al. Homeodomain-Interacting Protein Kinase (HPK-1) regulates stress responses and ageing in C. elegans. Sci Rep 2016;6:19582.

[199] Lee W, Swarup S, Chen J, Ishitani T, Verheyen EM. Homeodomain-interacting protein kinases (Hipks) promote Wnt/Wg signaling through stabilization of beta-catenin/Arm and stimulation of target gene expression. Development 2009;136:241–51.

[200] Louie SH, Yang XY, Conrad WH, Muster J, Angers S, Moon RT, et al. Modulation of the β-Catenin Signaling Pathway by the Dishevelled-Associated Protein Hipk1. PLoS ONE 2009;4:e4310.

[201] Keil W, Kutscher LM, Shaham S, Siggia ED. Long-Term High-Resolution Imaging of Developing *C. elegans* Larvae with Microfluidics. Dev Cell 2017;40:202–14.

[202] Sulston JE, Albertson DG, Thomson JN. The *Caenorhabditis elegans* male: postembryonic development of nongonadal structures. Dev Biol 1980;78:542–76.

[203] Botelho RJ, Teruel M, Dierckman R, Anderson R, Wells A, York JD, et al. Localized biphasic changes in phosphatidylinositol-4,5-bisphosphate at sites of phagocytosis. J Cell Biol 2000;151:1353–68.

[204] Andersen MH, Graversen H, Fedosov SN, Petersen TE, Rasmussen JT. Functional analyses of two cellular binding domains of bovine lactadherin. Biochemistry 2000;39:6200–6.

[205] Venegas V, Zhou Z. Two alternative mechanisms that regulate the presentation of apoptotic cell engulfment signal in *Caenorhabditis elegans*. Mol Biol Cell 2007;18:3180–92.

[206] LaMunyon CW, Ward S. Assessing the viability of mutant and manipulated sperm by artificial insemination of *Caenorhabditis elegans*. Genetics 1994;138:689–92.

[207] Sato M, Sato K, Liou W, Pant S, Harada A, Grant BD. Regulation of endocytic recycling by *C. elegans* Rab35 and its regulator RME-4, a coated-pit protein. Embo J 2008;27:1183–96.

[208] Allaire PD, Marat AL, Dall'Armi C, Di Paolo G, McPherson PS, Ritter B. The Connecdenn DENN domain: a GEF for Rab35 mediating cargo-specific exit from early endosomes. Mol Cell 2010;37:370–82.

[209] Chaineau M, Ioannou MS, McPherson PS. Rab35: GEFs, GAPs and effectors. Traffic 2013;14:1109–17.

[210] Shi A, Liu O, Koenig S, Banerjee R, Chen CC-H, Eimer S, et al. RAB-10-GTPase-mediated regulation of endosomal phosphatidylinositol-4,5-bisphosphate. Proc Natl Acad Sci USA 2012;109:E2306–15.

[211] Macia E, Luton F, Partisani M, Cherfils J, Chardin P, Franco M. The GDP-bound form of Arf6 is located at the plasma membrane. J Cell Sci 2004;117:2389–98.

[212] Ismail SA, Vetter IR, Sot B, Wittinghofer A. The structure of an Arf-ArfGAP complex reveals a Ca2+ regulatory mechanism. Cell 2010;141:812–21.

[213] Macia E, Chabre M, Franco M. Specificities for the small G proteins ARF1 and ARF6 of the guanine nucleotide exchange factors ARNO and EFA6. J Biol Chem 2001;276:24925–30.

[214] D'Souza-Schorey C, Stahl PD. Myristoylation is required for the intracellular localization and endocytic function of ARF6. Exp Cell Res 1995;221:153–9.

[215] Egami Y, Fukuda M, Araki N. Rab35 regulates phagosome formation through recruitment of ACAP2 in macrophages during FcγR-mediated phagocytosis. J Cell Sci 2011;124:3557–67.

[216] Kobayashi H, Fukuda M. Rab35 regulates Arf6 activity through centaurin-β2 (ACAP2) during neurite outgrowth. J Cell Sci 2012;125:2235–43.

[217] Chesneau L, Dambournet D, Machicoane M, Kouranti I, Fukuda M, Goud B, et al. An ARF6/Rab35 GTPase Cascade for Endocytic Recycling and Successful Cytokinesis. Curr Biol 2012;22:147–53.

[218] Allaire PD, Seyed Sadr M, Chaineau M, Seyed Sadr E, Konefal S, Fotouhi M, et al. Interplay between Rab35 and Arf6 controls cargo recycling to coordinate

cell adhesion and migration. J Cell Sci 2013;126:722–31.

[219] Miyamoto Y, Yamamori N, Torii T, Tanoue A, Yamauchi J. Rab35, acting through ACAP2 switching off Arf6, negatively regulates oligodendrocyte differentiation and myelination. Mol Biol Cell 2014;25:1532–42.

[220] Egami Y, Fujii M, Kawai K, Ishikawa Y, Fukuda M, Araki N. Activation-Inactivation Cycling of Rab35 and ARF6 Is Required for Phagocytosis of Zymosan in RAW264 Macrophages. J Immunol Res 2015;2015:429439–12.

[221] Shi A, Grant BD. Interactions between Rab and Arf GTPases regulate endosomal phosphatidylinositol-4,5-bisphosphate during endocytic recycling. Small GTPases 2013;4:106–9.

[222] Wood W, Turmaine M, Weber R, Camp V, Maki RA, McKercher SR, et al. Mesenchymal cells engulf and clear apoptotic footplate cells in macrophageless PU.1 null mouse embryos. Development 2000;127:5245–52.

[223] Parnaik R, Raff MC, Scholes J. Differences between the clearance of apoptotic cells by professional and non-professional phagocytes. Curr Biol 2000;10:857–60.

[224] Abdu Y, Maniscalco C, Heddleston JM, Chew T-L, Nance J. Developmentally programmed germ cell remodelling by endodermal cell cannibalism. Nat Cell Biol 2016;18:1302–10.

[225] Cannon GJ, Swanson JA. The macrophage capacity for phagocytosis. J Cell Sci 1992;101 (Pt 4):907–13.

[226] Herbomel P, Thisse B, Thisse C. Ontogeny and behaviour of early macrophages in the zebrafish embryo. Development 1999;126:3735–45.

[227] Rittig MG, Burmester GR, Krause A. Coiling phagocytosis: when the zipper jams, the cup is deformed. Trends Microbiol 1998;6:384–8.

[228] Ge X, Zhao X, Nakagawa A, Gong X, Skeen-Gaar RR, Shi Y, et al. A novel mechanism underlies caspase-dependent conversion of the dicer ribonuclease into a deoxyribonuclease during apoptosis. Cell Res 2014;24:218–32

[229] Weaver BP, Zabinsky R, Weaver YM, Lee E-S, Xue D, Han M. CED-3 caspase acts with miRNAs to regulate non-apoptotic gene expression dynamics for robust development in C. elegans. Elife 2014;3:e04265.

[230] Weaver BP, Weaver YM, Mitani S, Han M. Coupled Caspase and N-End Rule Ligase Activities Allow Recognition and Degradation of Pluripotency Factor LIN-28 during Non-Apoptotic Development. Dev Cell 2017;41:665–6.

[231] Arama E, Agapite J, Steller H. Caspase activity and a specific cytochrome C are required for sperm differentiation in Drosophila. Dev Cell 2003;4:687–97.

[232] Nakagawa A, Sullivan KD, Xue D. Caspase-activated phosphoinositide binding by CNT-1 promotes apoptosis by inhibiting the AKT pathway. Nat Struct Mol Biol 2014;21:1082–90.

[233] Honarpour N, Du C, Richardson JA, Hammer RE, Wang X, Herz J. Adult Apaf-1-deficient mice exhibit male infertility. Dev Biol 2000;218:248–58.

[234] Gould TW, Buss RR, Vinsant S, Prevette D, Sun W, Knudson CM, et al. Complete dissociation of motor neuron death from motor dysfunction by Bax deletion in a mouse model of ALS. J Neurosci 2006;26:8774–86.

[235] Kutscher LM, Shaham S. Non-apoptotic cell death in animal development. Cell Death Differ 2017;24:1326–36.

[236] Edison N, Zuri D, Maniv I, Bornstein B, Lev T, Gottfried Y, et al. The IAP-antagonist ARTS initiates caspase activation upstream of cytochrome C and SMAC/Diablo. Cell Death Differ 2012;19:356–68.

[237] Thuret G, Chiquet C, Herrag S, Dumollard J-M, Boudard D, Bednarz J, et al. Mechanisms of staurosporine induced apoptosis in a human corneal endothelial cell line. Br J Ophthalmol 2003;87:346–52.

[238] Nakajima Y-I, Kuranaga E. Caspase-dependent non-apoptotic processes in development. Cell Death Differ 2017;24:1422–30.

[239] la Vega de L, Grishina I, Moreno R, Krüger M, Braun T, Schmitz ML. A redox-regulated SUMO/acetylation switch of HIPK2 controls the survival threshold to oxidative stress. Mol Cell 2012;46:472–83.

[240] Brenner S. The genetics of Caenorhabditis elegans. Genetics 1974;77:71–94.

[241] Kutscher LM, Shaham S. Forward and reverse mutagenesis in *C. elegans.* WormBook 2014:1–26. doi:10.1895/wormbook.1.167.1.

[242] Lewis JA, Fleming JT. Basic culture methods. Methods Cell Biol 1995;48:3–29.

[243] Wicks SR, Yeh RT, Gish WR, Waterston RH, Plasterk RH. Rapid gene mapping in *Caenorhabditis elegans* using a high density polymorphism map. Nat Genet 2001;28:160–4.

[244] Zuryn S, Le Gras S, Jamet K, Jarriault S. A strategy for direct mapping and identification of mutations by whole-genome sequencing. Genetics 2010;186:427–30.

[245] Shaham S. galign: a tool for rapid genome polymorphism discovery. PLoS ONE 2009;4:e7188.

[246] Mello C, Fire A. DNA transformation. Methods Cell Biol 1995;48:451–82.

[247] Kamath RS, Fraser AG, Dong Y, Poulin G, Durbin R, Gotta M, et al. Systematic functional analysis of the *Caenorhabditis elegans* genome using RNAi. Nature 2003;421:231–7.

[248] Arribere JA, Bell RT, Fu BXH, Artiles KL, Hartman PS, Fire AZ. Efficient marker-free recovery of custom genetic modifications with CRISPR/Cas9 in *Caenorhabditis elegans*. Genetics 2014;198:837–46.

[249] Ward JD. Rapid and precise engineering of the Caenorhabditis elegans genome with lethal mutation co-conversion and inactivation of NHEJ repair. Genetics 2015;199:363–77.

[250] Liu H, Naismith JH. An efficient one-step site-directed deletion, insertion, single and multiple-site plasmid mutagenesis protocol. BMC Biotechnol 2008;8:91.

[251] Dickinson DJ, Ward JD, Reiner DJ, Goldstein B. Engineering the *Caenorhabditis elegans* genome using Cas9-triggered homologous recombination. Nat Methods 2013;10:1028–34.

[252] Peng H, Long F, Liu X, Kim SK, Myers EW. Straightening *Caenorhabditis elegans* images. Bioinformatics 2008;24:234–42.

[253] Lu N, Zhou Z. Membrane trafficking and phagosome maturation during the clearance of apoptotic cells. Int Rev Cell Mol Biol 2012;293:269–309.